Predicting state of health and remaining useful lifetime of lithium-ion batteries for eVTOLs using data-driven machine learning

Thesis defense date: 10^{th} June 2022

Birgitte Hennink
4463064
Air Transport & Operations
Aerospace Engineering

TU Delft

Abbreviations

CC Constant Current.

CV Constant Voltage.

EOL end of life.

EV Electric Vehicle.

eVTOL Electric Vertical Take-off and Landing.

GPR gaussian process regression.

IR Internal Resistance.

MAE Mean Absolute Error.

MAPE Mean Absolute Percentage Error.

ML machine learning.

MLP Multi-layer Perceptron.

MP mission profile.

NN Neural Network.

RF random forest.

RMSE Root Mean Squared Error.

RUL remaining useful lifetime.

SOC State of Charge.

SOH state of health.

SVM support vector machine.

SVR support vector regression.

Nomenclature

$\Delta^{CC,m,c}$	Duration of CC charging phase of capacity test c of mission profile m	s
$\Delta^{CV,m,c}$	Duration of CV charging phase of capacity test c of mission profile m	s
$\Delta^{phase,m,c}$	Duration of flight phase of capacity test c of mission profile m	s
$\Delta^{rest,m,c}$	Duration of CV charging phase of capacity test c of mission profile m	s
$\hat{RUL}^{m,c}$	Predicted Remaining Useful Lifetime of capacity test c of mission profile m	#missions
$\hat{SOH}^{m,c}$	Predicted State of Health of capacity test c of mission profile m	%
C^m	The total number of capacity tests in mission profile m	-
$I_i^{m,c}$	Current at timestep i of capacity test c of mission profile m	A
MAE_{RUL}^m	Mean Absolute Error of RUL of mission profile m	#missions
MAE_{SOH}^m	Mean Absolute Error of SOH of mission profile m	%
MAE_{RUL}	Average Mean Absolute Error of RUL	#missions
MAE_{SOH}	Average Mean Absolute Error of SOH	%

$MAPE^m_{RUL}$	Mean Absolute Percentage Error of RUL of mission profile m	–
$MAPE^m_{SOH}$	Mean Absolute Percentage Error of SOH of mission profile m	–
$MAPE_{RUL}$	Average Mean Absolute Percentage Error of RUL	–
$MAPE_{SOH}$	Average Mean Absolute Percentage Error of SOH	–
Q_{nom}	Nominal capacity	Ah
$Qcharge_i^{phase,m,c}$	Charge capacity of flight phase at timestep i of capacity test c of mission profile m	mAh
$Qdis_i^{phase,m,c}$	Discharge capacity of flight phase at timestep i of capacity test c of mission profile m	mAh
$Qdis_{max}^{phase,m,c}$	Maximum discharge capacity of flight phase of capacity test c of mission profile m	Ah
$Qdis_{mean}^{phase,m,c}$	Mean discharge capacity of flight phase of capacity test c of mission profile m	Ah
$Qdis_{min}^{phase,m,c}$	Minimum discharge capacity of flight phase of capacity test c of mission profile m	Ah
$Qdis_{var}^{phase,m,c}$	Variance discharge capacity of flight phase of capacity test c of mission profile m	Ah
$RMSE^m_{RUL}$	Root Mean Squared Error of RUL of mission profile m	#missions
$RMSE^m_{SOH}$	Root Mean Squared Error of SOH of mission profile m	%
$RMSE_{RUL}$	Average Root Mean Squared Error of RUL	#missions
$RMSE_{SOH}$	Average Root Mean Squared Error of SOH	%
$RUL^{m,c}$	True Remaining Useful Lifetime of capacity test c of mission profile m	#missions
$SOH^{m,c}$	True State of Health of capacity test c of mission profile m	%
$T^{m,c}_{cc}$	Current mission number of capacity test c of mission profile m	#missions
$t_{end}^{charge,m,c}$	Time step when charging phase of capacity test c of mission profile m ends	s
$t_{end}^{phase,m,c}$	Time step when phase of capacity test c of mission profile m ends	s
T^m_{EOL}	Mission number when capacity is below EOL of mission profile m	#missions
$T_i^{phase,m,c}$	Temperature of flight phase at timestep i of capacity test c of mission profile m	°C
$T_{max}^{phase,m,c}$	Maximum temperature of flight phase of capacity test c of mission profile m	Ah
$t_s^{charge,m,c}$	Time step when charging phase of capacity test c of mission profile m starts	s
$t_s^{phase,m,c}$	Time step when phase of capacity test c of mission profile m starts	s
$V_i^{phase,m,c}$	Voltage of flight phase at timestep i of capacity test c of mission profile m	V
$V_{max}^{phase,m,c}$	Maximum voltage of flight phase of capacity test c of mission profile m	V
$V_{mean}^{phase,m,c}$	Mean voltage of flight phase of capacity test c of mission profile m	V
$V_{min}^{phase,m,c}$	Minimum voltage of flight phase of capacity test c of mission profile m	V
$V_{var}^{phase,m,c}$	Variance voltage of flight phase of capacity test c of mission profile m	V

Predicting state of health and remaining useful lifetime of lithium-ion batteries for eVTOLs using data-driven machine learning

Author: Birgitte Hennink* (master thesis paper)
Supervisors: Mihaela Mitici, Marilena Pavel, Jianning Dong

Delft University of Technology, Delft, The Netherlands

Abstract

The health management of batteries is a key enabler for adopting Electric Vertical Take-off and Landing vehicles (eVTOLs). Currently, only a few studies consider the health management of eVTOL batteries. One characteristic of eVTOL batteries is that the battery discharge rates are significantly larger during take-off and landing. In turn, such discharge protocols are expected to impact the long-run health of batteries. This paper proposes a data-driven machine learning (ML) framework to estimate the state of health (SOH) and the remaining useful lifetime (RUL) of eVTOL batteries. This framework is illustrated using an open-source dataset of battery measurements taken during realistic eVTOL flights. Three main features are proposed for assessing the battery's health: charge, discharge and temperature. The paper quantifies the importance of these features for SOH and RUL prediction. Taking into account the type of battery charging before flight, it is also proposed a selection of eVTOL missions to be used for SOH and RUL prediction. The results demonstrate that indeed, discharge-related features have the highest importance when predicting battery SOH and RUL. Using five different ML algorithms, it is shown that the battery SOH and RUL are well estimated using random forest regression and XGBoost, respectively. To the best of our knowledge, this is the first study that proposes a framework dedicated to SOH and RUL prediction for eVTOL batteries.

1 Introduction

Electric Vertical Take-off and Landing vehicles (eVTOLs) are seen as a solution to growing traffic congestion in large cities, traffic-related pollution and intercity connectivity needs. Several companies such as Airbus, Bell, Embraer, Joby Aviation, Kitty Hawk, Pipistrel, Volocopter, and Aurora Flight Sciences have been designing, building, and testing eVTOLs in the last years [27].

One of the challenges the eVTOL industry faces is the management of the batteries, and in particular, the estimation of the state of health (SOH) and of the remaining useful lifetime (RUL) of batteries. The most frequently considered battery chemistry for e-mobility is lithium-ion due to its high energy-density, low self-discharge rates, very good low-temperature performance, and acceptable costs [13]. Several studies have focused on the health management of lithium-ion batteries for electric (ground) vehicles [37], on their SOH estimation [24] and RUL estimation [13; 46]. The batteries considered in these studies have been subject to constant current (CC) and constant voltage (CV) cycling with a constant discharge C-rates. For eVTOLs, however, the take-off and landing require larger discharge rates than the cruise phase. In the long-run, this is expected to have a direct impact on the health of the batteries. Since batteries are safety and cost-efficient critical for eVTOLs, the health management of batteries is a priority for eVTOLs.

Studies on battery SOH and RUL estimation propose either physics-informed approaches, model-based approaches or data-driven approaches. With the increasing availability of datasets on battery condition monitoring, several data-driven machine-learning approaches for battery SOH and RUL prediction have been proposed in the last years [15; 20].

In [13; 33; 41; 44; 46], several machine-learning algorithms are proposed to estimate the lifetime of batteries. In [33] and [44] an elastic net and a gradient boosting regression tree, respectively, are used to estimate the battery lifetime. The features considered in [44] regard the voltage, capacity, and temperature of the battery. A hydrid model (a random forest, an artificial bee colony and a general regression neural network), together with features generated based on the current (capacity, voltage, Internal Resistance (IR), and current) is proposed in [46]. In [13], an Elastic net, gaussian process regression (GPR), support vector machine (SVM), random forest (RF), a Gradient Boosting regression tree, and a Neural Network (NN) are used to predict the battery lifetime. The features used in this study are based on the charge, discharge, capacity, temperature, and IR recorded in the first 100-cycles of the battery. In contrast to [13], we estimate the battery SOH and RUL multiple time throughout the lifetime

*Msc Student, Air Transport and Operations, Faculty of Aerospace Engineering, Delft University of Technology

of the eVTOL batteries. In fact, the SOH and RUL estimates are updated as more measurements become available.

For SOH prediction, a random forest with features based on the charge current, voltage and temperature during charging and discharging is proposed in [24]. In [22] and [38], the authors propose a support vector regression algorithm for SOH estimation. Here, [22] argues that the SOH could be estimated using only the charge and discharge-related measurements. Also in this paper, we show that charge and discharge-related features have a high importance when estimating SOH and RUL of batteries. Nevertheless, we demonstrate that the temperature at which the batteries are exposed is an important feature for predicting SOH. In [21], a RF regression is proposed, together with features related to the charging voltage and the capacity of the battery.

Some of the most frequently used datasets for battery SOH and RUL predictions are [3], [7], [32], and [11],[24]. These batteries, however, are subject to constant CC and CV cycling. For dataset [32], lithium-ion batteries are charged and discharged at different temperatures, but still at constant CC and CV cycling. The measured parameters are the capacity, internal resistance, voltage, current, and temperature [12]. For dataset [3], LFP/Graphite cells are cycled. Here, the cells are always discharged at a 4C-rate. For dataset [24], data was recorded during real-life EVs usage over seven years of intensive usage.

To the best of our knowledge, dataset [Bills et al.] released by Carnegie Mellon University is the first battery dataset generated specifically for eVTOLs. In contrast with the previously discussed datasets, these batteries are subject to different C-rates during the discharge phase of a flight. Specifically, the take-off and landing of eVTOLs are performed at a larger C-rate than the cruise phase. Also, this eVTOL dataset cycles all battery sells until they reach end of life (EOL) [Bills et al.], instead of containing only early-cycle measurements, as is the case for [3]. Having run-to-EOL measurements, we are able to estimate the SOH and RUL of the batteries multiple times throughout the life of the batteries. Another novel aspect for this eVTOL dataset is that several parameters such as the temperature, power during discharge, and cruise length [Bills et al.] are varied across multiple eVTOL missions. Using this database specific for eVTOLs, this paper proposes for the first time a framework for battery SOH and RUL prediction for eVTOLs performing realistic flights [Bills et al.].

Using the eVTOL dataset [Bills et al.], we identified the missions relevant for SOH and RUL prediction. These are the missions where the battery is first charged to 100% State of Charge (SOC) before performing a flight. This is relevant because the maximum available capacity test can determine the battery's static capacity, which is critical when estimating the SOH. In practical applications, real-time dynamic capacity is more important to determine than the static capacity, because real-time dynamic capacity can better reflect the battery's SOH levels. However, estimating dynamic capacity accurately in real time is a challenge [40]. As a result, regular static capacity calibration becomes an option and will be used in this paper.

This paper proposed a framework for battery SOH and RUL estimation dedicated to eVTOLs. Using the dedicated eVTOLs database [Bills et al.], we first generate features based on measured variables and original voltage-capacity/time curves. These features are generated based on the battery charging/discharging protocols, and on the temperature at which the batteries are exposed. We quantify the importance of these features for SOH and RUL prediction. The results show that the (variation in the) voltage during take-off is of most importance for both SOH and RUL prediction. This makes the take-off not only safety-critical from a flight perspective, but also of high importance for SOH and RUL prognostics. The results also show that the length of the cruise has a lower importance for SOH and RUL prediction. Several machine learning algorithm are considered for SOH and RUL prediction: support vector regression (SVR), RF regression, GPR, XGBoost, and Multi-layer Perceptron (MLP). The results show that for the prediction of the SOH, the RF regression model has the best performance, with an Mean Absolute Error (MAE) of 1.33% and Root Mean Squared Error (RMSE) of 1.80%. For RUL prediction, the XGBoost leads to the best performance with an MAE of 54.53 missions and an RMSE of 67.92 missions. We also discuss the impact of the characteristics of the eVTOL mission on the battery SOH and RUL predictions. To the best of our knowledge, this is the first framework for battery SOH and RUL prediction for realistic eVTOL flights.

The remainder of this paper is structured as follows. In Section 2, the [Bills et al.] dataset on eVTOL batteries is analyzed. In Section 3, features are generated based on charge-related, discharge-related, and temperature-related. The determination of SOH and RUL is discussed in Section 4. In Section 5, an end-to-end machine learning framework is proposed for battery SOH and RUL prediction. In Sections 6 and 7 the SOH and RUL prediction results are presented. Besides, in Sections 6 and 7 the importance of features is quantified for SOH and RUL prediction, respectively. In section 8 we discuss the impact of the characteristics of the eVTOL missions on SOH and RUL prediction. Final conclusions are provided in Section 9.

2 Data description

We consider the health-monitoring dataset for Sony-Murata 18650 VTC-6 cell lithium-ion batteries available at [Bills et al.]. These batteries are used to perform short-range missions with the Vahana eVTOL.

Vahana is an eVTOL designed by Acubed (Airbus) for urban air mobility. It is an all-electric, single-seat, tilt-wing vehicle with a range of 50 km [2]. During cruise Vahana achieves an average speed of 190 km/h,

with a maximum of 220 km/h. The longest flight performed by Vahana had a total duration of 19 minutes and 56 seconds [1].

Figure 1: Vahana [2].

Figure 2 shows a generic mission profile for Vahana: vertical take-off, transition to forward flight, cruise for a specified distance, a transition back to a hover, and a vertical landing. (see Figure 1).

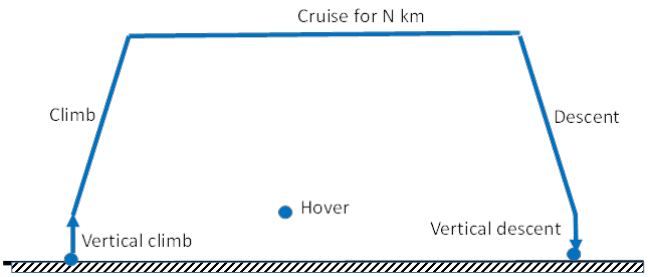

Figure 2: Generic mission profile eVTOL.

To discuss the dataset of [Bills et al.], we define a mission profile (MP) for Vahana as a set of mission tasks whose specifications are unchanged across a sequence of missions. From the beginning to the end of a mission, these tasks are Constant Current (CC) battery Charging phase, Constant Voltage (CV) battery Charging phase, Rest period, eVTOL Take-off, eVTOL Cruise, eVTOL Landing, and Rest period.

The dataset[Bills et al.] contains 22 mission profiles (MP1-MP22), see Table 1. Under each 22 mission profile, one Sony-Murata 18650 VTC-6 cell lithium-ion battery is used to perform a sequence of missions with Vahana (see Table 1 for the number of missions performed under each mission profile).

Baseline mission profiles

Mission profiles VAH01, VAH17, and VAH27 are baseline mission profiles (see Table 1). We refer to them as baseline mission profiles because the other mission profiles are obtained by changing the specification of mission tasks of one of these baseline mission profile.

Under a baseline mission profile, the battery is charged with 1 C-rate (CC charging phase). The CC charging phase ends as soon as the battery's voltage reaches 4.2 V. Hereafter, the CV charging phase starts with a constant voltage of 4.2 V until the current is below $C/30$. After charging, the battery cell rests until the cell temperature reaches 35 $°C$. After this Rest period, the eVTOL performs a flight. The take-off phase has a duration of 75 seconds, with a discharge power of $54W$, a C-rate of $5C$, and $1.12Wh$ discharge energy. Afterwards, the cruise phase takes 800 seconds, at a discharge power of 16 W, a C-rate of $1.48C$, and 3.55 Wh discharge energy. Hereafter, the landing phase takes place with a duration of 105 seconds, a discharge power of 54 W, a C-rate of $5C$, and 1.57 Wh discharge energy. Finally, the battery rests until its temperature decreases to 27 $°C$.

Table 1 shows how the 22 mission profiles are obtained by changing the following mission tasks of baseline mission profiles: the duration of the cruise phase, the power used during flight (i.e., take-off, cruise, and landing), the CC current, the CV voltage, and the (chamber) temperature.

Measurements

During every mission, the following measurements are recorded every time step: time (sec), cell voltage (V), cell current (mA), energy supplied to the cell during charge (Wh), charge supplied to the cell during charge (mAh), energy extracted from the cell during discharge (Wh), charge extracted the from the battery cell during discharge (mAh), cell surface temperature ($°C$), cycle number ($-$) and cycle segment ($-$).

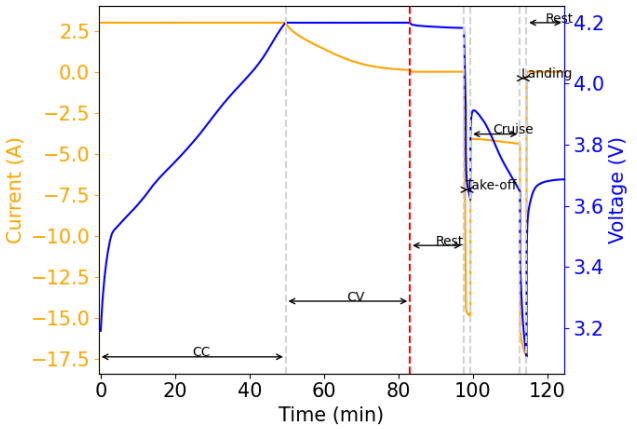

Figure 3: The charging and discharging phases of the first capacity test, mission profile VAH01. The battery is first discharged to 0% SOC. Then, the battery is charged to 100% SOC. With a battery with 100% SOC, the 1^{st} flight is performed. During take-off, cruise and landing, the battery is discharged.

Capacity tests

Given a mission profile, after every 50^{th} mission, the residual battery charge is reduced to 0% SOC at a discharge rate of C/5 until the voltage drops below 2.5V. Then, the battery is charged to 100% SOC at a charging rate of 1 C-rate and a constant voltage of 4.2V. After the battery is fully charged, the eVTOL performs

a flight (take-off, cruise, and landing). This "special" mission when the battery is charged to 100% and only afterwards the eVTOL takes off, is referred to as a capacity test. Table 1 shows the total number of capacity tests under each of the 22 mission profiles.

Figure 3 shows the charging and discharging protocol of the first capacity test of VAH01. The CC charging phase in Figure 3 has a duration of 50 minutes, and the battery is charged with 3.0 A. Afterwards, the CV charging phase takes place with 4.2 V for 33 minutes. The Rest period following charging has a duration of 14 minutes. The discharge phase starts with the take-off of the eVTOL. The duration of the take-off is 75 seconds. During take-off, the voltage drops from 3.92 V to 3.62 V. The cruise phase has a duration of 800 seconds. Hereafter, the landing phase has a duration of 105 seconds. During landing, the voltage drops from 3.57 V to 3.1 V. Finally, the mission ends with a Rest period of 605 seconds. At the end of the Rest period, the battery reaches a temperature of 27.3 $°C$.

To estimate the SOH and RUL of the batteries, we consider the battery capacity during capacity tests only, i.e., when the battery is charged to 100% SOC before flight. We only focus on the capacity tests because dynamic capacity estimation would require an extensive analysis and hyperparameter tuning, which may be prone to estimation errors [40]. In contrast, regular static capacity calibration is more reliable for testing purposes. The battery cell capacity during a cycle is given by the maximum amount of charge (in Ah) supplied to the cell during the charging phase of this cycle. In Figure 3, the red dotted line shows the end of this charging phase of the 1^{st} capacity test of VAH01.

Figure 4 shows the mission immediately following the 1^{st} capacity test of VAH01. It can be seen that the battery follows the same mission profile as in Figure 3. However, the battery is now charged only from 3.8 V to 4.2 V. As a result, the duration of the CC and CV charging period is shorter (83 min in the 1^{st} capacity test vs. 55 min in this mission immediately following this 1^{st} capacity test). In contrast, during the capacity test, the battery is charged from 3.2 V to 4.2V, and the CC and CV charging duration is more extensive (28 min).

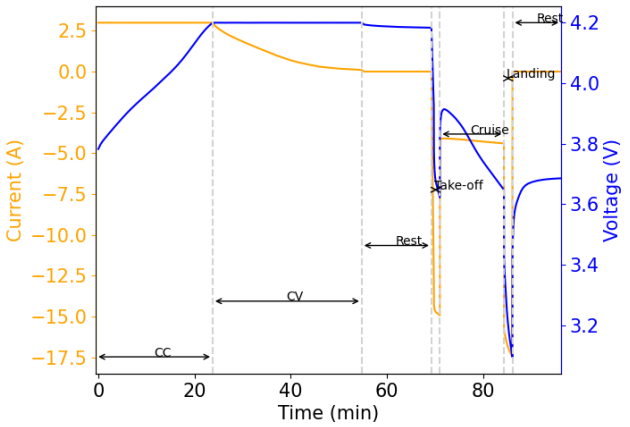

Figure 4: Charging and discharging phase of the 2^{nd} mission, mission profile VAH01.

Selection of mission profiles for SOH and RUL prediction

For our analysis, we consider only 19 mission profiles of the total 22 profiles (see Table 1). Mission profiles VAH06, VAH07, and VAH09 are not considered due to the inconsistencies in the battery characteristics recorded over time.

For VAH06, the degradation of the battery capacity follows an unexpected trend. During mission 766 (15^{th} capacity test), the capacity of the battery is 2.51 Ah. However, during the following capacity tests, from mission 903 until mission 8942, the battery's capacity varies between 1.8 - 1.9 Ah. Afterwards, VAH06 consists of four standard capacity tests where the battery's capacity degrades from 2.51 Ah to 2.44 Ah (see also Figure 5). This is unexpected as the battery's capacity should degrade over time, and not decrease and then increase again.

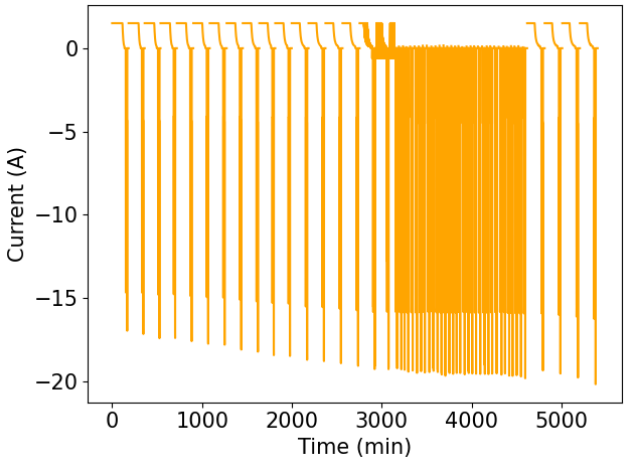

Figure 5: Capacity tests - VAH06.

Figure 6 shows the capacity tests during mission profile VAH07. For VAH07, the battery's capacity increases over time as more capacity tests are performed. However, this pattern is unexpected since the battery's capacity is expected to decrease over time.

	Cruise duration	Power Take-off	Power Cruise	Power Landing	CC	CV	Temperature	VAHXX	#Missions	#Capacity tests
MP1	**800** s	**54** W	**16** W	**54** W	**1** C	**4.2** V	**25** $°C$	**VAH01**	**847**	**17**
MP2	125% of 800 s	54 W	16 W	54 W	1 C	4.2 V	25 $°C$	VAH02	625	13
MP3	800 s	90% of 54 W	90% of 16 W	90% of 54 W	1 C	4.2 V	25 $°C$	VAH05	1615	31
MP4	800 s	54 W	16 W	54 W	50% of 1 C	4.2 V	25 $°C$	VAH06	9290	28
MP5	800 s	54 W	16 W	54 W	1 C	95.24% of 4.2 V	25 $°C$	VAH07	339	44
MP6	800 s	54 W	16 W	54 W	1 C	4.2 V	80% of 25 $°C$	VAH09	8527	46
MP7	800 s	54 W	16 W	54 W	1 C	4.2 V	120% of 25 $°C$	VAH10	1431	28
MP8	800 s	80% of 54 W	80% of 16 W	80% of 54 W	1 C	4.2 V	25 $°C$	VAH11	2249	44
MP9	50% of 800 s	54 W	16 W	54 W	1 C	4.2 V	25 $°C$	VAH12	2349	46
MP10	75% 800 s	54 W	16 W	54 W	1 C	4.2 V	25 $°C$	VAH13	1042	20
MP11	125% of 800 s	54 W	16 W	54 W	1 C	4.2 V	25 $°C$	VAH15	554	11
MP12	800 s	54 W	16 W	54 W	150% of 1 C	4.2 V	25 $°C$	VAH16	559	11
MP13	**800** s	**54** W	**16** W	**54** W	**1** C	**4.2** V	**25** $°C$	**VAH17**	**1002**	**20**
MP14	800 s	54 W	16 W	54 W	150% of 1 C	4.2 V	25 $°C$	VAH20	611	12
MP15	125% of 800 s	54 W	16 W	54 W	1 C	4.2 V	25 $°C$	VAH22	579	12
MP16	800 s	54 W	16 W	54 W	1 C	97.62% of 4.2 V	25 $°C$	VAH23	697	13
MP17	800 s	54 W	16 W	54 W	50% of 1 C	4.2 V	25 $°C$	VAH24	801	16
MP18	800 s	54 W	16 W	54 W	1 C	4.2 V	80% of 25 $°C$	VAH25	554	11
MP19	75% of 800 s	54 W	16 W	54 W	1 C	4.2 V	25 $°C$	VAH26	1164	22
MP20	**800** s	**54** W	**16** W	**54** W	**1** C	**4.2** V	**25** $°C$	**VAH27**	**587**	**12**
MP21	800 s	90% of 54 W	90% of 16 W	90% of 54 W	1 C	4.2 V	25 $°C$	VAH28	1182	23
MP22	800 s	54 W	16 W	54 W	1 C	4.2 V	140% of 25 $°C$	VAH30	919	18

Table 1: Mission profile characteristics, based on [Bills et al.].

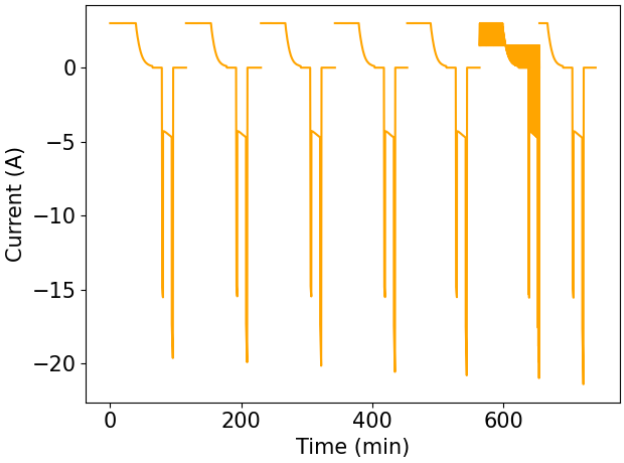

Figure 6: Capacity tests - VAH07.

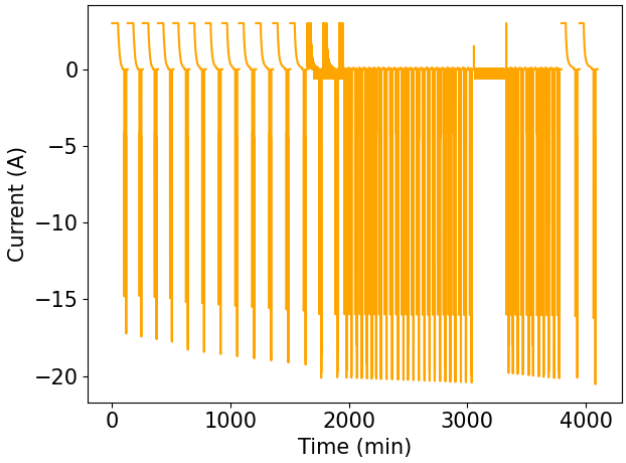

Figure 7: Capacity tests - VAH09.

Figure 7 shows the capacity tests for VAH09. For capacity tests corresponding to mission 728 until mission 6074, the battery capacity varies between 1.8-1.9 Ah. This pattern can be seen in Figure 7. Afterwards, from mission 6277 until mission 6306, the battery's capacity increases to 2.46 Ah. Then, from mission 6480 until mission 8352, the capacity varies again between 1.8-1.9 Ah. Finally, during the last two capacity tests, the battery's capacity degraded from 2.43 to 2.41 Ah. This pattern is unexpected as we expect the capacity to decrease over time, and not decrease, increase, and then decrease again.

Discussion of selected mission profiles

Figure 20 (Appendix A) shows the current during the capacity tests of the 19 selected mission profiles. Figures 20(a), 20(j), and 20(q) show the capacity tests of the baseline mission profile VAH01, VAH17, and VAH27, respectively.

Figures 20(d), 20(o), and 20(s) show the capacity tests for mission profiles VAH10, VAH25, and VAH30, which are obtained by varying the temperature in the baseline mission profiles. As expected, a lower temperature leads to fewer missions (and thus fewer capacity tests) than a 20% increase of thermal chamber temperature. Figure 20(o) shows that the one last capacity test is different than the others. The reason for this abnormal pattern is that during this mission, two capacity tests are being performed one after the other and reported as one capacity test in the dataset [Bills et al.].

Figures 20(c), 20(e), and 20(r) show the capacity tests of VAH05, VAH11, and VAH28, where the power during the flight (i.e., during take-off, cruise, and landing) has been reduced. For these mission profiles, it can be seen that the current values are lower during the discharge phase. This is expected because the power is obtained by multiplying the current with the voltage. Therefore, a reduction in power leads to lower current values. In Figure 20(r), it can be seen that there is a different capacity test present at 750 minutes because two capacity tests are being performed one after the other and reported as one capacity test in the dataset [Bills et al.].

Figures 20(b), 20(f), 20(g), 20(h), 20(l), and 20(p) show the capacity tests of VAH02, VAH12, VAH13, VAH15, VAH22, and VAH26, where the cruise length is varied. We note that the mission profiles with the longest cruise duration also have the least total number of flights performed.

Figures 20(i) and 20(k) show the capacity tests for VAH16 and VAH20, where the CC charge current is increased to 1.5 C. As a result, the duration of the CC charging period decreases. Figure 20(n) shows the capacity tests during mission profile VAH24, where the CC charge current is reduced to C/2. As a result, the duration of the CC charging phase increases.

Figure 20(m) shows the capacity tests during mission profile VAH23, where the CV charge voltage is reduced to 4.1 V. As expected, in this case, the CV charging phase has a longer duration than in the baseline mission profile.

Figure 8 shows the capacity degradation for each of the 19 selected mission profile. The capacity is given at every capacity test of each mission profile.

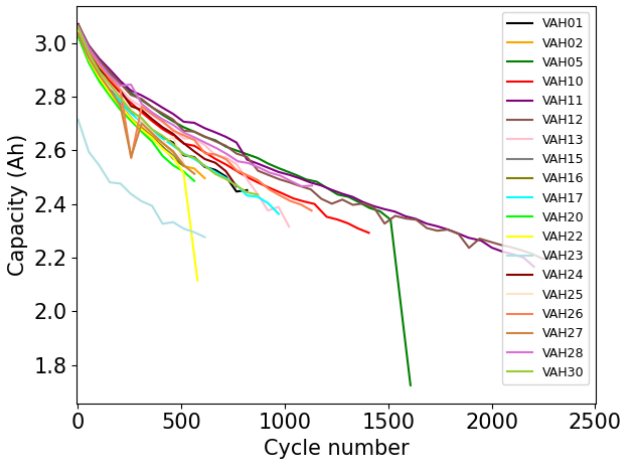

Figure 8: Capacity degradation for all 19 selected mission profiles.

Figure 9 shows boxplots of the duration of the CC charging phase during capacity tests of the 19 selected mission profiles. Most mission profiles consider a CC charging phase duration of 2000-3000 seconds. For mission profile VAH24, the duration of the charging phase is longer since the CC charge current is reduced to C/2. Moreover, there are outliers present in mission profiles VAH05, VAH22, VAH25, and VAH28. These outliers are present due to one abnormal capacity test in VAH05, VAH22, VAH25, and VAH28. These abnormal capacity tests can be seen in Figure 20(c), Figure 20(l), Figure 20(o), and Figure 20(r) accordingly.

3 Feature generation

To discuss the generation of features, we first introduce the following notations. Let C^m denote the total number of capacity tests of a mission profile m, $1 \leq m \leq M$.

Let $t_s^{phase,m,c}$, $1 \leq m \leq M$, $1 \leq c \leq C^m$, denote the time step when phase $\in$ {take-off, cruise, landing} of capacity test c of mission profile m starts. Let $t_e^{phase,m,c}$, $1 \leq m \leq M$, $1 \leq c \leq C^m$, denote the time step when phase $\in$ {take-off, cruise, landing} of capacity test c of mission profile m ends.

Let $t_s^{charge,m,c}$, $1 \leq m \leq M$, $1 \leq c \leq C^m$, denote the time step when the charging phase of capacity test c of mission profile m starts. Let $t_e^{charge,m,c}$, $1 \leq m \leq M$, $1 \leq c \leq C^m$, denote the time step when the charging phase of capacity test c of mission profile m ends.

Let $T_i^{phase,m,c}$ denote the temperature recorded at time step i during a flight phase of a capacity test c of mission profile m, with phase $\in$ {take-off, cruise, landing}, $t_s^{phase,m,c} \leq i \leq t_e^{phase,m,c}$, $1 \leq c \leq C^m$, $1 \leq m \leq M$.

Let $V_i^{phase,m,c}$ denote the voltage recorded during a flight phase at time step i of capacity test c of mission profile m, with phase $\in$ {take-off, cruise, landing}, $t_s^{phase,m,c} \leq i \leq t_e^{phase,m,c}$, $1 \leq c \leq C^m$, m, $1 \leq m \leq M$.

Let $Qdis_i^{phase,m,c}$ denote the discharge capacity during a flight phase at time step i of capacity test c of mission profile m, with phase $\in$ {take-off, cruise, landing}, $t_s^{phase,m,c} \leq i \leq t_e^{phase,m,c}$, $1 \leq c \leq C^m$, $1 \leq m \leq M$.

Let $Qcharge_i^{m,c}$ denote the charge capacity at time step i during capacity test c of mission profile m, with $t_s^{charge,m,c} \leq i \leq t_e^{charge,m,c}$, $1 \leq c \leq C^m$, $1 \leq m \leq M$.

We consider a total of 33 features (see Table 2). These features are related to the charging, discharging and temperature of the battery, as follows.

3.1 Battery charge-related features

Figure 10(a) shows the charging time vs. the charging voltage for the capacity tests of the baseline mission profile VAH01. Mission profile VAH01 has 847 missions, out of which every 50^{th} mission is a capacity test. Figure 10(a) shows that as the number of missions increases, the duration of the CC charging phase decreases. The first capacity test has a CC charging duration of 50 minutes, whereas the last capacity test has a CC charging duration of 37 minutes. Hence, there is a 26% decrease in the CC charging duration. When the duration of the CC charging phase is reduced, the cut-off voltage of 4.2 V is reached earlier. Due to the reduction of the duration of the CC charging phase, the

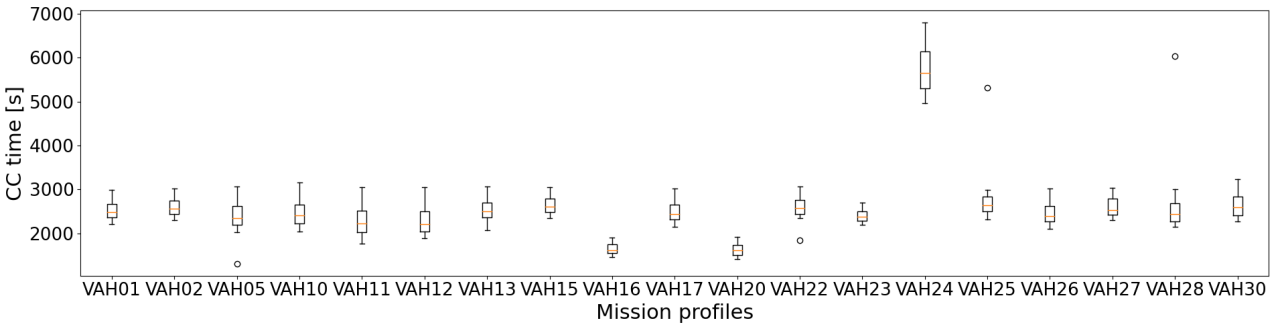

Figure 9: Duration CC charging phase.

CV charging phase begins earlier and has a longer duration. During the first capacity test the CV charging phase takes 33 minutes. In contrast the CV charging phase has a duration of 64 minutes during the last capacity. Thus, for VAH01, the duration of the CV charging phase increases with 92%. The observed decrease in the CC charging duration and the increase of the CV charging duration over the number of missions is due to the battery polarization phenomenon [45].

Analyzing the charging of the battery, we consider as features: 1) $\Delta^{CC,m,c}$, the duration of the CC charging phase of capacity test c of mission profile m; 2) $\Delta^{CV,m,c}$, the duration of the CV phase of capacity test c of mission profile m, and 3) $\Delta^{rest,m,c}$, the duration of the Rest period after charging. The Rest period starts when the current is below $C/30$. The Rest period ends as soon as the battery's temperature reaches $35°C$. Table 2 gives an overview of the features considered.

3.2 Battery discharge-related features

Regarding discharge-related features, we consider features related to the discharge voltage of the battery, the discharge capacity, and the duration of each discharge phase (see Table 2).

Discharge voltage: Figure 10(b) shows the discharge capacity vs. the discharge voltage during capacity tests of the baseline mission profile VAH01. For landing and take-off, a higher C-rate is considered than for the cruise phase. During the take-off and landing the C-rate is 5C, whereas during cruise the C-rate is 1.48C. Figure 10(b) shows that as the number of missions increases, the minimum discharge voltage decreases during each phase. Besides, it can be seen that during the take-off and landing phases, the discharge voltage drop is higher then during the cruise phase. This is expected, because the take-off and landing phases occur at a higher C-rate.

Since the discharge voltage varies for every flight phase and across missions, we aim to capture the impact of these variations by considering voltage-related features. Therefore, we consider the following battery-discharge related features: 1) $V_{max}^{phase,m,c}$, the maximum voltage during phase $\in$ {take-off, landing, cruise} of capacity test c of mission profile m, 2) $V_{min}^{phase,m,c}$, the minimum voltage during phase $\in$ {take-off, landing, cruise} of capacity test c of mission profile m, 3) $V_{mean}^{phase,m,c}$, the mean voltage during phase $\in$ {take-off, landing, cruise} of capacity test c of mission profile m, and 4) $V_{var}^{phase,m,c}$, the variance voltage during phase $\in$ {take-off, landing, cruise} of capacity test c of mission profile m.

These voltage related featured are considered since they reflect the open circuit voltage and internal resistance, which are closely related to the remaining capacity and the aging of the battery [28; 40].

Discharge capacity: Figure 10(b) shows that the discharge capacity increases from take-off to cruise to landing. The discharge capacity also increases as the number of missions increases. To capture these patterns, we consider the following features related to the discharge capacity of the battery (see also Table 2): 1) $Qdis_{max}^{phase,m,c}$, the maximum discharge capacity recorded during phase $\in$ {take-off, landing, cruise} of capacity test c of each mission profile m, 2) $Qdis_{min}^{phase,m,c}$, the minimum discharge capacity recorded during phase $\in$ {take-off, landing, cruise} of capacity test c of each mission profile m, 3) $Qdis_{mean}^{phase,m,c}$, the mean discharge capacity recorded during phase $\in$ {take-off, landing, cruise} of capacity test c of each mission profile m, and 4) $Qdis_{var}^{phase,m,c}$, the variance of the discharge capacity recorded during phase $\in$ {take-off, landing, cruise} of capacity test c of each mission profile m.

The discharge capacity and its variation reflect the load characteristics of the battery, which directly impacts the aging of the battery. As such, we consider as features the maximum, minimum, mean and variance of the discharge capacity.

Duration of the discharge phase: We consider $\Delta^{phase,m,c}$, the duration of each discharge phase $\in$ {take-off, landing, cruise} of capacity test c of mission profile m (see also Table 2). Since the cruise duration varies across mission profiles, we also consider the duration of the cruise phase as a feature.

3.3 Temperature-related features

Figure 10(c) shows the maximum, minimum, and average battery temperature recorded during all missions of mission profile VAH01. During every capacity test, the maximum and average battery temperature drop. This is because the battery cell is allowed to rest at the end of a capacity test until the battery tempera-

ture reduces to 27 $°C$. Figure 10(c) also shows that, as the battery is used for a longer time, its maximum temperature increases.

During a capacity test, Figure 10(d) shows that the highest battery temperature is reached during landing. Figure 10(d) also shows that the temperature reaches a peak during take-off and decreases during cruise. In Figure 10(d), the tasks of the first capacity test are highlighted in orange, while the last capacity test is highlighted in blue. When considering both the take-off, landing, and cruise phases, the temperature increases as the number of capacity tests increases.

To capture the change in battery temperature as more missions are performed, we consider as feature $T_{max}^{phase,m,c}$, the maximum battery temperature (in $°C$) recorded during the discharge phase $\in$ {take-off, landing, cruise} of capacity test c of each mission profile m, see also Table 2.

4 Estimating the SOH and RUL of the batteries

In general, the state of health (SOH) of a battery is defined as the ratio between the measured charging capacity during a capacity test, and the nominal capacity of the battery. Formally, [35; 39]:

$$SOH^{m,c} = \frac{\int_{t_s}^{t_e} I_i^{m,c}(t)\, dt}{Q_{nom}} \cdot 100\%, \tag{1}$$

where $I_i^{m,c}$ is the cell current at time step i, during capacity test c of mission profile m. The integral is taken over the full charging phase. In Figure 3, the end of the charging phase is indicated with a red dotted line. The dataset [Bills et al.] also contains $Qcharge_i^{m,c}$ (mAh), the amount of charge supplied to the cell during charge. Using this, SOH could be determined as:

$$SOH^{m,c} = \frac{\max_i(Qcharge_i^{m,c})}{Q_{nom}} \cdot 100\%, \tag{2}$$

where $t_s^{CCstart,m,c} \leq i \leq t_e^{CVend,m,c}$, $1 \leq m \leq M$, $1 \leq c \leq C^m$.

Although in [5] a nominal battery capacity of 3.0 Ah is indicated in the dataset [Bills et al.], all mission profiles, except VAH23, have during the first capacity test a battery capacity of more than 3.0 Ah. For example, for mission profile VAH01 the first capacity test has a battery capacity of 3.03 Ah. For mission profile VAH23 the battery's capacity during the first capacity test is 2.71 Ah. Thus, a capacity of 3.0 Ah does not seem to be the nominal capacity for all battery cells considered in [5].

Therefore, we choose to determine the SOH of a battery, following [31], as:

$$SOH^{m,c} = \frac{\max_i(Qcharge_i^{m,c})}{\max_i(Qcharge_i^{m,0})} \cdot 100\%, \tag{3}$$

with $Qcharge_i^{m,c}$ the maximum measured capacity during a capacity test c of mission profile m, and $charge_i^{m,0}$ the maximum battery capacity measured during the first capacity test ($c = 0$) of mission profile m.

The remaining useful lifetime (RUL) of a battery is defined as the remaining number of missions/cycles for this battery until end of life (EOL), given that the battery has already been used for $c >= 0$ missions/cycles. Formally, the RUL of a battery, estimated after c missions/cycles under mission profile m, is defined as:

$$RUL^{m,c} = T_{EOL}^m - T_{cc}^{m,c}, \tag{4}$$

where $T_{cc}^{m,c}$ is the current mission/cycle number under mission profile m, and T_{EOL}^m is the mission/cycle number when the battery capacity drops for the first time below an EOL-threshold for mission profile m.

Existing studies based on experimental battery datasets set the EOL-threshold to 80% of the nominal battery capacity [13; 33; 44; 47]. To the best of our knowledge, EOL-thresholds for eVTOL batteries have not yet been formally established. For eVTOL batteries, it is expected that conservative safety margins will be considered. In [17], a conservative EOL-threshold of 85% of a nominal battery capacity of an eVTOL is considered. This eVTOL is designed for a total capacity of 5 persons with a range of 400 km [17]. Following [17], for our analysis, we also consider an EOL-threshold of 85% of the initially measured battery capacity.

The choice of the EOL-threshold has also an effect on the selection of the mission profiles. Using an EOL-threshold of 80%, not all mission profiles in the dataset [Bills et al.] will have their batteries reaching EOL. Specifically, for mission profiles VAH01, VAH02, VAH15, VAH16, VAH20, VAH23, VAH24, VAH25, VAH27, and VAH28 the series of measurements stop before the battery capacity reaches 80% of the initially measured battery capacity (see also Table 20). In other words, using an EOL-threshold of 80% of the initial battery capacity, these mission profiles will not have run-to-EOL series of measurements.

Considering an EOL-threshold of 85% of the initially measured battery capacity, all mission profiles in the dataset [Bills et al.] have batteries that reach their EOL. Table 3 shows the number of missions until each battery reaches its EOL, as well as the number of capacity tests until this battery reaches its EOL.

However, one capacity test has been removed from the dataset for two mission profiles. In Figure 11, the capacity degradation for VAH26 and VAH27 and their EOL value can be seen, with the EOL-threshold set at 85%.

Figure 10: Capacity tests - mission profile VAH01.

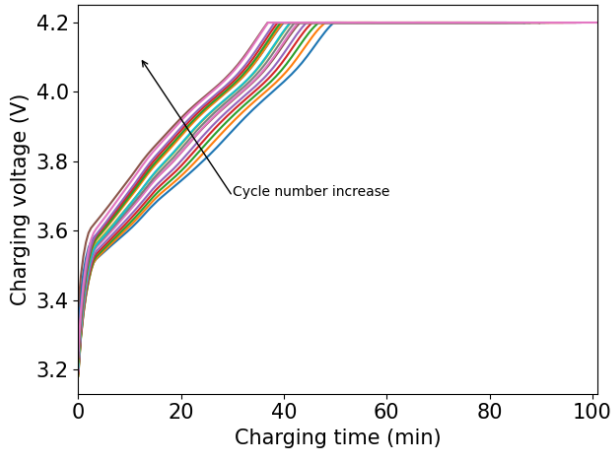

(a) Charging curves during all capacity tests - VAH01.

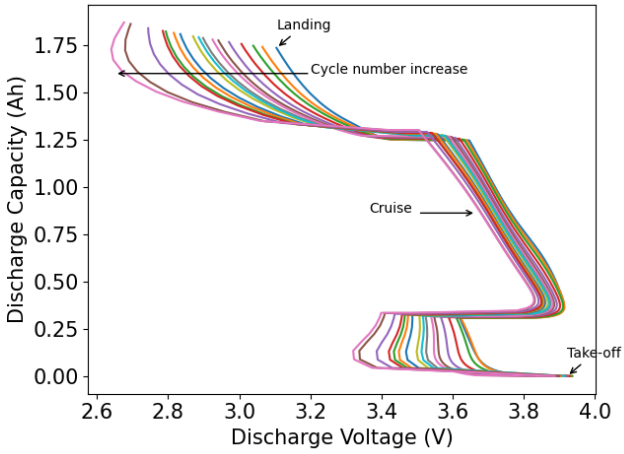

(b) Discharge capacity during all capacity tests - VAH01.

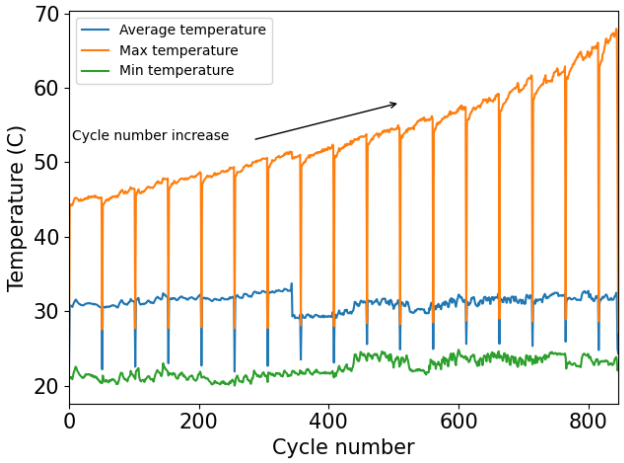

(c) Average, max and min temperature during all missions - VAH01.

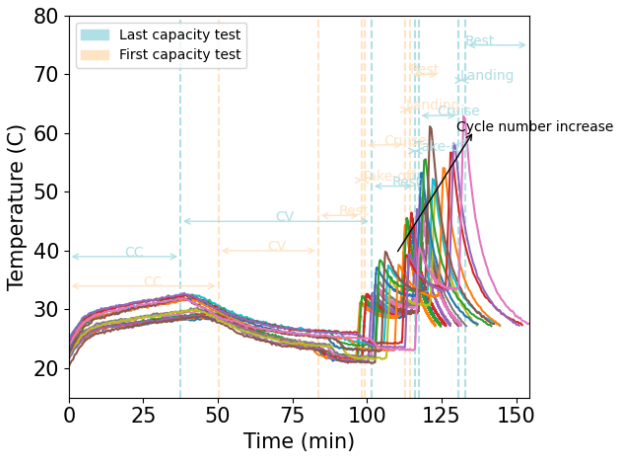

(d) Temperature during all capacity tests - VAH01.

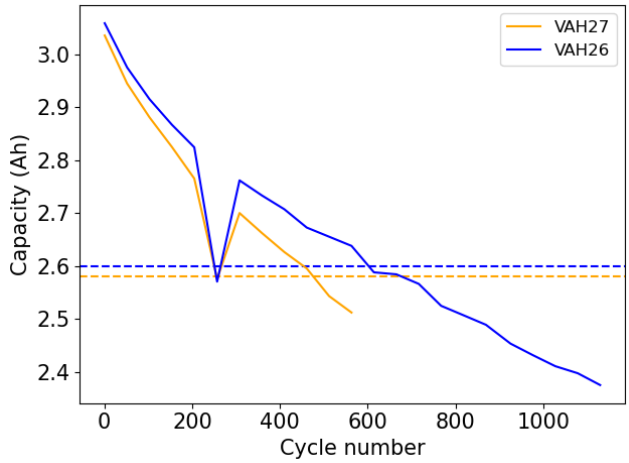

Figure 11: Capacity degradation for VAH26 and VAH27 with EOL-threshold set to 85% of the initial capacity.

Figure 11 shows that both mission profiles exhibit a battery capacity drop at mission/cycle 257. Afterwards, the capacity of the battery decreases steadily, as expected, without large capacity drops. Given these unexpected large capacity drop, we consider this mission as an outlier. Therefore, we do not consider mission 257 in the analysis of both mission profiles. As a result, the EOL mission of VAH26 is adjusted to mission 614, and for mission profile VAH27 to mission 512. The number of missions until the battery has reached its EOL is then adjusted for VAH26 from 6 to 12 missions. For VAH27 the number of missions until the battery has reached its EOL is then adjusted from 6 to 11 missions.

Feature	Unit	Description	Formula
$\Delta^{CC,m,c}$	$[s]$	Duration of CC charging phase of capacity test c of mission m	
$\Delta^{CV,m,c}$	$[s]$	Duration of CV charging phase of capacity test c of mission m	
$\Delta^{rest,m,c}$	$[s]$	Duration of rest phase after charging of capacity test c of mission m	
$\Delta^{phase,m,c}$	$[s]$	Duration of flight phase of capacity test c of mission m	
$V_{max}^{phase,m,c}$	$[V]$	Maximum voltage during flight phase of capacity test c of mission m	
$V_{min}^{phase,m,c}$	$[V]$	Minimum voltage during flight phase of capacity test c of mission m	
$V_{mean}^{phase,m,c}$	$[V]$	Mean voltage during flight phase of capacity test c of mission m	$\frac{1}{t_e - t_s + 1} \sum_{t_s}^{t_e} V_i^{phase,m,c}$, $1 \leq m \leq M, 1 \leq c \leq C^m$
$V_{var}^{phase,m,c}$	$[V]$	Variance voltage during flight phase of capacity test c of mission m	
$Qdis_{max}^{phase,m,c}$	$[Ah]$	Maximum discharge capacity during flight phase of capacity test c of mission m	
$Qdis_{min}^{phase,m,c}$	$[Ah]$	Minimum discharge capacity during flight phase of capacity test c of mission m	
$Qdis_{mean}^{phase,m,c}$	$[Ah]$	Mean discharge capacity during flight phase of capacity test c of mission m	$\frac{1}{t_e - t_s + 1} \sum_{t_s}^{t_e} Qdis_i^{phase,m,c}$, $1 \leq m \leq M, 1 \leq c \leq C^m$
$Qdis_{var}^{phase,m,c}$	$[Ah]$	Variance discharge capacity during flight phase of capacity test c of mission m	
$T_{max}^{phase,m,c}$	$[°C]$	Maximum temperature during flight phase of capacity test c of mission m	

Table 2: Charge-related, discharge-related and temperature-related features considered.

	Missions until EOL	Capacity tests until EOL
VAH01	613	13
VAH02	511	11
VAH05	766	16
VAH10	614	13
VAH11	817	17
VAH12	766	16
VAH13	562	12
VAH15	460	10
VAH16	460	10
VAH17	562	12
VAH20	460	10
VAH22	460	10
VAH23	562	12
VAH24	562	12
VAH25	513	11
VAH26	614	12
VAH27	512	11
VAH28	722	15
VAH30	511	11

Table 3: Mission profiles and their number of missions and capacity tests until EOL is reached, EOL-threshold of 85% of the initial measured battery capacity.

For completeness, Appendix I shows the RUL estimation when an EOL-threshold of 80% of the initially measured battery capacity is considered.

5 Machine learning framework for SOH and RUL prediction

Figure 12 shows the framework considered for estimating the SOH and RUL for eVTOL batteries. We first generate features (see Section 3) based on charge-related, discharge-related, and temperature-related battery measurements. We next select those features with the highest importance for SOH and RUL prediction. With the selected features, we estimate SOH and RUL using the following machine learning (ML) algorithms: support vector regression (SVR), random forest (RF) regression, XGBoost, gaussian process regression (GPR), and multi-layer Perceptron (MLP). The hyperparameters of these algorithms are also tuned using a Bayesian hyperparameter tuning algorithm. The SOH and RUL of the batteries are obtained using a 5-fold cross validation. Below is a short description of the ML algorithms considered.

Support vector regression (SVR)

SVR is a supervised machine learning algorithm based on kernels [36]. The SVR is related to SVM, but SVR is capable to solve regression problems instead of classification problems [25]. SVR is ideal for SOH/RUL estimation because it excels at characterizing nonlinear relationships between inputs and outputs [22]. Besides, the benefit of SVR is that no computationally costly mathematical procedures are required in the formulation [25]. SVR solves nonlinear prediction tasks by converting a low-dimensional problem into a linear problem in a high-dimensional feature space using a nonlinear mapping [13].

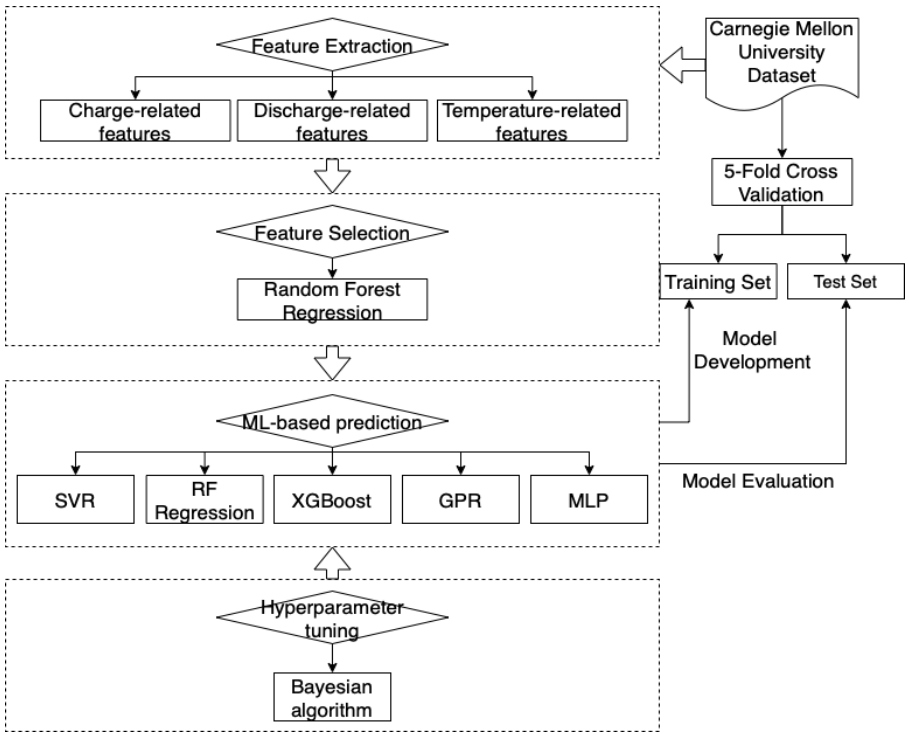

Figure 12: ML framework for battery SOH and RUL prediction.

Random forest (RF) regression

The RF regression is a supervised ensemble machine learning model that combines heterogeneous decision trees [8]. Only a randomly selected portion of the training set is used to construct each forest tree. Besides, it uses averaging to improve the prediction accuracy and control over-fitting [21]. Each tree consists of decision nodes and leaf nodes. The decision nodes asses each fed-in sample with a test function and pass it to different branches based on the features of the sample [21]. After all of the forest trees have been generated, each sample in the test set is classified by combining the predictions of each tree using majority voting.

XGBoost

XGBoost is a gradient-boosted tree used for classification and regression problems. It is based on gradient boosting, however gradient-boosted trees are built continuously which results in slow learning from the data to improve its prediction in succeeding iteration [29]. In contrast, XGBoost builds trees in parallel in a fast way compared to a RF [9]. Hence, the XGBoost model is based on optimized distributed gradient boosting. The XGBoost is designed to improve performance and speed. Besides, the XGBoost controls the model complexity and reduces overfitting with the built-in regularization [29].

Gaussian process regression

GPR is a probabilistic non-parametric kernel model. The Gaussian distribution computes the probability of an input vector with mean and variance as its features [30; 34]. For each time step, the probability of an input time series vector is computed. As a result, rather than having scalar mean and variance, the GPR model produces a mean and covariance vector [34]. GPR is based on a kernel that predicts the output by incorporating prior knowledge and obtaining a hypothesis of posterior probability via a Bayesian framework. As GPR is constructed on a Bayesian framework, its predicted output can be interpreted in a probability-based fashion, demonstrating the result's reliability [10]. Besides, GPR has the advantages of hyper-parameter adaptive acquisition, reasonably simple implementation, and use without loss of performance when compared to neural networks and SVM [43].

Multi-layer Perceptron (MLP) regressor

MLP is a feed-forward neural network with multiple layers and adaptive weights [14]. All hidden layers include batch normalization to improve the neural network's stability. Figure 13 shows a general representation of a MLP regressor with three hidden layers. In Figure 13, it can be seen that the input layer consists of a set of neurons, which represent the number of features in the dataset. Each neuron in the hidden layer transforms the values of the previous layer with a weighted linear summation and is followed by an activation function. Finally, the output layer collects the value of the last output layer and transforms it into output values.

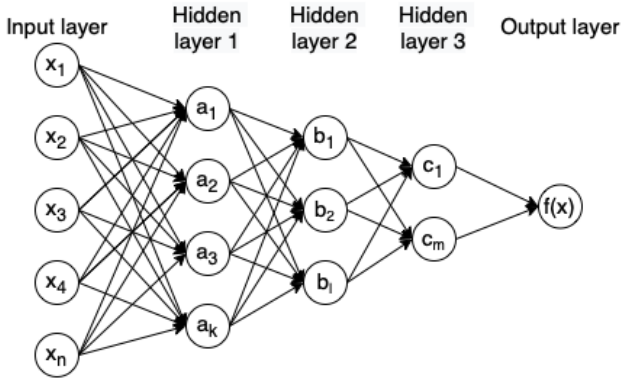

Figure 13: MLP regressor with three hidden layers.

Data normalisation

For SVR, GPR, and MLP, the values of the features considered in Section 3 are normalized as follows:

$$y = \frac{x - \mu}{\sigma}, \tag{5}$$

with μ the mean of the feature, and σ the standard deviation of the feature.

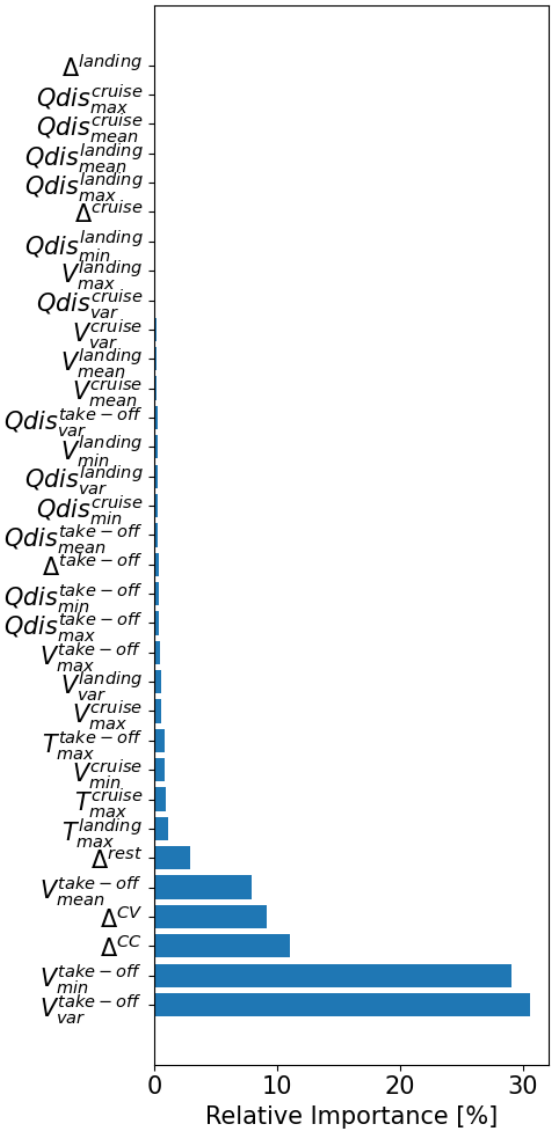

Figure 14: Feature importance - SOH estimation.

6 Predicting battery SOH

6.1 Feature selection and importance quantification

In Section 3, a total of 33 features have been considered. From these 33 features, we select for SOH prediction only the features with high importance. The importance of the features is obtained using a random forest regression model.

Figure 14 shows the the importance of the 33 features considered. We select the top 65% of these 33 features with the highest importance, i.e., we select the following 21 features:

Selected charge-related features: duration of CC charging phase ($\Delta^{CC,m,c}$), duration of CV charging phase ($\Delta^{CV,m,c}$), duration of the Rest period ($\Delta^{rest,m,c}$);

Selected discharge-related features: variance of the voltage during take-off and landing ($V^{phase,m,c}_{var}$), mean voltage during take-off ($V^{phase,m,c}_{mean}$); minimum voltage during take-off, cruise, and landing ($V^{phase,m,c}_{min}$); maximum voltage during take-off, and cruise ($V^{phase,m,c}_{max}$); minimum discharge capacity during take-off, and cruise ($Qdis^{phase,m,c}_{min}$); maximum discharge capacity during take-off ($Qdis^{phase,m,c}_{max}$), variance discharge capacity during take-off, and landing ($Qdis^{phase,m,c}_{var}$); mean discharge capacity during take-off ($Qdis^{phase,m,c}_{mean}$), duration of take-off ($\Delta^{phase,m,c}$);

Selected temperature-related features: maximum temperature during take-off, cruise and landing ($T^{phase,m,c}_{max}$).

Figure 14 shows that the variance of the voltage during take-off has the highest importance, followed by the minimum voltage during take-off, and the dura-

tion of the CC charging phase. The results show that the features related to take-off have a high importance, This can be explained by the fact that the battery experiences a high discharge voltage during take-off. During high discharge voltages, the internal resistance increases, which impacts the SOH [16]. Also, the duration of the CC charging phase has a high importance for the prediction of the SOH. As the battery performs more missions, the SOH decreases while the duration of the CC charging phase increases (see Figure 10(a)).

6.2 5-fold cross-validation

We estimate the battery SOH using 5-fold cross validation. The folds are generated using group K-fold [26] such that each fold contains a unique set of mission profiles used for testing. In each fold, the number of mission profiles selected for testing is approximately the same (3-4 mission profiles per fold). Also, the number of capacity tests of these selected 3-4 mission profiles is approximately the same (75 capacity tests used for testing). In other words, having a total of 19 mission profiles (see Section 2) with a total of 380 capacity tests, we aim to allocate mission profiles to folds such that each of the 5 folds contains approximately 380/5 capacity tests used for testing. Each mission profile is allocated only once to a fold. Hence, we obtained the following 5 folds:

- Fold 1: the test dataset consists of mission profiles VAH12, VAH22, and VAH24 (with a total of 74 capacity tests). The remaining 16 mission profiles (with a total of 306 capacity tests) are the training dataset.
- Fold 2: the test dataset consists of mission profiles VAH11, VAH27, and VAH30 (with a total of 74 capacity tests). The remaining 16 mission profiles (with a total of 306 capacity tests) are the training dataset.
- Fold 3: the test dataset consists of mission profiles VAH02, VAH05, VAH13 and VAH15 (with a total of 75 capacity tests). The remaining 15 mission profiles (with a total of 305 capacity tests) are the training dataset.
- Fold 4: the test dataset consists of mission profiles VAH10, VAH17, VAH20 and VAH23 (with a total of 84 capacity tests). The remaining 15 mission profiles (with a total of 296 capacity tests) are the training dataset.
- Fold 5: the test dataset consists of mission profiles VAH01, VAH16, VAH26 and VAH28 (with a total of 73 capacity tests). The remaining 15 mission profiles (with a total of 307 capacity tests) are the training dataset.

6.3 Hyperparameter tuning

Table 4 shows the optimal hyperparameters obtained for each of the five ML algorithms considered. We performed hyperparameter tuning based on Bayesian optimisation algorithm [13] using the Hyperopt library of Python [4]. For hyperparameter tuning, we used Fold 5 (see Section 6.2).

	Hyperparameters
SVR	$Kernel = Linear$ $Tolerance = 0.186$
RF Regression	$Trees = 797$ $MaxDepth = 30$ $MinSampleLeaf = 2$ $MinSampleSplit = 4$
XGBoost	$Trees = 3100$ $MaxDepth = 19$ $LearningRate = 0.25$ $Subsample = 0.80$
GPR	$Alpha = 0.069$ $Kernel = Dotproduct + Whitekernel$
MLP	$BatchSize = 96$ $Neurons 1^{st} Layer = 90$ $Neurons 2^{nd} Layer = 90$ $Neurons 3^{rd} Layer = 40$

Table 4: Optimized hyperparameters - SOH.

6.4 Performance metrics

For every mission profile used for testing, we predict the SOH at each capacity test. The performance of our SOH predictions is evaluated using the Mean Absolute Error (MAE), Root Mean Squared Error (RMSE), and the Mean Absolute Percentage Error (MAPE). These performance metrics are defined, for the estimated SOH of a battery under mission profile $m, 1 \leq m \leq M$, as follows:

$$MAE^m_{SOH} = \frac{1}{C^m} \sum_{i=1}^{C^m} \left| SOH^{m,i} - \hat{SOH}^{m,i} \right|,$$

$$RMSE^m_{SOH} = \sqrt{\frac{1}{C^m} \sum_{i=1}^{C^m} \left(\hat{SOH}^{m,i} - SOH^{m,i} \right)^2}$$

$$MAPE^m_{SOH} = \frac{1}{C^m} \sum_{i=1}^{C^m} \frac{\left| SOH^{m,i} - \hat{SOH}^{m,i} \right|}{SOH^{m,i}} \cdot 100\%,$$

where $SOH^{m,i}$ is the true battery SOH at capacity test i of mission profile m, $\hat{SOH}^{m,i}$ is the predicted SOH at capacity test i of mission profile $m, 1 \leq m \leq M$.

The overall performance of our SOH predictions across all M mission profiles is evaluated using:

$$MAE_{SOH} = \frac{1}{M} \sum_{j=1}^{M} MAE^j_{SOH}$$

$$RMSE_{SOH} = \frac{1}{M} \sum_{j=1}^{M} RMSE^j_{SOH}$$

$$MAPE_{SOH} = \frac{1}{M} \sum_{j=1}^{M} MAPE^j_{SOH}$$

6.5 Results - SOH prediction

Table 5 shows the MAE, RMSE, and MAPE obtained across all mission profiles for SOH estimation. The results show that the lowest SOH estimation errors are obtained using RF regression, this was also concluded by [11].

	MAE	RMSE	MAPE
SVR	1.48	2.20	0.02
RF Regression	**1.33**	**1.80**	**0.02**
XGBoost	1.39	1.91	0.02
GPR	1.48	2.27	0.79
MLP	2.75	7.49	0.03

Table 5: Results - predicting the SOH [%].

Table 6 shows the MAE, RMSE, and MAPE obtained for SOH prediction for each mission profile. The last row of Table 6 gives the average of these metrics. The results show that the lowest estimation errors are obtained when using RF regression. Moreover, the SOH estimation errors obtained for the baseline mission profiles are below the average MAE, RMSE and MAPE. The lowest prediction errors are obtained for mission profiles VAH02, VAH10, VAH12, VAH13, VAH15, VAH16, VAH26 and VAH28, when considering RF regression.

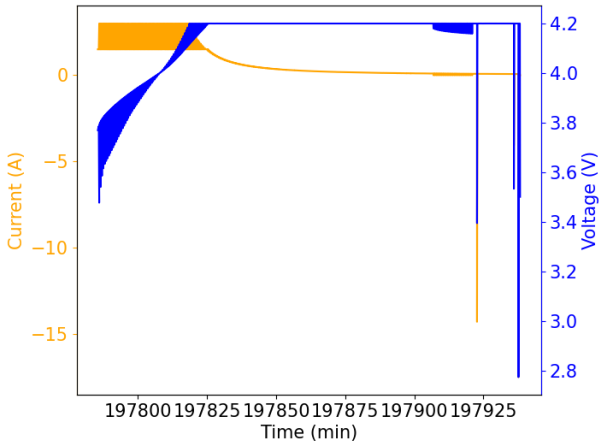

Figure 15: Second last capacity test - VAH05.

The highest prediction errors are obtained for VAH05, regardless of the ML algorithms (see Table 6). For the second last capacity test of VAH05, the RF regression predicts a SOH of 88.98%, whereas the true SOH is 76.29%. For the last capacity test of VAH05, the RF regression predicts the SOH to be 72.63%, while the true SOH is 56.21%. The high SOH prediction errors for VAH05 for the second last capacity can be explained by analyzing the current and voltage during that specific second last capacity test (see Figure 20(c)). Figure 15 shows the second second last capacity test of VAH05. In Figure 15 it can be seen that the current oscillates during the CC phase. Also, the current during the discharge phases does not follow the pattern of standard capacity tests (see Figure 3). In fact, during discharge the voltage exhibits 4 peaks. Besides, the current is often close to zero.

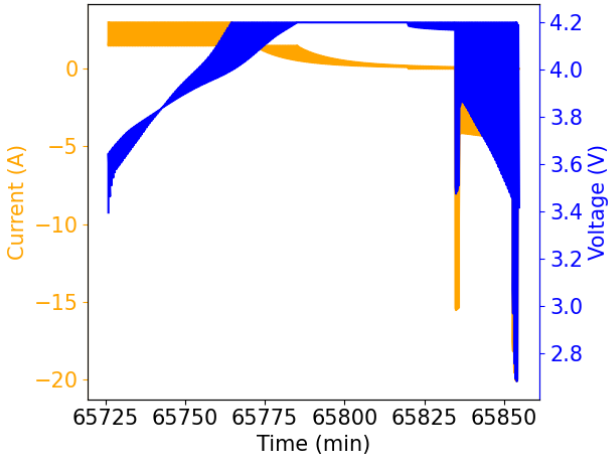

Figure 16: Second last capacity test - VAH22.

The second-highest value of the RMSE, when using RF regression, is achieved for mission profile VAH22 (see Table 6). Figure 20(l) shows that during the second last capacity test of VAH22, the current does not follow the pattern of a standard capacity test. During the second last capacity test of VAH22, the SOH is estimated to be 89.79%, while the true SOH is 82.64%. The SOH for the last capacity test is estimated to be 80.21% , while the true SOH is 69.53%. This could be explained by the fact that the current and voltage oscillate during the charging, take-off, cruise and landing of the second capacity test of VAH22 (see Figure 16).

7 Predicting battery RUL

7.1 Feature selection and feature importance quantification

In Section 3, 33 features have been generated. In this section we quantify the importance of the features using a RF regression model.

Figure 17 shows the importance of all the 33 features considered. For RUL prediction, of these 33 features we select the top 65% (21 features) with the highest importance. The following 21 features are selected:

Selected charge-related features: duration of CC charging phase ($\Delta^{CC,m,c}$), duration of CV charging phase ($\Delta^{CV,m,c}$), duration of the Rest period ($\Delta^{rest,m,c}$)

Selected discharge-related features: variance voltage during take-off and landing ($V_{var}^{phase,m,c}$); mean voltage during take-off, cruise and landing ($V_{mean}^{phase,m,c}$); minimum voltage during take-off ($V_{min}^{phase,m,c}$); maximum discharge capacity during take-off, cruise and landing ($Qdis_{max}^{phase,m,c}$); mean discharge capacity during take-off ($Qdis_{mean}^{phase,m,c}$); variance discharge capacity during cruise and landing ($Qdis_{var}^{phase,m,c}$); minimum discharge

	SVR			**RF Regression**			XGBoost			GPR			MLP		
	MAE	RMSE	MAPE	MAE	RMSE	MAPE	MAE	RMSE	MAPE	MAE	RMSE	MAPE	MAE	RMSE	MAPE
VAH01	1.09	1.47	0.01	1.29	1.51	0.01	1.2	1.53	0.01	1.18	1.57	0.01	2.14	2.3	0.02
VAH02	0.89	1.07	0.01	0.85	1.01	0.01	2.13	2.64	0.02	0.61	0.85	0.01	1.91	2.2	0.02
VAH05	2.82	7.62	0.04	1.82	3.88	0.03	2.02	3.85	0.03	3.04	9.74	0.04	18.36	94.69	0.24
VAH10	0.55	0.71	0.01	0.87	1.01	0.01	0.86	1.04	0.01	0.65	0.87	0.01	2.08	2.44	0.03
VAH11	1.79	1.91	0.02	1.51	1.7	0.02	1.92	2.41	0.02	1.33	1.49	0.02	1.47	1.69	0.02
VAH12	2.78	2.99	0.04	0.65	0.84	0.01	0.91	1.16	0.01	3.52	3.73	0.04	1.71	1.9	0.02
VAH13	0.87	1.13	0.01	0.58	0.71	0.01	0.84	1.07	0.01	0.89	1.09	0.01	1.12	1.55	0.01
VAH15	1.0	1.2	0.01	0.31	0.46	0.0	0.72	1.03	0.01	0.79	0.98	0.01	1.75	2.03	0.02
VAH16	0.66	1.13	0.01	1.26	1.45	0.01	0.82	0.97	0.01	0.65	1.05	0.01	0.7	1.03	0.01
VAH17	1.24	1.4	0.01	0.46	0.63	0.01	1.08	1.4	0.01	0.89	1.07	0.01	0.56	0.86	0.01
VAH20	1.13	1.44	0.01	1.85	2.34	0.02	1.17	1.53	0.01	0.92	1.25	0.01	0.78	1.19	0.01
VAH22	2.54	5.52	0.03	1.79	3.74	0.02	1.95	4.19	0.03	2.02	4.72	0.02	5.21	12.92	0.07
VAH23	2.11	2.72	0.02	2.95	3.74	0.03	2.45	3.19	0.03	2.31	2.69	0.03	7.27	7.62	0.08
VAH24	3.9	4.0	0.04	1.55	2.08	0.02	2.55	2.71	0.03	4.28	4.39	0.05	1.19	1.48	0.01
VAH25	0.94	1.62	0.01	2.0	2.71	0.02	1.85	2.46	0.02	0.86	1.44	0.01	2.06	2.76	0.02
VAH26	1.32	2.14	0.02	1.17	1.64	0.01	0.8	1.31	0.01	1.5	2.35	0.02	1.34	2.11	0.02
VAH27	1.33	1.84	0.01	1.03	1.32	0.01	1.05	1.39	0.01	1.46	1.9	0.02	1.21	1.64	0.01
VAH28	0.63	1.07	0.01	0.89	1.1	0.01	0.69	0.86	0.01	0.61	1.14	0.01	0.57	0.86	0.01
VAH30	0.56	0.8	0.01	2.36	2.43	0.03	1.36	1.58	0.02	0.63	0.82	0.01	0.89	1.04	0.01
Average	1.48	2.20	0.02	1.33	1.80	0.02	1.39	1.91	0.02	1.48	2.27	0.02	2.75	7.49	0.03

Table 6: Error metrics SOH [%]

capacity during take-off and cruise ($Qdis_{min}^{phase,m,c}$); duration of take-off ($\Delta^{phase,m,c}$).

Selected temperature-related features: maximum temperature during take-off, cruise and landing ($T_{max}^{phase,m,c}$).

Figure 17 shows that the mean and the variance of the voltage during take-off are the most important features. This is expected since the take-off is performed at a high C-rate, which leads to a high internal impedance during take-off. In turn, a higher internal impedance is expected to affect the battery lifetime.

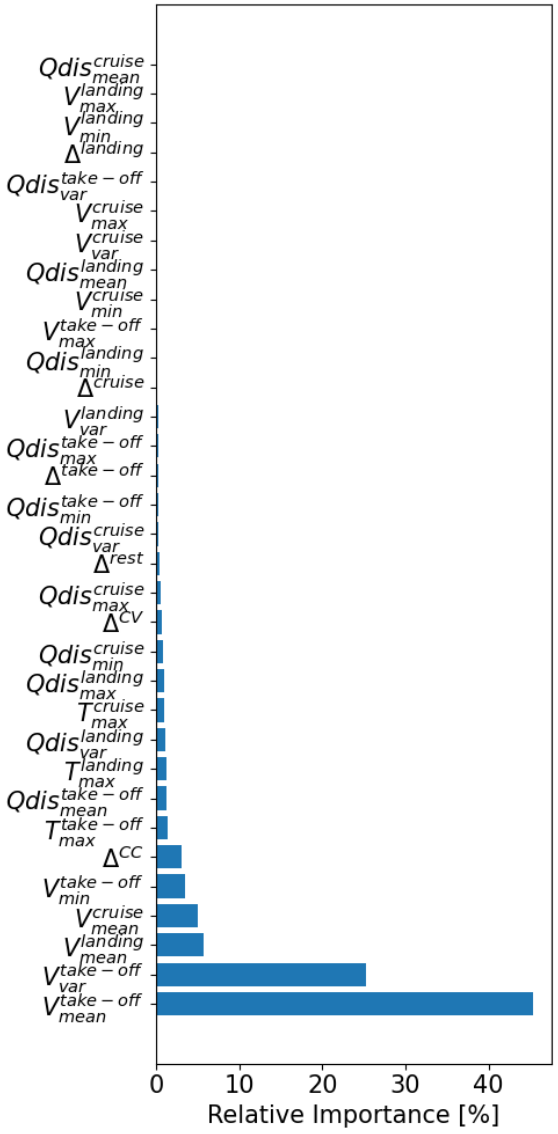

Figure 17: Feature importance - RUL estimation.

7.2 5-fold cross-validation

We estimate the battery RUL using 5-fold cross validation. Compared with the estimation of SOH, where we consider a total of 380 capacity tests, for RUL estimation, we consider only a total of 215 capacity tests. This is because we set an EOL of 85% of the initially measured battery capacity. Also, two outliers (capacity tests) have been removed for mission profiles VAH26 and VAH27, as discussed in Section 4.

The 5 folds are generated using group K-fold [26] such that each fold contains a unique set of mission profiles used for testing. In each fold, the number of mission profiles selected for testing is approximately the same (4 mission profiles per fold). Also, the number of capacity tests of these selected 4 mission profiles is approximately the same (45 capacity tests used for testing). In other words, having a total of 19 mission profiles (see Section 2) with a total of 215 capacity tests, we aim to allocate mission profiles to folds such that each of the 5 folds contains approximately 215/5 capacity tests used for testing. Each mission profile is allocated only once to a fold. Hence, we obtained the following 5 folds:

- Fold 1: the test data consists of the mission profiles VAH11, VAH16, VAH20, and VAH24 (with a total of 45 capacity tests). The remaining 15 mission profiles (with a total of 170 capacity tests) are the training dataset.
- Fold 2: the test data consists of mission profiles VAH05, VAH15, VAH17, and VAH26 (with a total of 45 capacity tests). The remaining 15 mission profiles (with a total of 170 capacity tests) are the training dataset.
- Fold 3: the test data consists of mission profiles VAH02, VAH12, VAH23, and VAH27 (with a total of 45 capacity tests). The remaining 15 mission profiles (with a total of 170 capacity tests) are the training dataset.
- Fold 4: the test data consists of mission profiles VAH10, VAH28, and VAH30 (with a total of 36 capacity tests). The remaining 16 mission profiles (with a total of 179 capacity tests) are the training dataset.
- Fold 5: the test data consists of mission profiles VAH01, VAH13, VAH22, and VAH25 (with a total of 44 capacity tests). The remaining 15 mission profiles (with a total of 171 capacity tests) are the training dataset.

7.3 Hyperparameter tuning

Table 7 shows the optimal hyperparameters obtained for each ML model. The hyperparameter tuning is based on the Hyperopt Bayesian algorithm [4]. For the hyperparameter tuning Fold 5 is used (see section 7.2).

	Hyperparameters
SVR	$Kernel = linear$ $Tolerance = 88.75$
RF Regression	$Trees = 1951$ $MaxDepth = 104$ $MinSampleLeaf = 3$ $MinSampleSplit = 2$
XGBoost	$Trees = 5100$ $MaxDepth = 29$ $LearningRate = 0.25$ $Subsample = 0.91$
GPR	$Alpha = 1.0$ $Kernel = RationalQuadratic$
MLP	$BatchSize = 64$ $Neurons1^{st}Layer = 40$ $Neurons2^{nd}Layer = 10$ $Neurons3^{rd}Layer = 30$

Table 7: Optimized hyperparameters - RUL.

7.4 Performance metrics

For every mission profile used for testing, we predict the RUL at each capacity test. The performance of the RUL predictions is evaluated using the Mean Absolute Error (MAE), Root Mean Squared Error (RMSE), and the Mean Absolute Percentage Error (MAPE). These performance metrics are defined, for the estimated RUL of a battery under mission profile $m, 1 \leq m \leq M$, as follows:

$$MAE^m_{RUL} = \frac{1}{C^m} \sum_{i=1}^{C^m} \left| RUL^{m,i} - \hat{RUL}^{m,i} \right|,$$

$$RMSE^m_{RUL} = \sqrt{\frac{1}{C^m} \sum_{i=1}^{C^m} \left(\hat{RUL}^{m,i} - RUL^{m,i} \right)^2}$$

$$MAPE^m_{RUL} = \frac{1}{C^m} \sum_{i=1}^{C^m} \frac{\left| RUL^{m,i} - \hat{RUL}^{m,i} \right|}{RUL^{m,i}} \cdot 100\%,$$

where $RUL^{m,i}$ is the true battery RUL at capacity test i of mission profile m, $\hat{RUL}^{m,i}$ is the predicted RUL at capacity test c of mission profile $m, 1 \leq m \leq M$.

The overall performance of our RUL predictions across all M mission profiles is evaluated using:

$$MAE_{RUL} = \frac{1}{M} \sum_{j=1}^{M} MAE^j_{RUL}$$

$$RMSE_{RUL} = \frac{1}{M} \sum_{j=1}^{M} RMSE^j_{RUL}$$

$$MAPE_{RUL} = \frac{1}{M} \sum_{j=1}^{M} MAPE^j_{RUL}$$

7.5 Results - RUL prediction

Table 8 shows the MAE, RMSE, and MAPE obtained when considering all 19 mission profiles. From all

five considered machine learning algorithms, XGBoost leads to the lowest RUL estimation errors.

	MAE	RMSE	MAPE
SVR	66.48	79.03	0.38
RF Regression	63.25	75.81	0.39
XGBoost	**54.53**	**67.92**	**0.39**
GPR	59.37	72.86	0.27
MLP	75.45	87.97	0.44

Table 8: Results - RUL prediction [#missions].

Table 9 shows the MAE, RMSE, and MAPE obtained for RUL estimation when considering all 19 mission profiles. In the last row, each model's average MAE, RMSE, and MAPE is given.

The results show that the lowest RUL estimation errors (MAE, RMSE) are obtained when considering XGBoost, and mission profiles with an increase in cruise duration (VAH02, VAH15, VAH22) and 50% increase of CC charging current (VAH16 and VAH20).

Table 9 also shows that the highest RUL predictions errors are obtained for mission profile VAH11. Mission profile VAH11 has the largest power reduction (20%) during take-off, cruise, and landing.

XGBoost leads to the lowest RUL estimation errors. Compared with the results obtained for SOH estimation, RUL prediction errors are significantly lower for mission profiles VAH05 and VAH22. This is because the EOL (85% of initially measured capacity) of the batteries used for VAH05 and VAH22 is reached before the non-standard capacity tests of VAH05 and VAH22 (see Figures 20(c) and 20(l)).

For mission profile VAH25, XGBoost leads to RUL estimation errors above average. This can be explained by the non-standard capacity test in VAH25. In 20(o), it can be seen that during the second last capacity test there is a non-standard capacity test. In Figure 18, the second last capacity test of VAH25 is plotted with the voltage.

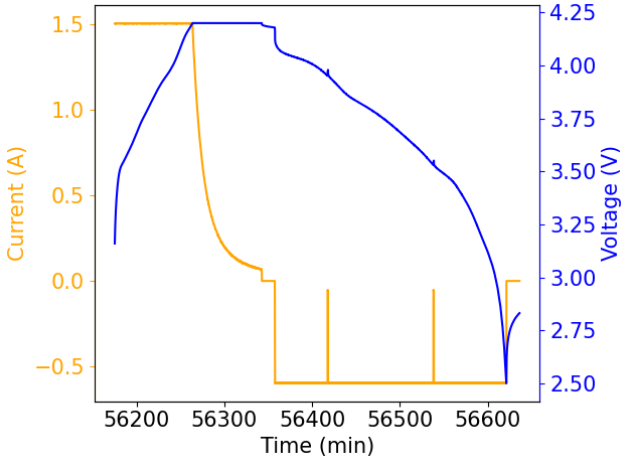

Figure 18: Second last capacity test - VAH25.

From Figure 18, it can be seen that the capacity test follows a different pattern than the standard capacity test (see Figure 3). The CC charging current is lower, and the discharge phases are not clearly distinguishable. This is known by [Bills et al.] because during the second to last capacity test two capacity tests are being performed one after the other and reported as one capacity test in the dataset. For this second last capacity test, the RUL is estimated to be 434 missions, while the true RUL is 52 missions. This large error for this capacity test increases significantly the overall error for this mission profile.

XGBoost also leads to large RUL estimation errors for mission profile VAH28. VAH28 has a 10% power reduction during take-off, cruise, and landing, compared with the baseline mission profiles. These results can be explained by the fact that the 6^{th} capacity test of this mission profile exhibits abnormal trends (see Figure 20(r)). In Figure 19, the current and voltage during the 6^{th} capacity test can be seen.

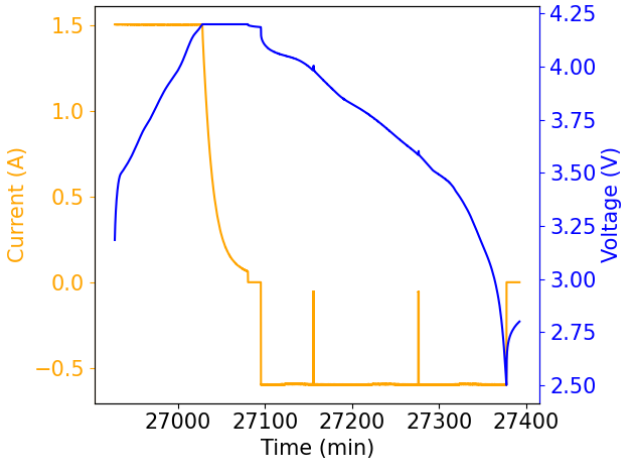

Figure 19: Second last capacity test - VAH28.

In Figure 19, it can be seen that the CC charging current is lower compared to the standard capacity test (see Figure 3). Besides, the current and voltage during the discharge phases do not follow the pattern of the standard capacity test (see Figure 3). During the discharge phase the take-off, cruise, and landing cannot be clearly distinguished. For this 6^{th} capacity test, RUL is estimated as 148 missions, while the true RUL is 466 missions. Also here, these large errors obtained for an early capacity test increase the overall RUL estimation errors for this mission.

8 Impact of eVTOL mission characteristics on the estimation of SOH and RUL

One of the mission characteristics that is varied across mission profiles is the duration of the cruise phase. Mission profiles VAH02, VAH15, and VAH22 have a cruise phase extended by 25% compared to the base-

	SVR			RF Regression			**XGBoost**			GPR			MLP		
	MAE	RMSE	MAPE	MAE	RMSE	MAPE	MAE	RMSE	MAPE	MAE	RMSE	MAPE	MAE	RMSE	MAPE
VAH01	99.21	104.42	0.53	105.72	117.74	0.34	62.64	75.85	0.28	70.28	80.3	0.32	69.91	85.41	0.42
VAH02	37.21	48.7	0.32	53.49	67.41	0.24	52.72	57.54	0.22	23.26	30.66	0.1	80.52	87.69	0.33
VAH05	75.78	91.53	0.32	34.48	45.09	0.15	35.99	47.14	0.12	24.38	34.42	0.14	121.01	129.48	0.63
VAH10	29.19	34.14	0.2	30.16	34.62	0.22	36.43	43.5	0.15	82.54	96.59	0.27	47.57	52.29	0.2
VAH11	139.37	173.13	0.96	163.78	187.94	0.98	199.58	224.73	1.1	145.87	173.34	0.71	367.18	383.3	1.93
VAH12	114.59	138.36	0.29	102.78	114.45	0.31	97.43	109.16	0.28	133.43	155.36	0.32	38.82	44.07	0.14
VAH13	52.43	61.41	0.19	20.87	25.01	0.1	24.91	28.7	0.11	16.94	18.96	0.07	27.3	32.41	0.14
VAH15	12.17	15.9	0.1	22.02	25.92	0.18	18.15	23.79	0.14	14.13	18.55	0.12	13.87	19.83	0.14
VAH16	67.75	70.88	0.41	50.78	55.66	0.32	30.77	34.77	0.21	73.73	75.08	0.43	74.94	89.47	0.34
VAH17	40.64	49.44	0.25	36.31	40.37	0.18	26.18	31.57	0.19	22.81	31.52	0.21	43.31	48.81	0.31
VAH20	59.21	61.67	0.41	41.84	46.07	0.31	19.63	27.21	0.18	63.19	63.93	0.39	66.32	78.78	0.25
VAH22	10.37	12.5	0.06	28.92	32.25	0.17	8.76	14.41	0.07	12.54	15.86	0.11	7.12	9.28	0.07
VAH23	133.27	169.15	0.38	126.67	149.08	0.94	115.34	131.3	0.67	124.96	154.4	0.41	129.93	145.97	0.85
VAH24	40.19	43.46	0.23	62.81	79.2	0.54	45.09	56.82	0.37	72.57	94.38	0.29	87.77	106.45	0.74
VAH25	69.66	112.77	0.82	73.85	161.69	1.09	65.27	126.31	0.88	29.14	44.76	0.33	72.94	114.6	0.74
VAH26	58.81	70.97	0.4	28.62	31.21	0.18	31.7	35.01	0.17	36.94	41.49	0.23	60.3	65.11	0.27
VAH27	55.31	59.54	0.38	13.3	17.67	0.09	14.91	19.19	0.06	36.07	41.73	0.14	30.45	34.06	0.13
VAH28	66.99	80.77	0.34	53.92	57.31	0.2	49.74	91.25	0.17	75.56	128.24	0.25	68.73	111.97	0.47
VAH30	100.98	102.77	0.66	151.42	151.74	0.9	100.76	112.24	0.75	69.77	84.71	0.32	25.63	32.51	0.19
Average	66.48	79.03	0.38	63.25	75.81	0.39	54.53	67.92	0.32	59.37	72.86	0.27	75.45	87.97	0.44

Table 9: Error metrics RUL [#missions], with EOL-threshold 85%

line mission profiles. Mission profiles VAH12, VAH13, and VAH26 have a decreased cruise duration with 50%, 25% and 25% respectively, compared with the baseline mission profiles.

When estimating SOH using RF regression, the estimation errors (MAE, RMSE, MAPE) for these mission profiles are bellow the average estimation errors (see Table 6). The exception is mission profile VAH22, where the second to last capacity test exhibits unexpected patterns in the voltage and the current of the charging and discharging phases (see also Figure 16). In this case study, thus, after increasing or decreasing the duration of the cruise phase, the SOH is still well estimated.

The importance of the duration of the cruise phase for SOH estimation was ranked as low in Section 6.1. This does not mean that the characteristics of the cruise phase are of no importance for SOH estimation. In fact, the following features related to the cruise phase have been ranked as of high importance (in decreasing order of importance): maximum temperature during cruise, minimum voltage during cruise, maximum voltage during cruise, and minimum discharge capacity during cruise. The results show that the maximum temperature during cruise is of high importance for SOH estimation. This is also in accordance to existing literature [19; 23] where the battery temperature is shown to be highly correlated with the SOH of the battery.

Similarly, when considering the RUL estimation using XGBoost, the RUL estimation errors for mission profiles VAH02, VAH15, VAH22 are below the average errors. Also in this case, the feature Duration of the cruise phase, Δ^{cruise}, is shown to have a low importance for RUL estimation (see Section 7.1). Nonetheless, several features related to cruise phase have been shown to have a high importance for RUL prediction. In decreasing order of importance, the following features have been selected for RUL estimation: mean voltage during cruise, maximum discharge capacity during cruise, variance discharge capacity during cruise, minimum discharge capacity during cruise, and maximum temperature during cruise.

Another mission characteristic that has been varied across several mission profiles is the CC charging current. Mission profiles VAH16 and VAH20 have a 50% increase of the CC charging current, while VAH24 has a 50% reduction of the CC charging current when compared to baseline mission profiles. For both VAH16, VAH20 and VAH24, the RUL estimation errors are below the average estimation errors. The change in the CC charging current is directly reflected in the change in the duration of the CC charging phase, i.e., an increase in the CC charging current leads to a decrease of the duration of the CC charging phase and vice versa. The importance of the CC charging current for RUL estimation is reflected by the fact that the Duration of the CC charging phase Δ^{CC} is shown to have a high importance for RUL estimation (see Section 7.1). This is also in accordance to existing literature [18] where the CC charging duration is related to the battery's degradation. As the battery's capacity decreases gradually, it takes less time to fully charge the battery [42].

Battery discharge power is another mission characteristic that is varied across mission profiles. Mission profiles VAH05 and VAH28 have a 10% power reduction during the discharge phase, i.e., during take-off, cruise and landing. Mission profile VAH11 has a 20% power reduction during discharge.

Using XGBoost, the RUL estimation errors obtained for VAH05 and VAH28 are below the average estimation errors (MAE). However, when reducing the discharge power to 20%, the RUL estimation errors for VAH11 are the highest. The importance of the discharge power for RUL estimation is reflected in the fact that multiple voltage-related features of shown to be of high importance for RUL estimation: mean, variance and minimum voltage during take-off. Indeed, the take-off is a critical phase of a flight when the battery voltage exhibits a peak.

9 Conclusions

In this paper a data-driven machine learning framework is proposed to predict the state of health and remaining useful lifetime of eVTOL batteries. We consider a dataset of eVTOL battery that are used to perform realistic eVTOL flights. The flights are performed under varying conditions: temperature, cruise duration, discharge power, CC charging current and CV charging voltage, The take-off and landing are performed at high C-rates (5 C-rate) compared to the cruise phase (1.48 C-rate).

A total of 33 features have been generated based on charge-related, discharge-related, and temperature-related parameters. The importance of these features for SOH and RUL estimation has been quantified. The results show that the features with the highest importance for SOH are the voltage recorded during take-off and the duration of the CC-CV charging phase. For RUL estimation, the voltage during take-off, landing and cruise are of highest importance.

We consider five machine learning algorithms for SOH and RUL prognostics: SVR, RF regression, XGBoost, GPR, and MLP. The lowest SOH estimation errors are obtained using a RF regression (MAE= 1.33%, RMSE= 1.80%). XGBoost leads to the lowest RUL estimation errors (MAE= 54.33 missions, RMSE= 54.53 missions). The results also show that when varying the cruise duration with up to a 25% increase, the SOH and RUL are well estimated by RF regression and XGBoost, respectively.

As future work we plan to extend this framework by extending the range of features considered. We are also interested in further analyzing the features with the highest importance for SOH and RUL and their impact on the degradation of the eVTOL battery capacities.

References

[1] Acubed (2019). Our story: Part 4. `https://acubed.airbus.com/blog/vahana/our-story-part-4/` (accessed: 11.03.2022).

[2] Airbus (2019). Vahana our single-set evtol demonstrator. `https://www.airbus.com/en/urbanairmobility/vahana` (accessed: 10.05.2022).

[3] Attia, P., Grover, A., and Jin, N. e. a. (2020). Closed-loop optimization of fast-charging protocols for batteries with machine learning. *Nature*, 578:397–402.

[4] Bergstra, J., Yamins, D., and Cox, D. D. (2013). Making a science of model search: Hyperparameter optimization in hundreds of dimensions for vision architectures. In *Proceedings of the 30th International Conference on International Conference on Machine Learning - Volume 28*, ICML'13, page I–115–I–123. JMLR.org.

[5] Bills, A., Sripad, S., Fredericks, W. L., Guttenberg, M., Charles, D., Frank, E., and Viswanathan, V. (2021). Universal battery performance and degradation model for electric aircraft. *ChemRxiv*, this content is a preprint and has not been peer-reviewed.

[Bills et al.] Bills, A., Viswanathan, V., Sripad, S., Frank, E., Charles, D., and Fredericks, W. L. evtol battery dataset. `https://kilthub.cmu.edu/articles/dataset/eVTOL_Battery_Dataset/14226830?file=26855063`, (accessed: 29.04.2022).

[7] Bole, B., Kulkarni, C., and Daigle, M. (2014). Adaptation of an electrochemistry-based li-ion battery model to account for deterioration observed under randomized use. *Annual Conference of the Prognostics and Health Management Society*.

[8] Breiman, L. (2001). Random forests. *Machine Learning*, 45:5–32.

[9] Chen, T. and Guestrin, C. (2016). Xgboost: A scalable tree boosting system. *22nd SIGKDD Conference on Knowledge Discovery and Data Mining*.

[10] Chen, T., Morris, J., and Martin, E. (2007). Gaussian process regression for multivariate spectroscopic calibration. *Chemometrics and Intelligent Laboratory Systems*, 87:59–71.

[11] Chen, Z., Sun, M., Shu, X., Shen, J., and Xiao, R. (2018). On-board state of health estimation for lithium-ion batteries based on random forest. *IEEE International Conference on Industrial Technology (ICIT)*, pages 1754–1759.

[12] dos Reis, G., Strange, C., Yadav, M., and Li, S. (2021). Lithium-ion battery data and where to find it. *Energy and AI*, 5.

[13] Fei, Z., Yang, F., Tsui, K.-L., Li, L., and Zhang, Z. (2021). Early prediction of battery lifetime via a machine learning based framework. *Elsevier*, 225:article 120205.

[14] Hinton, G. E. (1990). Connectionist learning procedures. *Machine Learning*, III:555–610.

[15] Hu, X., Jiang, J., Cao, D., and Egardt, B. (2016). Battery health prognosis for electric vehicles using sample entropy and sparse bayesian predictive modeling. *IEEE Transactions on Industrial Electronics*, 63(4):2645–2656.

[16] Huang, S.-C., Tseng, K.-H., Liang, J.-W., Chang, C.-L., and Pecht, M. G. (2017). An online soc and soh estimation model for lithium-ion batteries. *Energies*, 10(4):512–512.

[17] Javier Alba-Maestre, Koen Prud'homme van Reine, T. S. and Castro, S. G. P. (2021). Preliminary propulsion and power system design of a tandem-wing long-range evtol aircraft. 11(23):11083–11083.

[18] Keil, P. and Jossen, A. (2016). Charging protocols for lithium-ion batteries and their impact on cycle life—an experimental study with different 18650 high-power cells. *Journal of Energy Storage*, 6:125–141.

[19] Leng, F., Tan, C. M., and Pecht, M. (2015). Effect of temperature on the aging rate of li ion battery operating above room temperature. *Scientific Reports*, 5(12967).

[20] Li, Y., Liu, K., M.Foley, A., Zülke, A., Berecibar, M., Nanini-Maury, E., Mierlo, J. V., and E.Hoster, H. (2019). Data-driven health estimation and lifetime prediction of lithium-ion batteries: A review. *Renewable and Sustainable Energy Reviews*, 113.

[21] Li, Y., Zou, C., Berecibar, M., Nanini-Maury, E., Chan, J. C.-W., van den Bossche, P., Mierlo, J. V., and Omar, N. (2018). Random forest regression for online capacity estimation of lithium-ion batteries. *Applied Energy*, 232:197–210.

[22] Liu, Z., Zhao, J., Wang, H., and Yang, C. (2020). A new lithium-ion battery soh estimation method based on an indirect enhanced health indicator and support vector regression in phms. *Energies*, 13(4):830.

[23] Lv, S., Wang, X., Lu, W., Zhang, J., and Ni, H. (2022). The influence of temperature on the capacity of lithium ion batteries with different anodes. *Energies*, 15(60):60–60.

[24] Mawonou, K. S., Eddahech, A., Dumur, D., Beauvois, D., and Godoy, E. (2021). State-of-health estimators coupled to a random forest approach for lithium-ion battery aging factor ranking. *Journal of Power Sources*, 484.

[25] Patil, M. A., Tagade, P., Hariharan, K. S., Kolake, S. M., Song, T., Yeo, T., and Doo, S. (2015). A novel multistage support vector machine based approach for li ion battery remaining useful life estimation. *Applied Energy*, 159:285–297.

[26] Pedregosa, F., Varoquaux, G., Gramfort, A., Michel, V., Thirion, B., Grisel, O., Blondel, M., Prettenhofer, P., Weiss, R., Dubourg, V., Vanderplas, J., Passos, A., Cournapeau, D., Brucher, M., Perrot, M., and Duchesnay, E. (2011). Scikit-learn: Machine learning in Python. *Journal of Machine Learning Research*, 12:2825–2830.

[27] Polaczyk, N., Trombino, E., Wei, P., and Mitici, M. (2019). A review of current technology and research in urban on-demand air mobility applications. In *8th Biennial Autonomous VTOL Technical Meeting and 6th Annual Electric VTOL Symposium*, pages 333–343.

[28] Pop, V. (2008). Battery management systems : accurate state-of-charge indication for battery powered applications. *Springer*, Ser. Philips research book series, v. 9.

[29] Quinto, B. (2020). Next-generation machine learning with spark : covers xgboost, lightgbm, spark nlp, distributed deep learning with keras, and more. *Apress L.P. Retrieved May 11, 2022, from* *https://learning-oreilly-com.tudelft.idm.oclc.org/library/view/next-generation-machine-learning/9781484256695/html/488426_1_En_1_Chapter.xhtml*.

[30] Richardson, R. R., Osborne, M. A., and Howey, D. A. (2017). Gaussian process regression for forecasting battery state of health. *Journal of Power Sources*, 357:209–2019.

[31] Roman, D., Saxena, S., Robu, V., Pecht, M., and Flynn, D. (2021). Machine learning pipeline for battery state-of-health estimation. *Nature Machine Intelligence*, 3(5):447–456.

[32] Saha, B. and Goebel, K. (2017). Battery data set. *NASA Ames Prognostics Data Repository (http://ti.arc.nasa.gov/project/prognostic-data-repository)*. NASA Ames Research Center, Moffett Field, CA.

[33] Severson, K. A., Attia, P. M., Jin, N., Perkins, N., Jiang, B., Yang, Z., Chen, M. H., Aykol, M., Herring, P. K., Fraggedakis, D., Bazant, M. Z., Harris, S. J., Chueh, W. C., and Braatz, R. D. (2019). Data-driven prediction of battery cycle life before capacity degradation. *Nature Energy*, 4:383–391.

[34] Sharifzadeha, M., Sikinioti-Lock, A., and Shah, N. (2019). Machine-learning methods for integrated renewable power generation: A comparative study of artificial neural networks, support vector regression, and gaussian process regression. *Renewable and Sustainable Energy Reviews*, 108:513–538.

[35] Shu, X., Li, G., Shen, J., Lei, Z., Chen, Z., and Liu, Y. (2020). A uniform estimation framework for state of health of lithium-ion batteries considering feature extraction and parameters optimization. *Energy*, 204.

[36] Steinwart, I. and Christmann, A. (2008). Support vector machines. *1st ed., Ser. Information science and statistics*, Springer.

[37] Tian, H., Qin, P., Li, K., and Zhao, Z. (2020a). A review of the state of health for lithium-ion batteries: Research status and suggestions. *Journal of Cleaner Production*, 261.

[38] Tian, J., Xiong, R., and Shen, W. (2020b). State-of-health estimation based on differential temperature for lithium ion batteries. *IEEE Transactions On Power Electronics*, 35(10):10363–10373.

[39] Tian, J., Xu, R., Wang, Y., and Chen, Z. (2021). Capacity attenuation mechanism modeling and health assessment of lithium-ion batteries. *Energy*, 221.

[40] Xiong, R. (2020). Battery management algorithm for electric vehicles. *Springer*.

[41] Xu, F., Yang, F., Fei, Z., Huang, Z., and Tsui, K.-L. (2021). Life prediction of lithium-ion batteries based on stacked denoising autoencoders. *Reliability Engineering and System Safety,*, 208.

[42] Yang, A., Wang, Y., Yang, F., Wang, D., Zi, Y., Tsui, K. L., and Zhang, B. (2019). A comprehensive investigation of lithium-ion battery degradation performance at different discharge rates. *Journal of Power Sources*, 443.

[43] Yang, D., Zhang, X., Pan, R., Wang, Y., and Chen, Z. (2018). A novel gaussian process regression model for state-of-health estimation of lithium-ion battery using charging curve. *Applied Energy*, 384:387–395.

[44] Yang, F., Wang, D., Xu, F., Huang, Z., and Tsui, K.-L. (2020). Lifespan prediction of lithium-ion batteries based on various extracted features and gradient boosting regression tree model. *Journal of Power Sources*, 476.

[45] Zhang, C., Jiang, J., Gao, Y., Zhang, W., Liu, Q., and Hu, X. (2017). Charging optimization in lithium-ion batteries based on temperature rise and charge time. *Applied Energy*, 194:569–577.

[46] Zhang, Y., Peng, Z., Guan, Y., and Wu, L. (2021). Prognostics of battery cycle life in the early-cycle stage based on hybrid model. *Elsevier*, 221:article 119901.

[47] Zhang, Y., Xiong, R., He, H., and Pecht, M. G. (2018). Long short-term memory recurrent neural network for remaining useful life prediction of lithium-ion batteries. *IEEE Transactions on Vehicular Technology*, 67(7):5695–5705.

Appendices

A Appendix 1

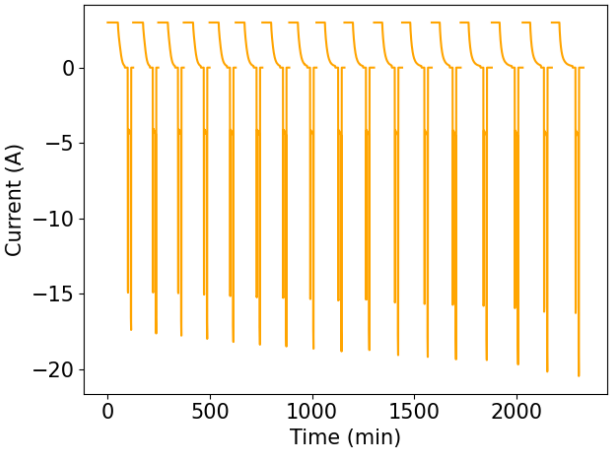

(a) Capacity tests in VAH01

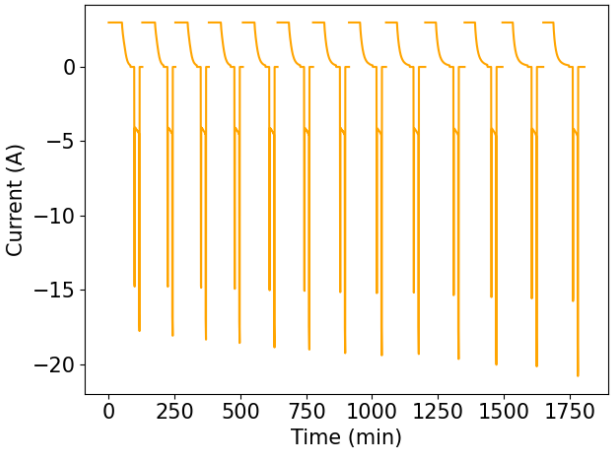

(b) Capacity tests in VAH02

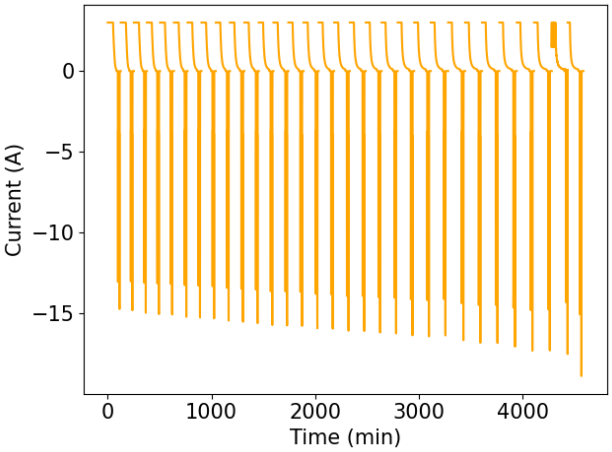

(c) Capacity tests in VAH05

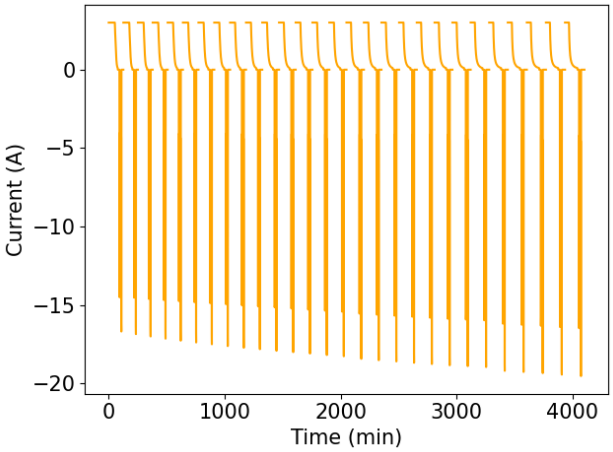

(d) Capacity tests in VAH10

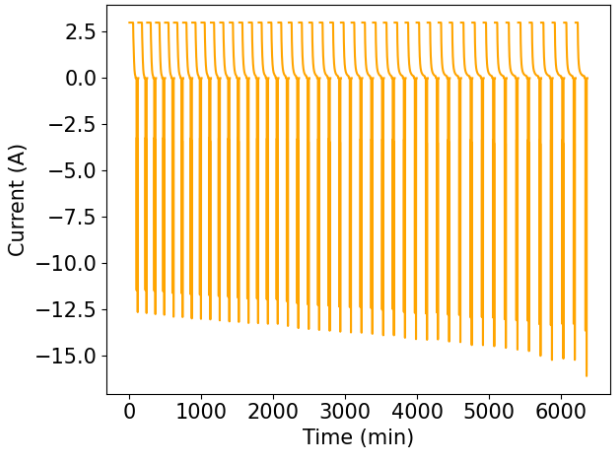

(e) Capacity tests in VAH11

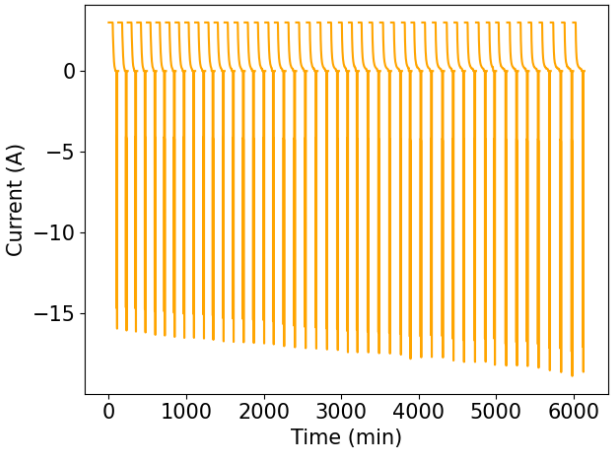

(f) Capacity tests in VAH12

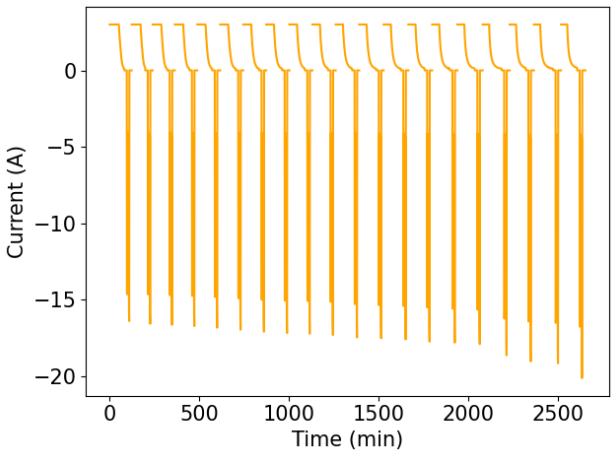

(g) Capacity tests in VAH13

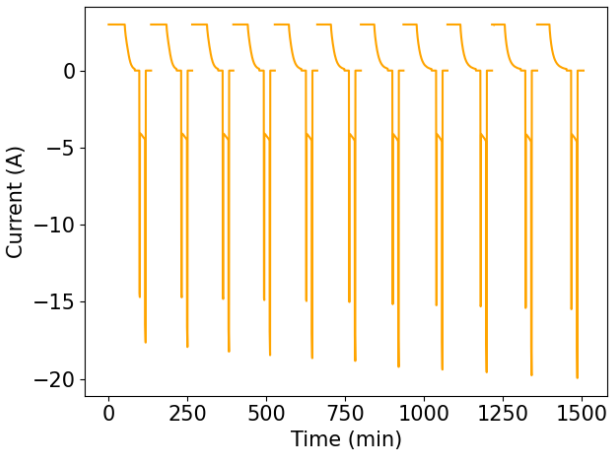

(h) Capacity tests in VAH15

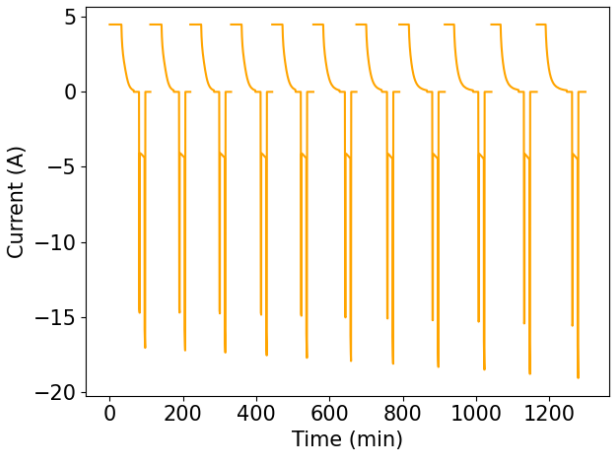

(i) Capacity tests in VAH16

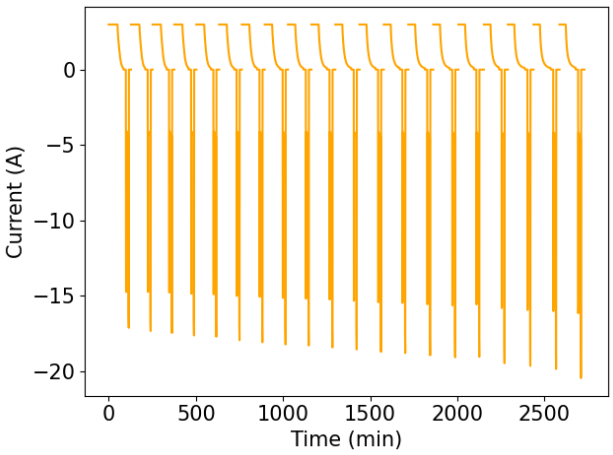

(j) Capacity tests in VAH17

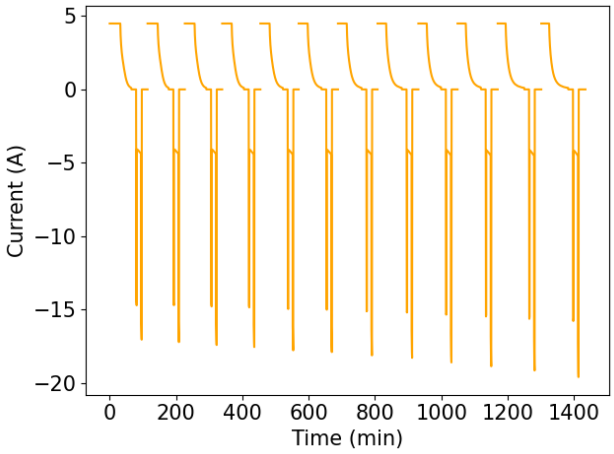

(k) Capacity tests in VAH20

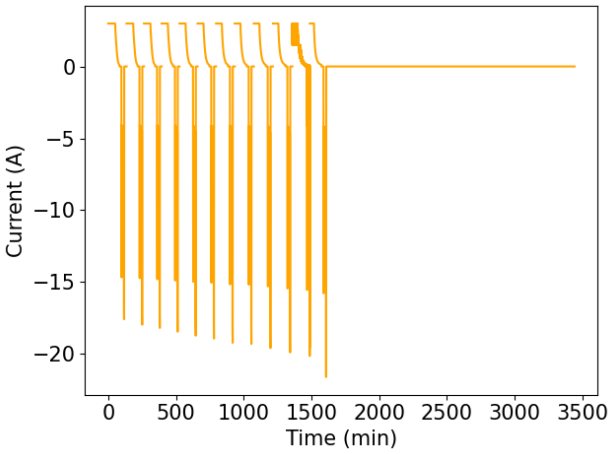

(l) Capacity tests in VAH22

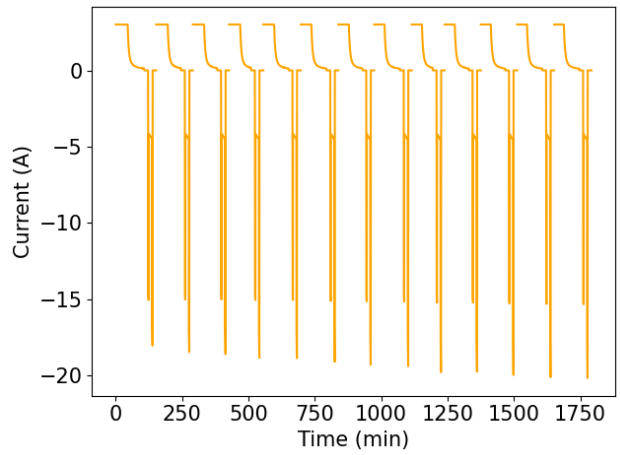

(m) Capacity tests in VAH23

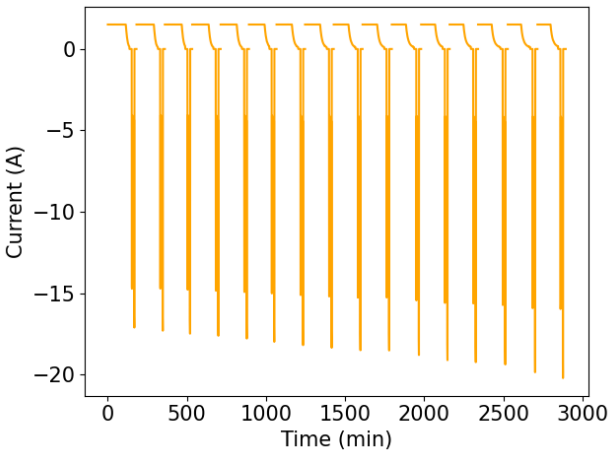

(n) Capacity tests in VAH24

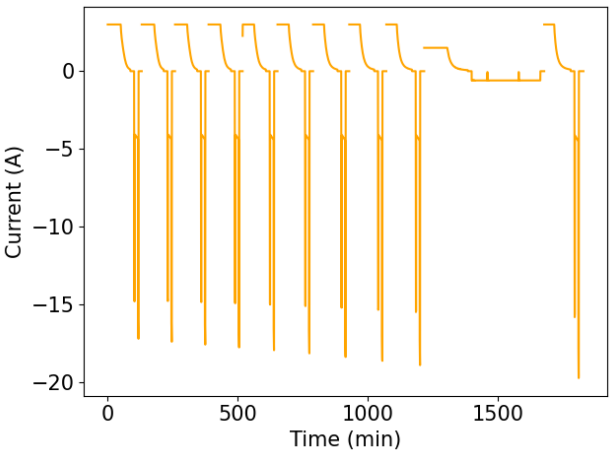

(o) Capacity tests in VAH25

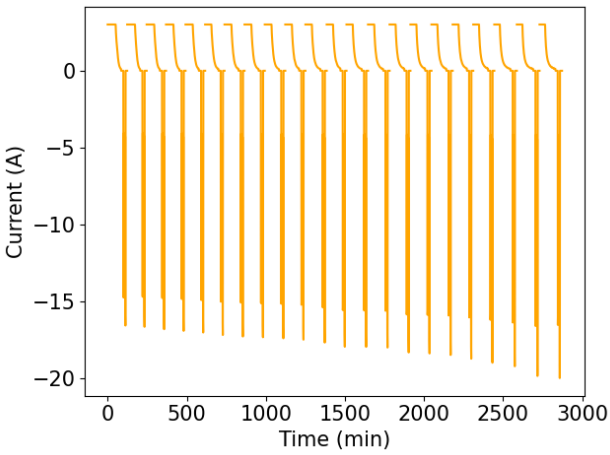

(p) Capacity tests in VAH26

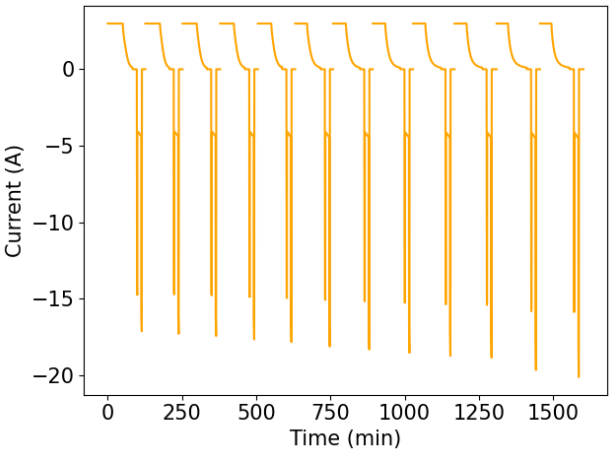

(q) Capacity tests in VAH27

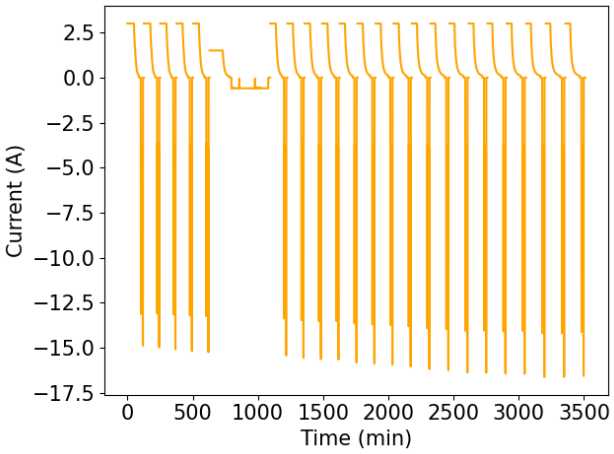

(r) Capacity tests in VAH28

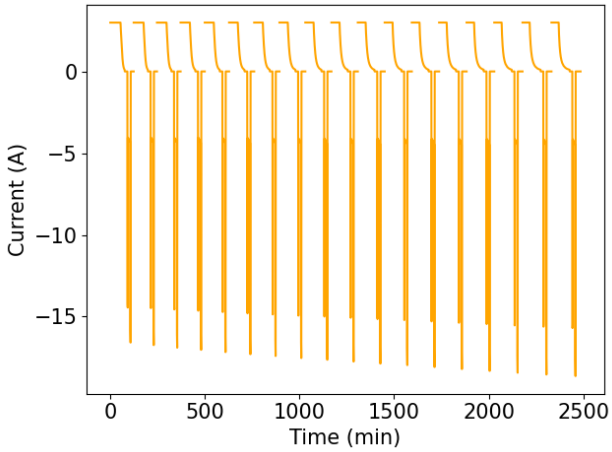

(s) Capacity tests in VAH30

Figure 20: The current during all capacity tests in all MPs, except the excluded MPs (i.e., VAH06, VAH07, and VAH09)

B Appendix 2

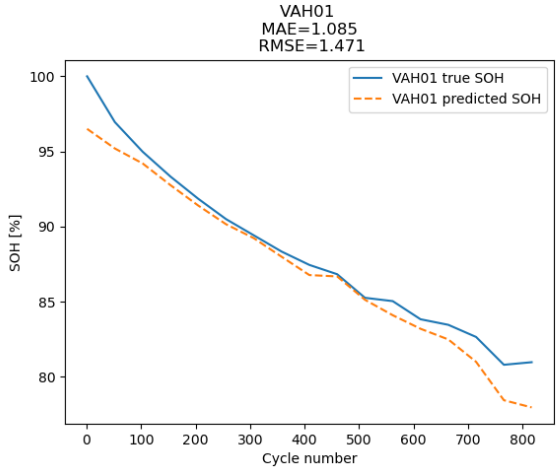

(a) Predicted and true SOH, with SVR, in VAH01

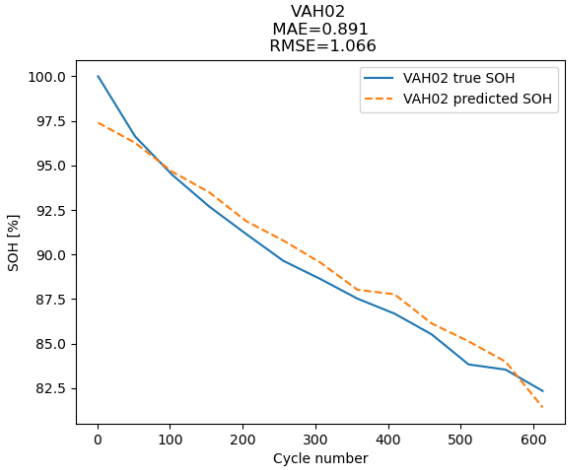

(b) Predicted and true SOH, with SVR, in VAH02

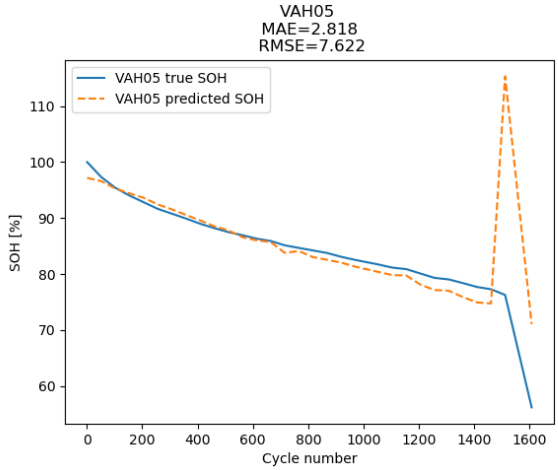

(c) Predicted and true SOH, with SVR, in VAH05

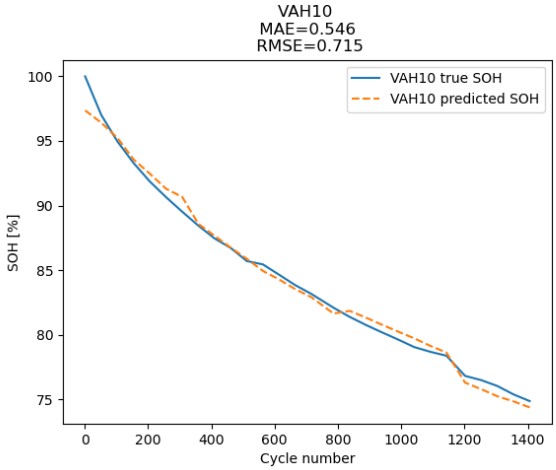

(d) Predicted and true SOH, with SVR, in VAH10

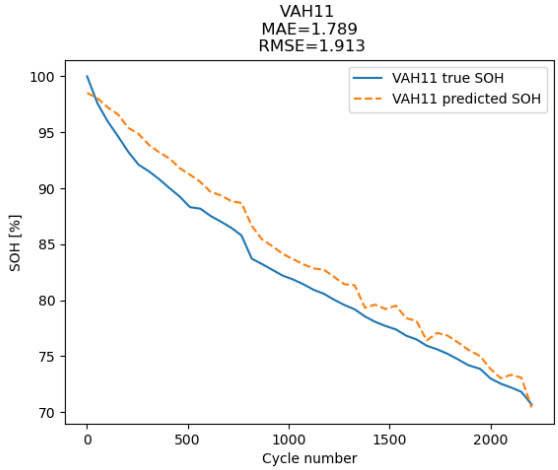

(e) Predicted and true SOH, with SVR, in VAH11

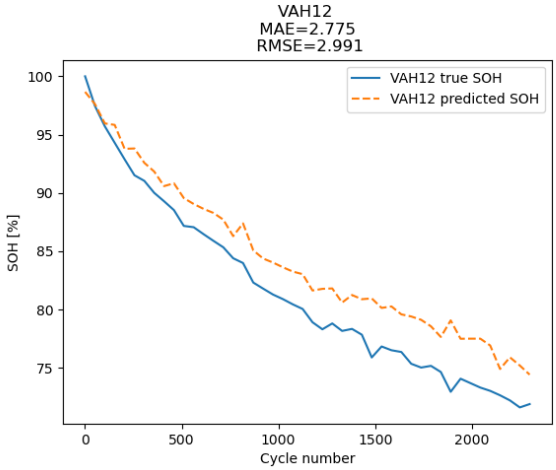

(f) Predicted and true SOH, with SVR, in VAH12

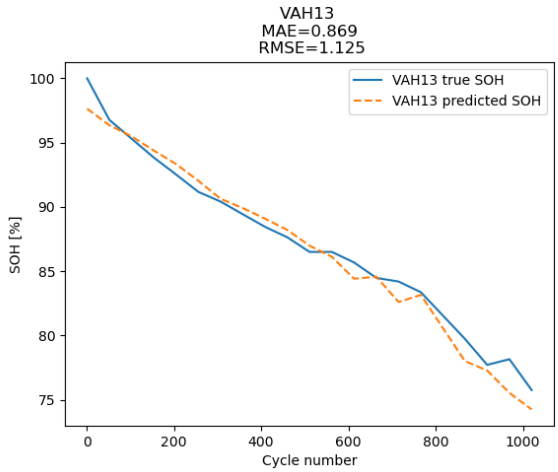

(g) Predicted and true SOH, with SVR, in VAH13

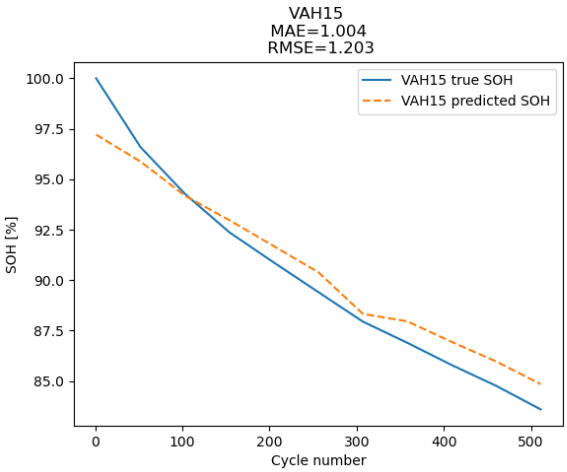

(h) Predicted and true SOH, with SVR, in VAH15

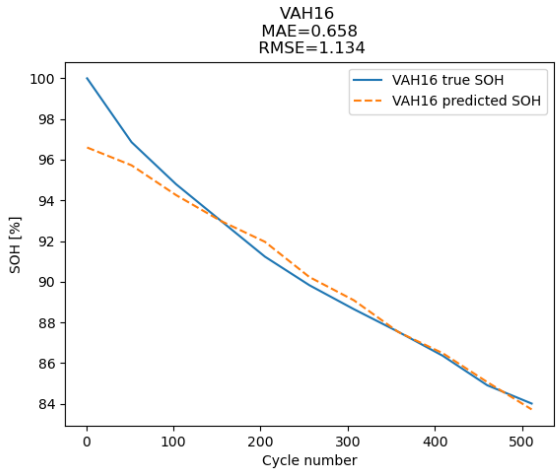

(i) Predicted and true SOH, with SVR, in VAH16

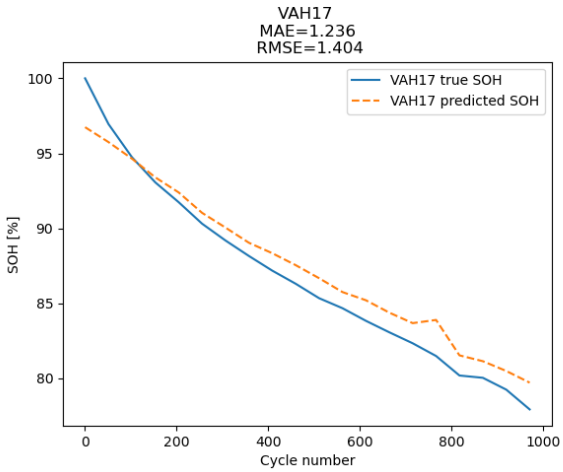

(j) Predicted and true SOH, with SVR, in VAH17

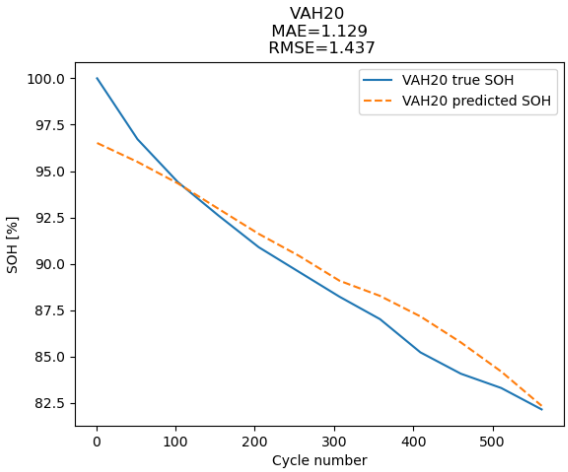

(k) Predicted and true SOH, with SVR, in VAH20

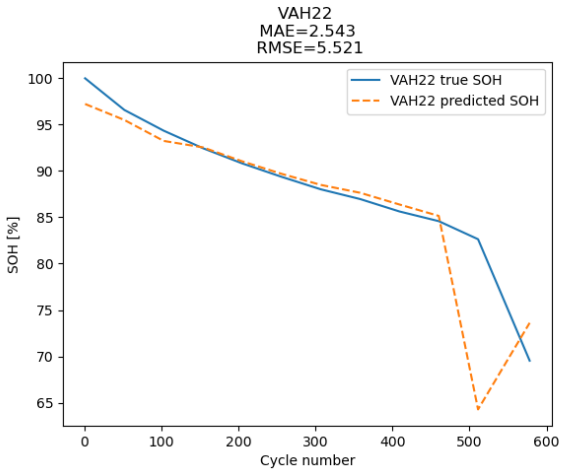

(l) Predicted and true SOH, with SVR, in VAH22

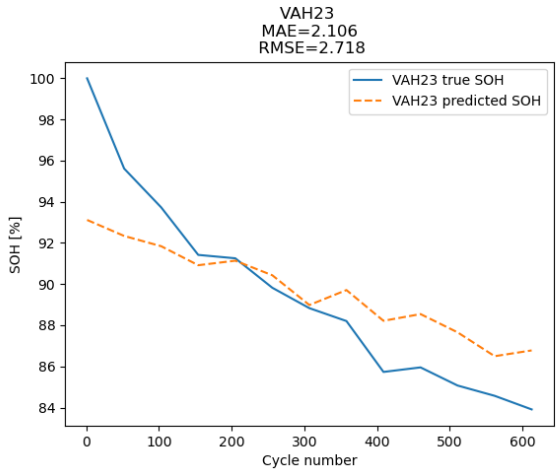

(m) Predicted and true SOH, with SVR, in VAH23

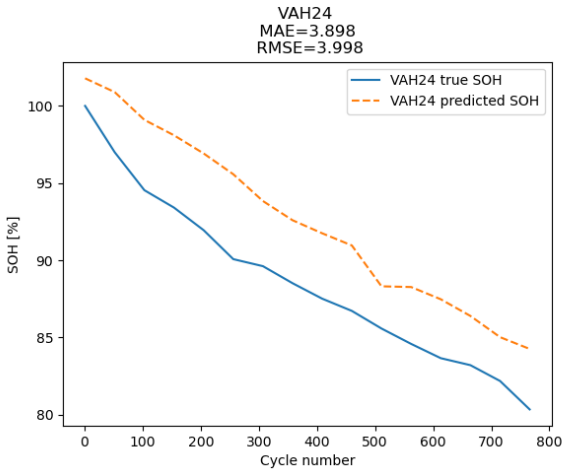

(n) Predicted and true SOH, with SVR, in VAH24

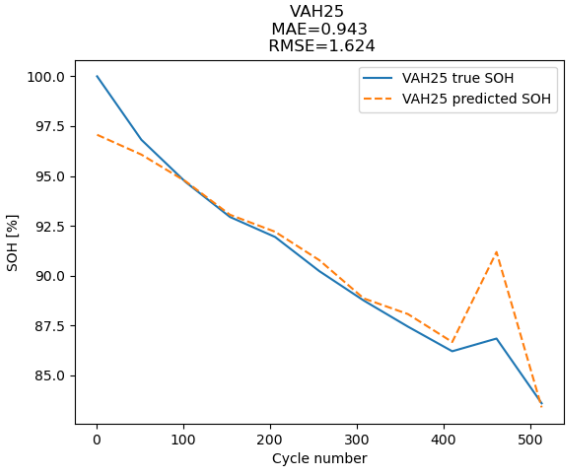

(o) Predicted and true SOH, with SVR, in VAH25

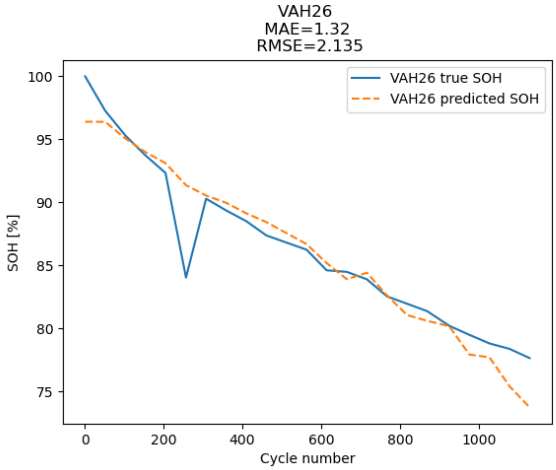

(p) Predicted and true SOH, with SVR, in VAH26

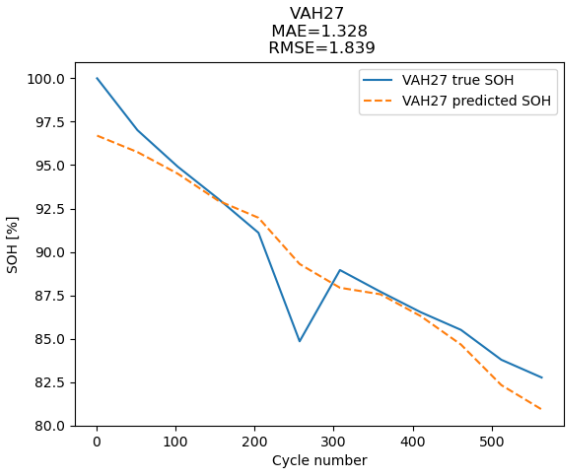

(q) Predicted and true SOH, with SVR, in VAH27

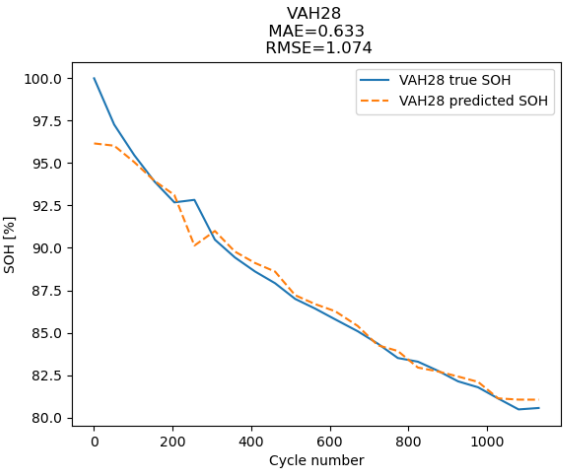

(r) Predicted and true SOH, with SVR, in VAH28

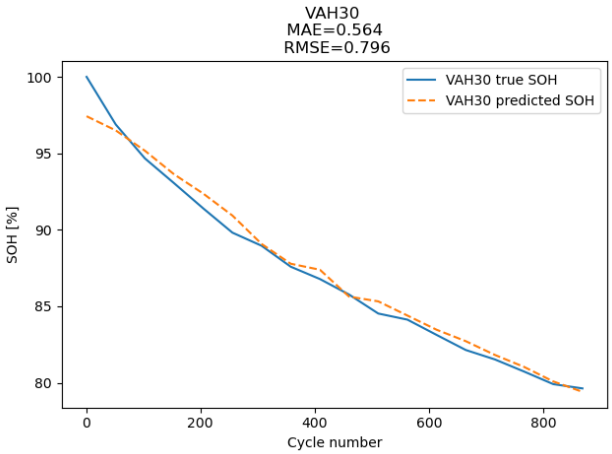

(s) Predicted and true SOH, with SVR, in VAH30

Figure 21: The results of SVR for SOH

C Appendix 3

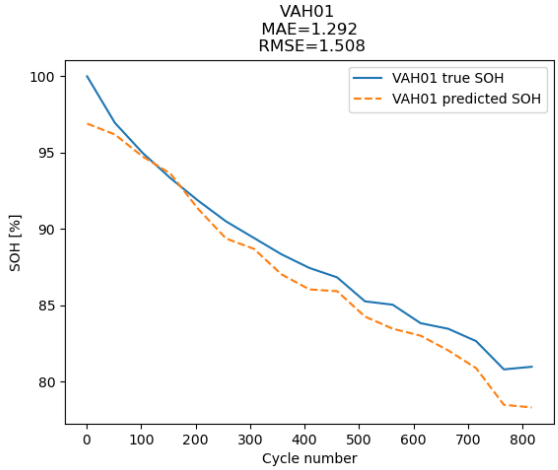

(a) Predicted and true SOH, with RF, in VAH01

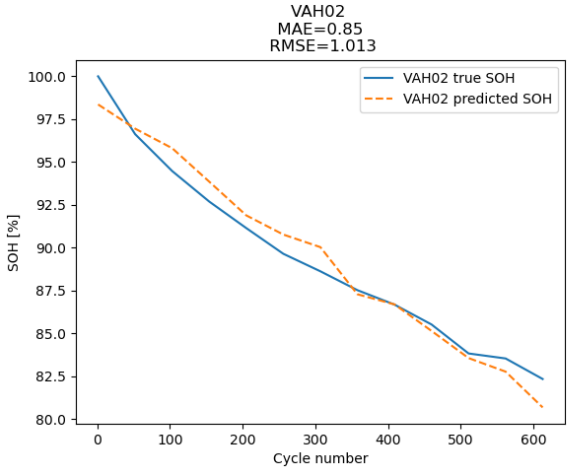

(b) Predicted and true SOH, with RF, in VAH02

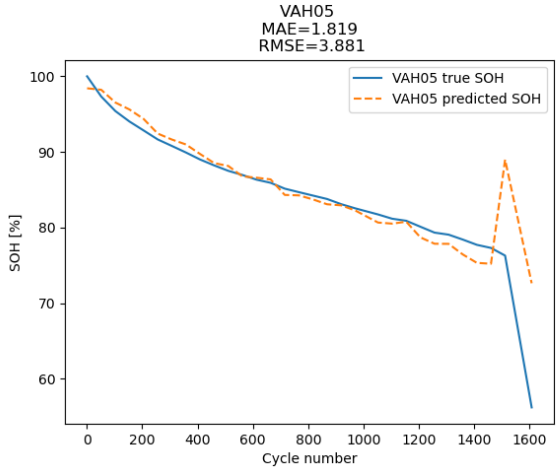

(c) Predicted and true SOH, with RF, in VAH05

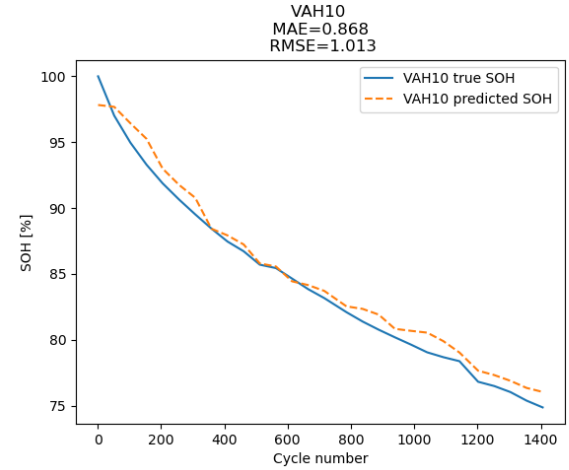

(d) Predicted and true SOH, with RF, in VAH10

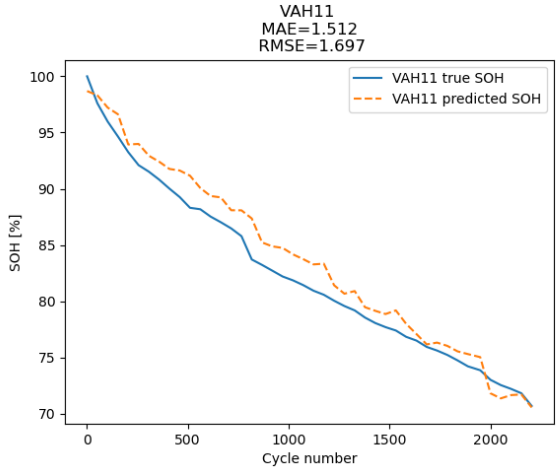

(e) Predicted and true SOH, with RF, in VAH11

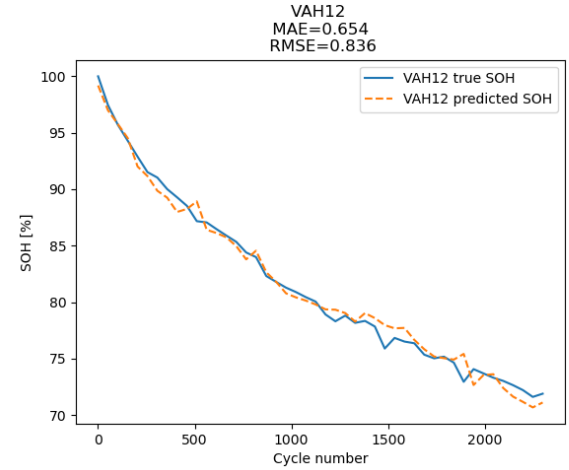

(f) Predicted and true SOH, with RF, in VAH12

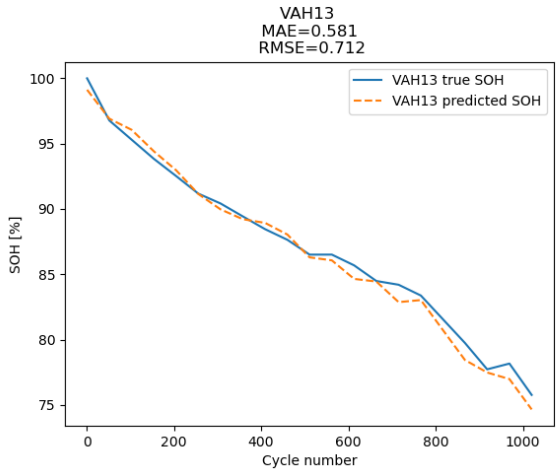

(g) Predicted and true SOH, with RF, in VAH13

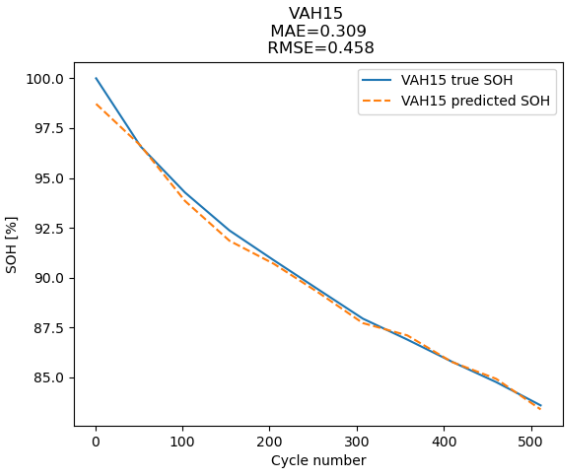

(h) Predicted and true SOH, with RF, in VAH15

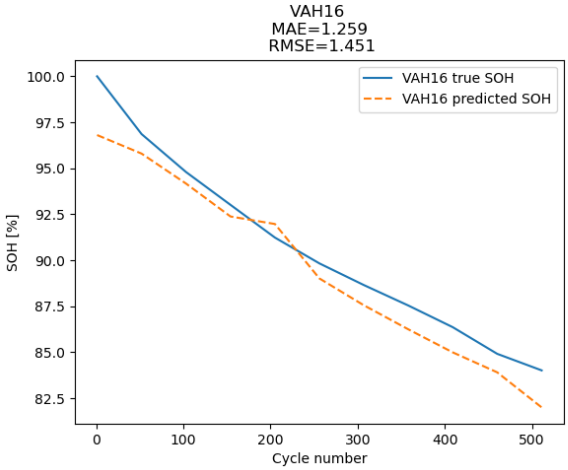

(i) Predicted and true SOH, with RF, in VAH16

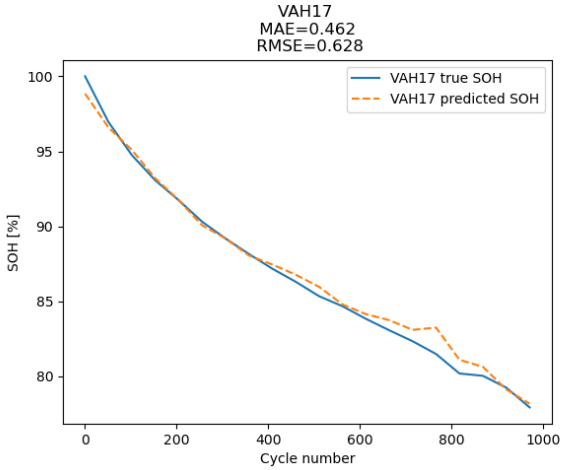

(j) Predicted and true SOH, with RF, in VAH17

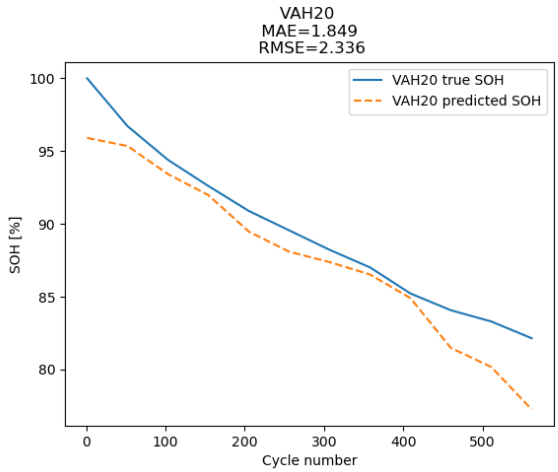

(k) Predicted and true SOH, with RF, in VAH20

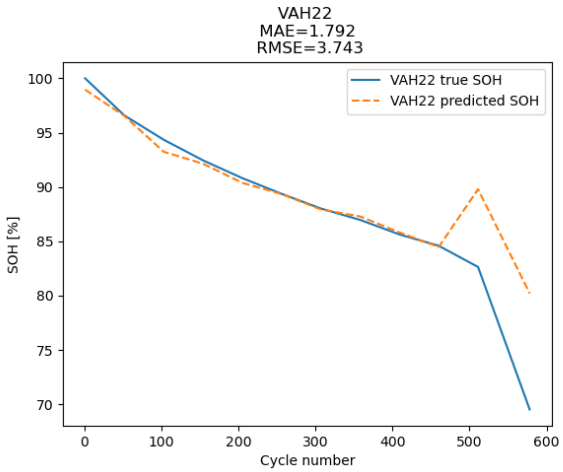

(l) Predicted and true SOH, with RF, in VAH22

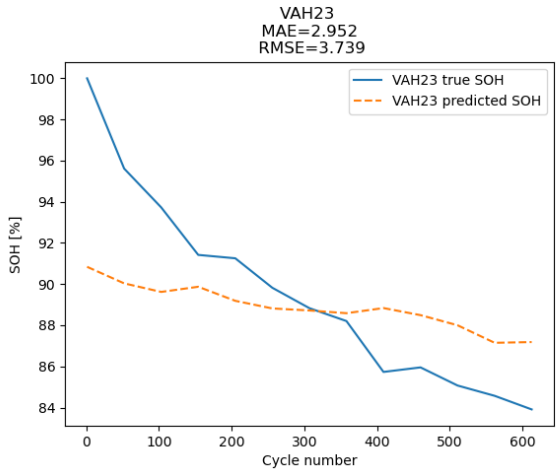

(m) Predicted and true SOH, with RF, in VAH23

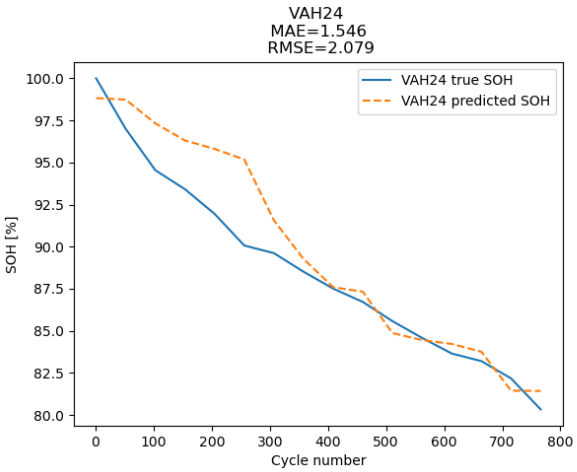

(n) Predicted and true SOH, with RF, in VAH24

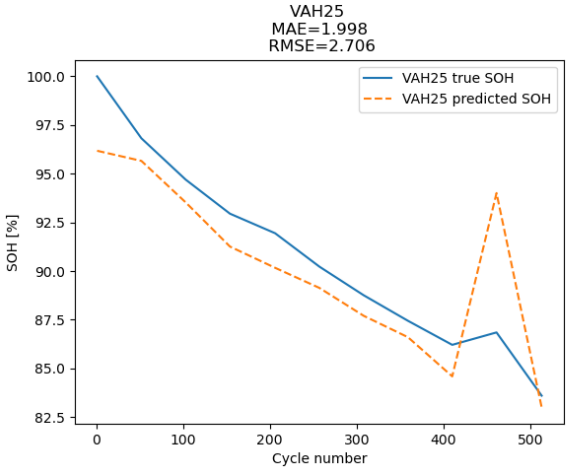

(o) Predicted and true SOH, with RF, in VAH25

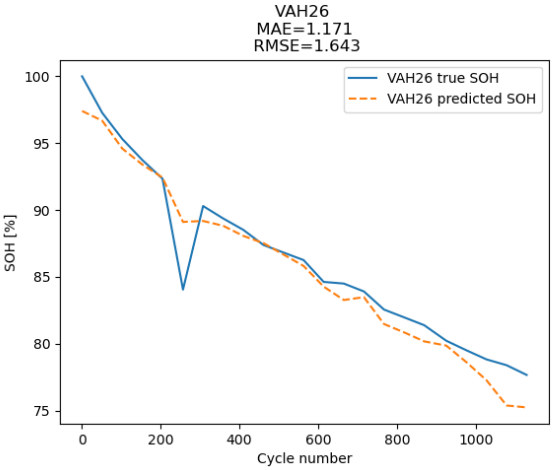

(p) Predicted and true SOH, with RF, in VAH26

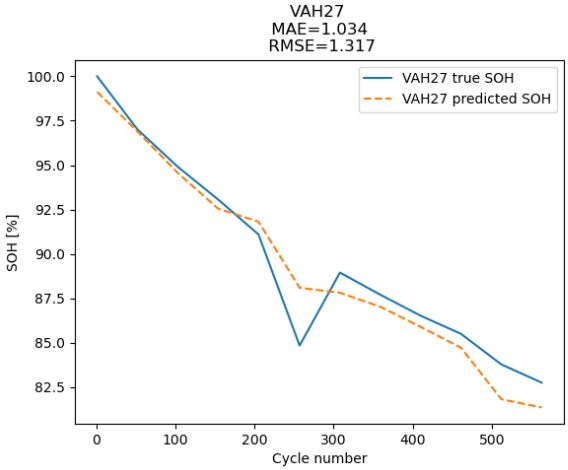

(q) Predicted and true SOH, with RF, in VAH27

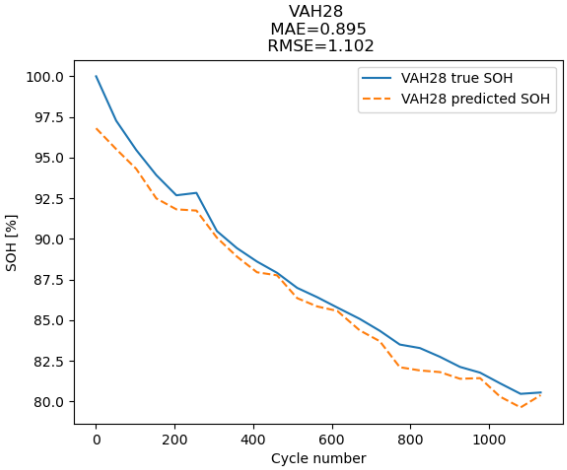

(r) Predicted and true SOH, with RF, in VAH28

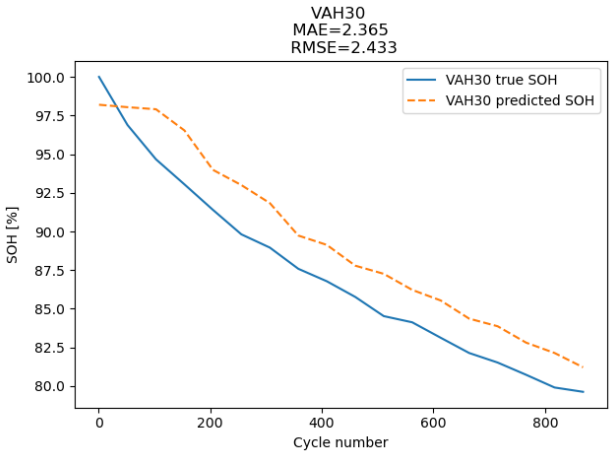

(s) Predicted and true SOH, with RF, in VAH30

Figure 22: The results of RF for SOH

D Appendix 4

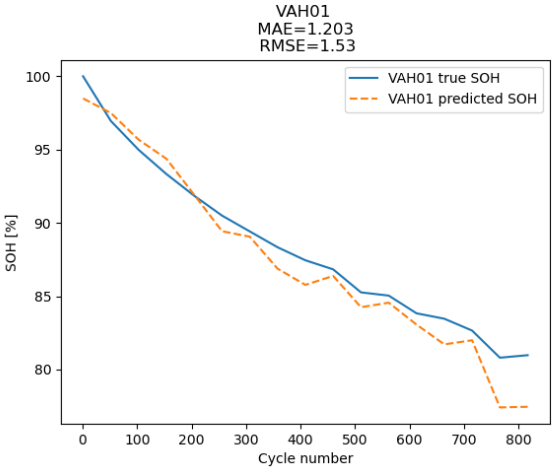

(a) Predicted and true SOH, with XGBoost, in VAH01

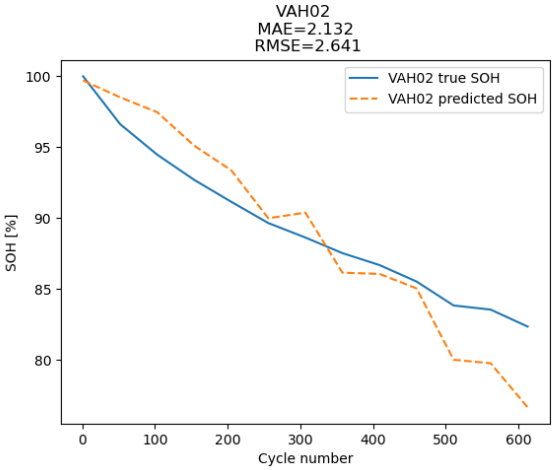

(b) Predicted and true SOH, with XGBoost, in VAH02

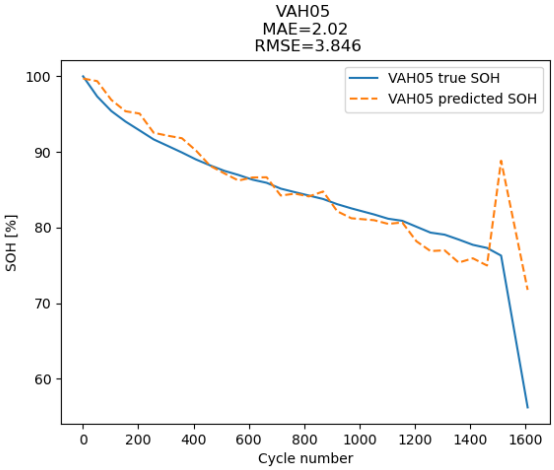

(c) Predicted and true SOH, with XGBoost, in VAH05

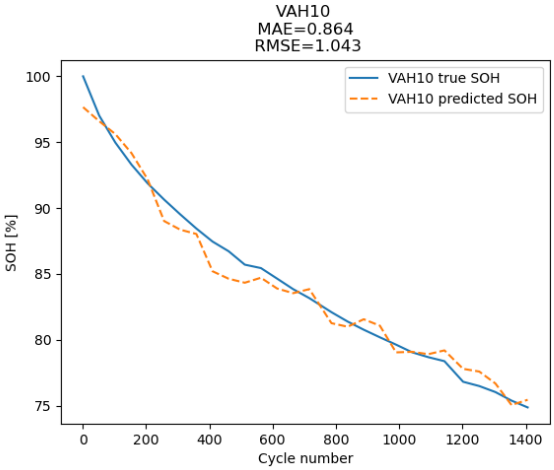

(d) Predicted and true SOH, with XGBoost, in VAH10

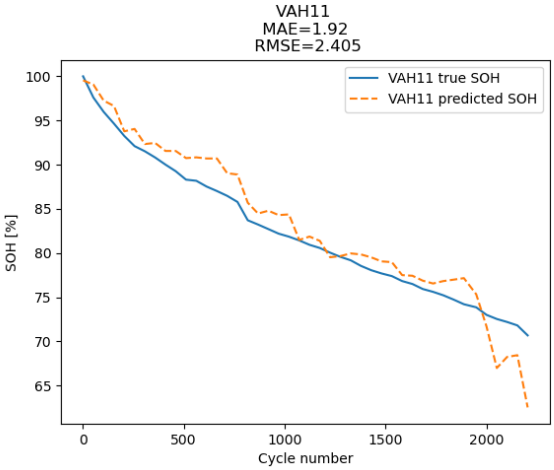

(e) Predicted and true SOH, with XGBoost, in VAH11

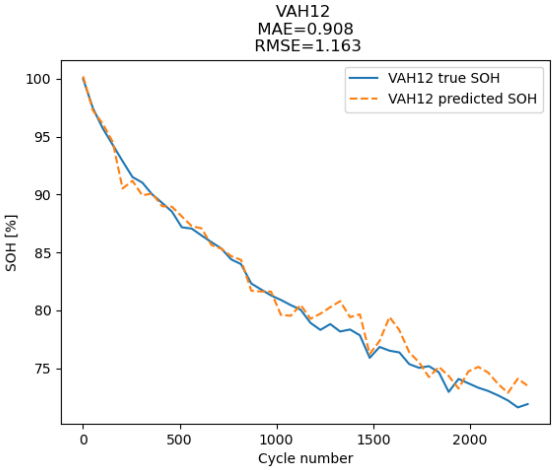

(f) Predicted and true SOH, with XGBoost, in VAH12

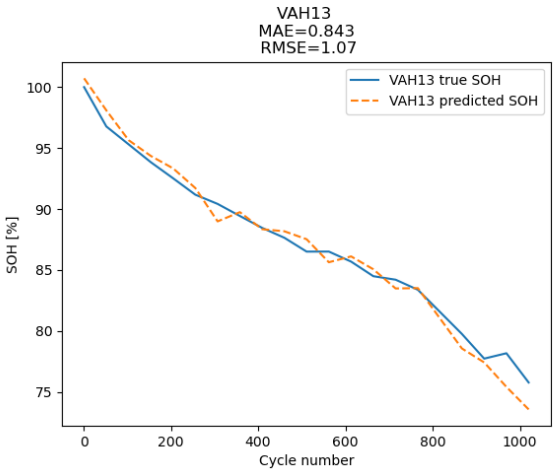

(g) Predicted and true SOH, with XGBoost, in VAH13

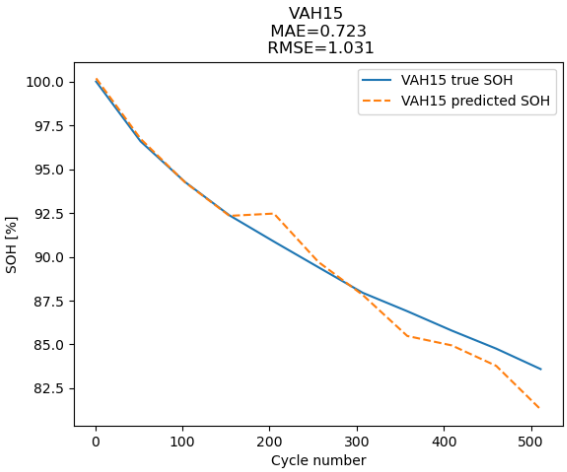

(h) Predicted and true SOH, with XGBoost, in VAH15

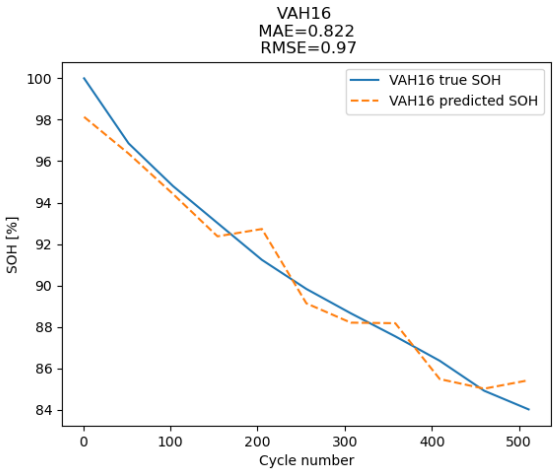

(i) Predicted and true SOH, with XGBoost, in VAH16

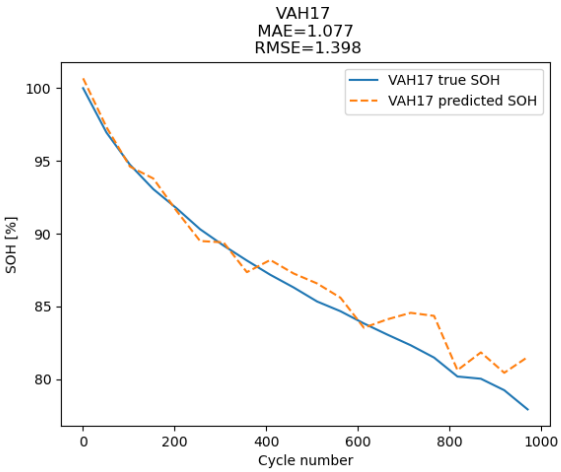

(j) Predicted and true SOH, with XGBoost, in VAH17

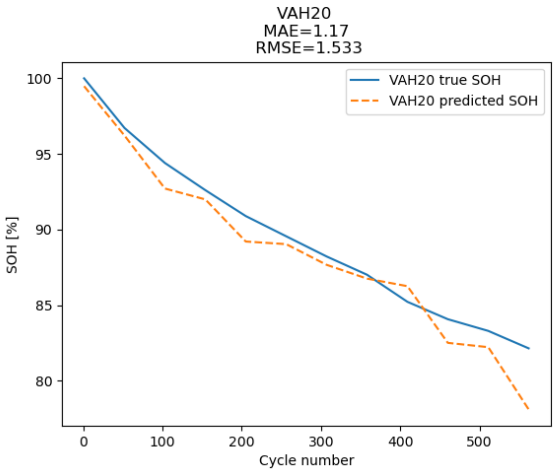

(k) Predicted and true SOH, with XGBoost, in VAH20

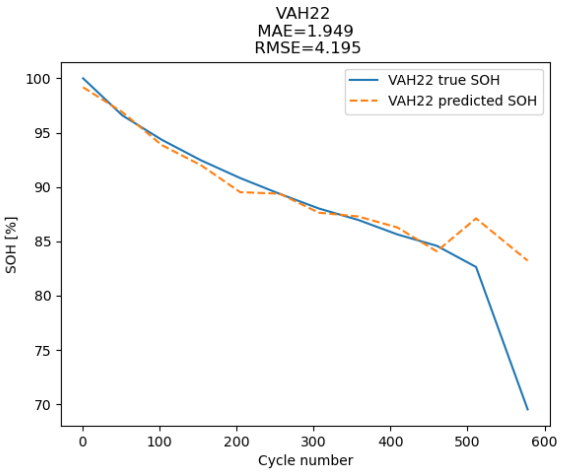

(l) Predicted and true SOH, with XGBoost, in VAH22

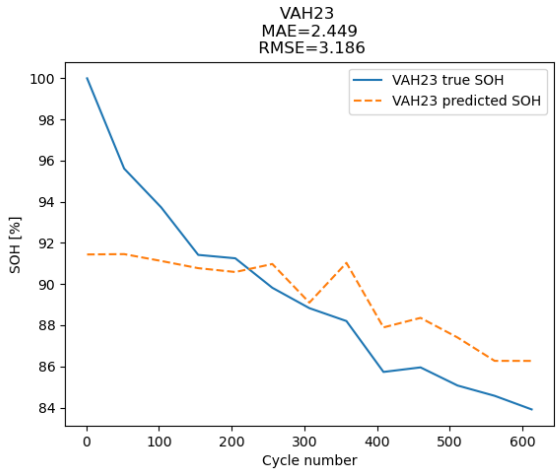

(m) Predicted and true SOH, with XGBoost, in VAH23

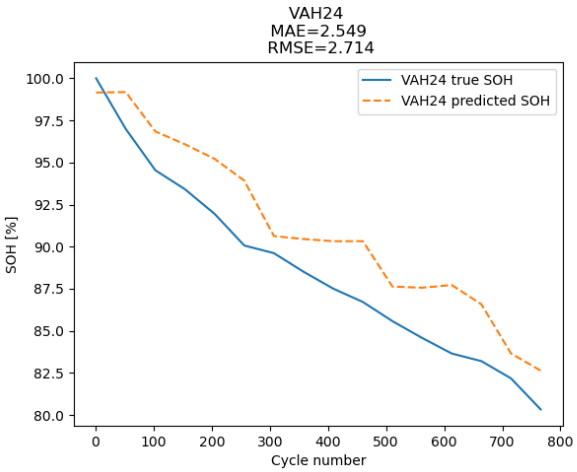

(n) Predicted and true SOH, with XGBoost, in VAH24

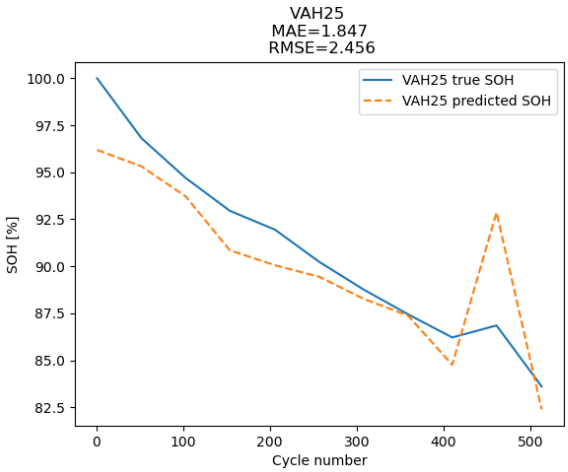

(o) Predicted and true SOH, with XGBoost, in VAH25

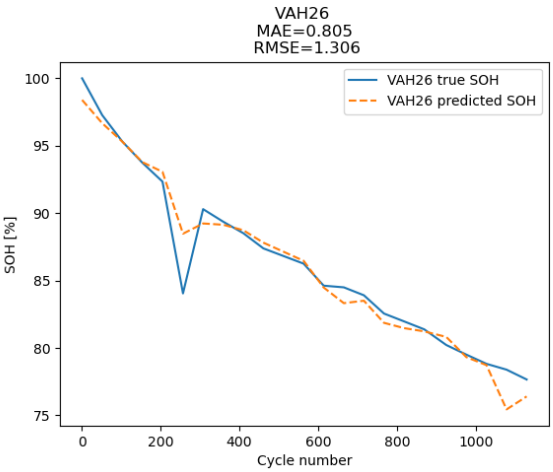

(p) Predicted and true SOH, with XGBoost, in VAH26

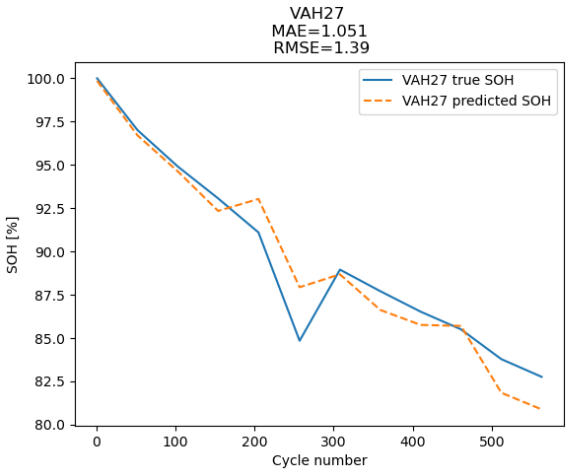

(q) Predicted and true SOH, with XGBoost, in VAH27

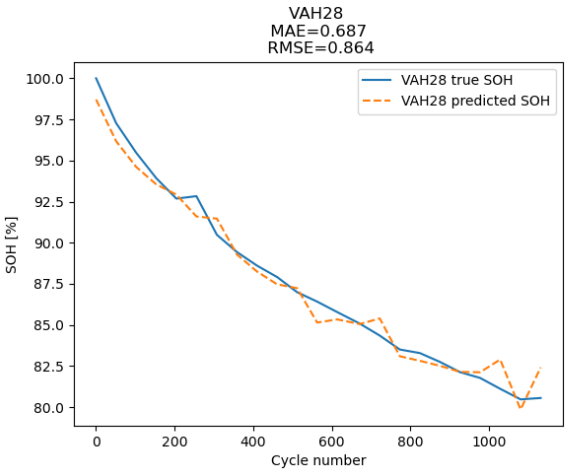

(r) Predicted and true SOH, with XGBoost, in VAH28

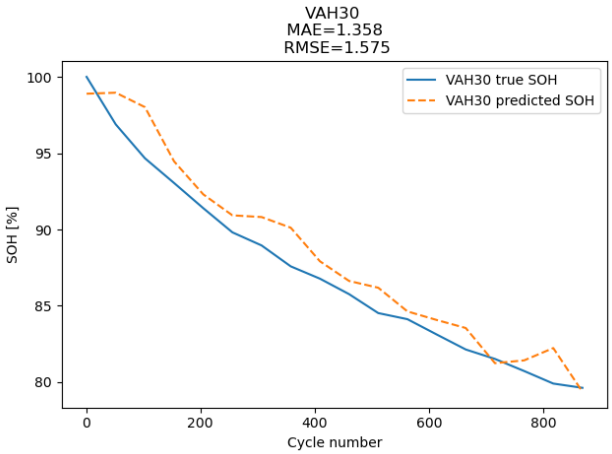

(s) Predicted and true SOH, with XGBoost, in VAH30

Figure 23: The results of XGBoost for SOH

E Appendix 5

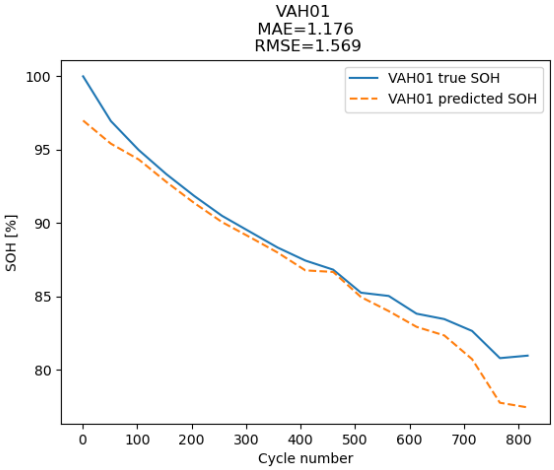

(a) Predicted and true SOH, with RF, in VAH01

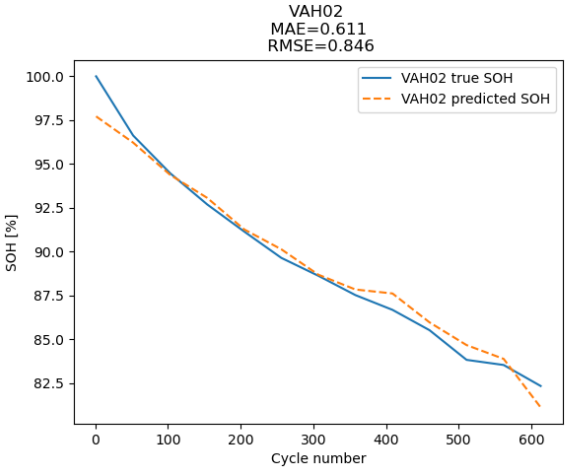

(b) Predicted and true SOH, with GPR, in VAH02

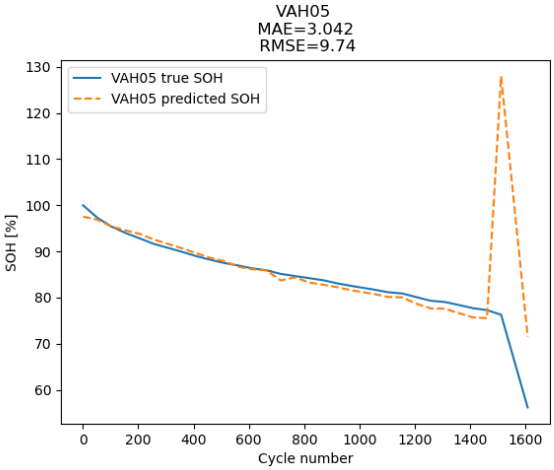

(c) Predicted and true SOH, with GPR, in VAH05

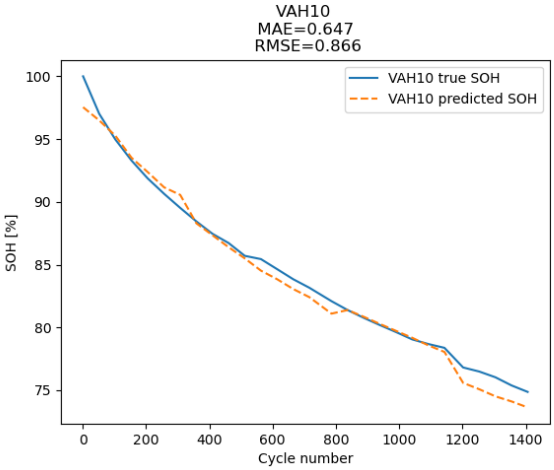

(d) Predicted and true SOH, with GPR, in VAH10

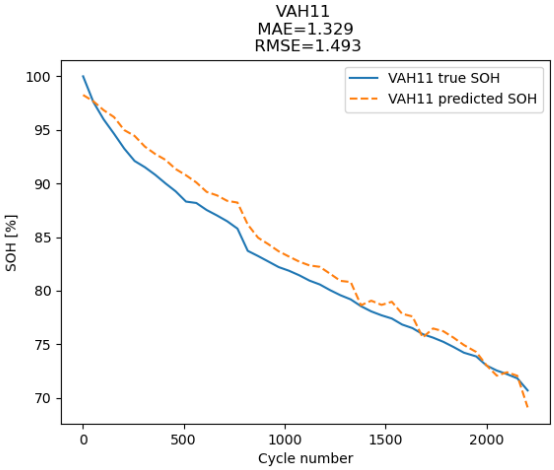

(e) Predicted and true SOH, with GPR, in VAH11

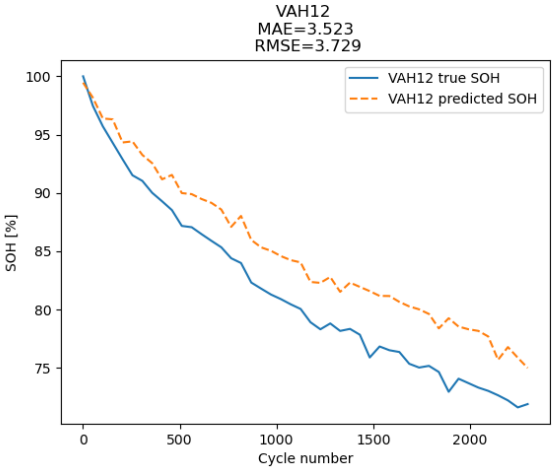

(f) Predicted and true SOH, with GPR, in VAH12

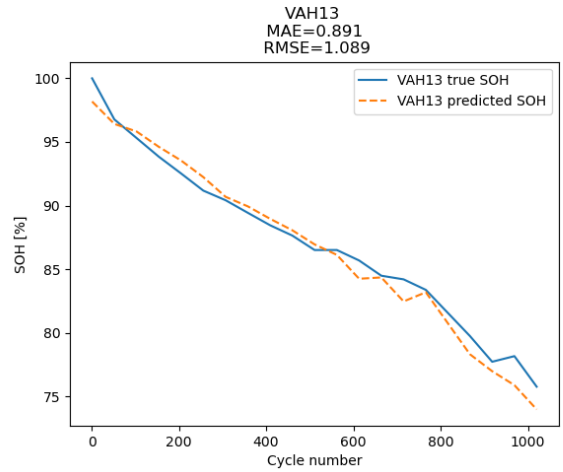

(g) Predicted and true SOH, with GPR, in VAH13

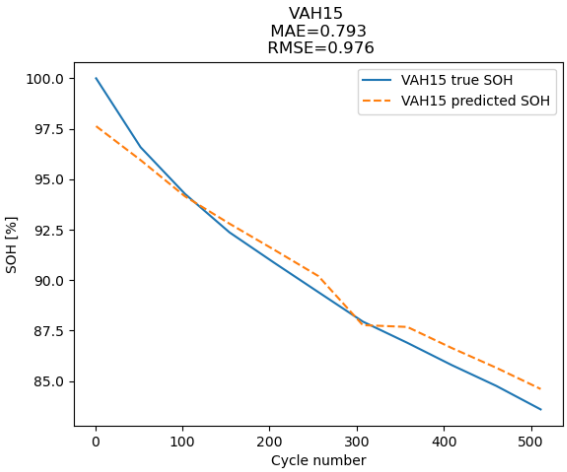

(h) Predicted and true SOH, with GPR, in VAH15

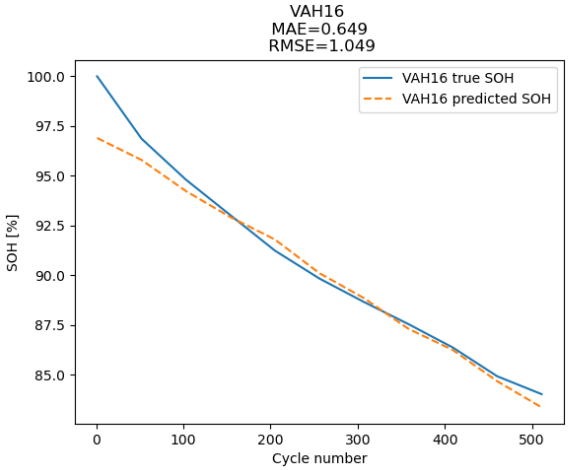

(i) Predicted and true SOH, with GPR, in VAH16

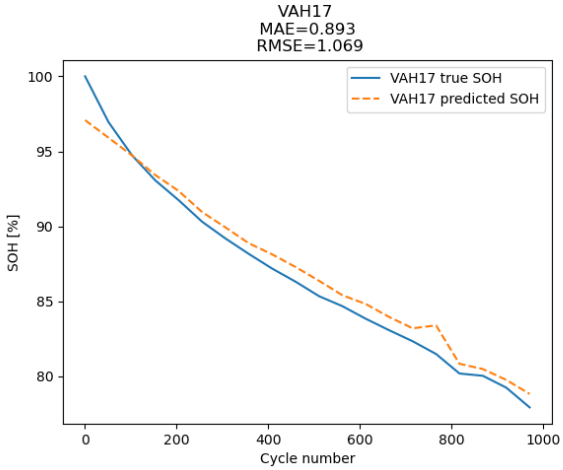

(j) Predicted and true SOH, with GPR, in VAH17

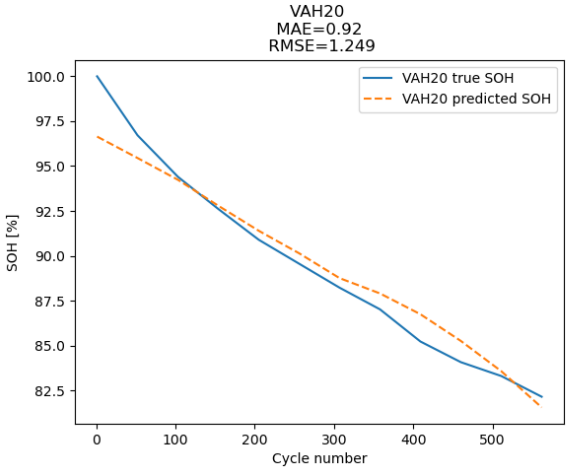

(k) Predicted and true SOH, with GPR, in VAH20

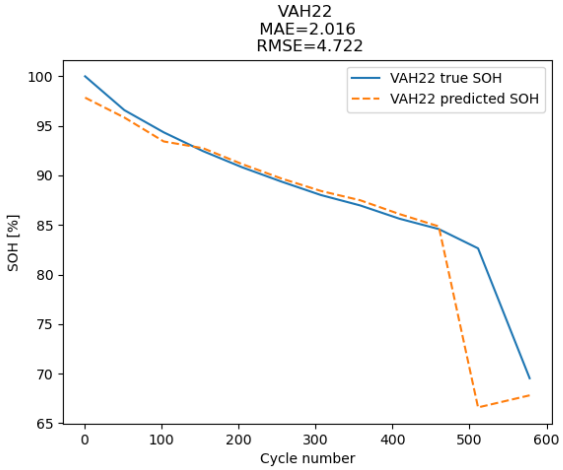

(l) Predicted and true SOH, with GPR, in VAH22

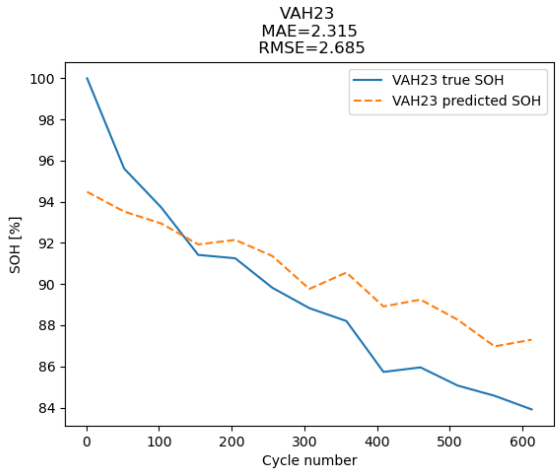

(m) Predicted and true SOH, with GPR, in VAH23

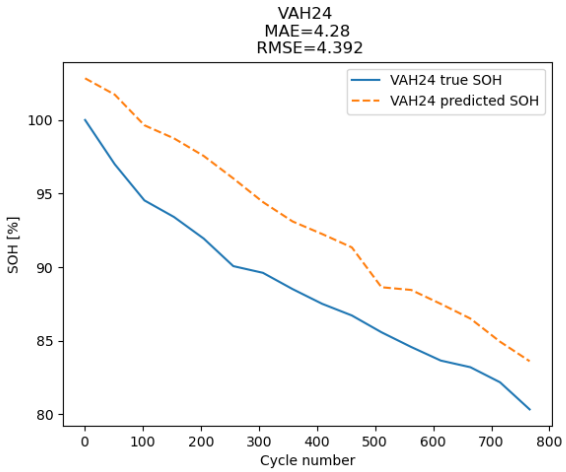

(n) Predicted and true SOH, with GPR, in VAH24

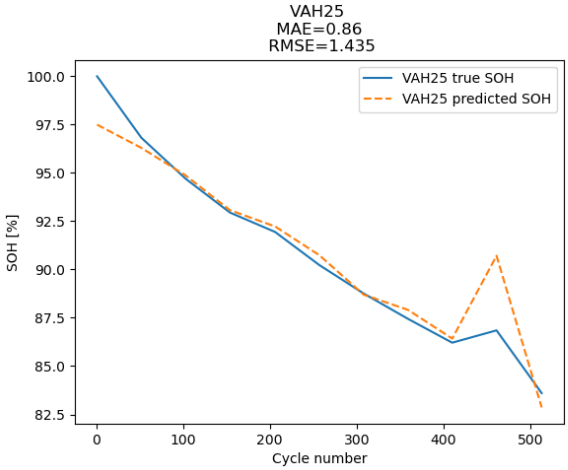

(o) Predicted and true SOH, with GPR, in VAH25

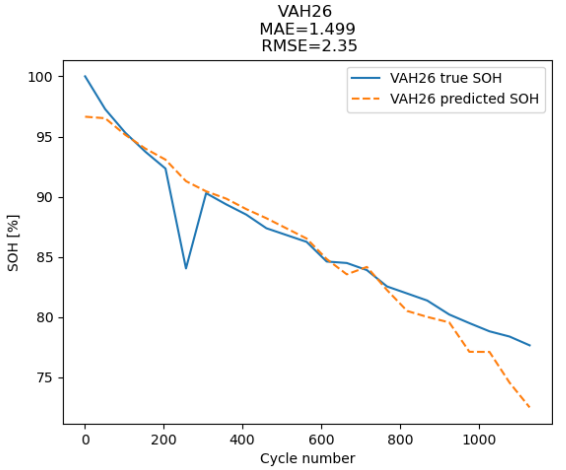

(p) Predicted and true SOH, with GPR, in VAH26

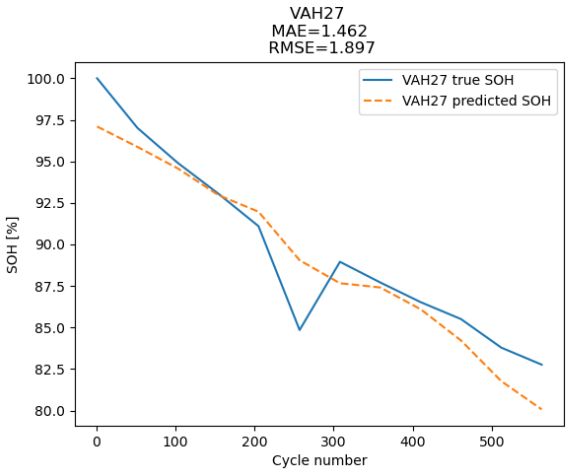

(q) Predicted and true SOH, with GPR, in VAH27

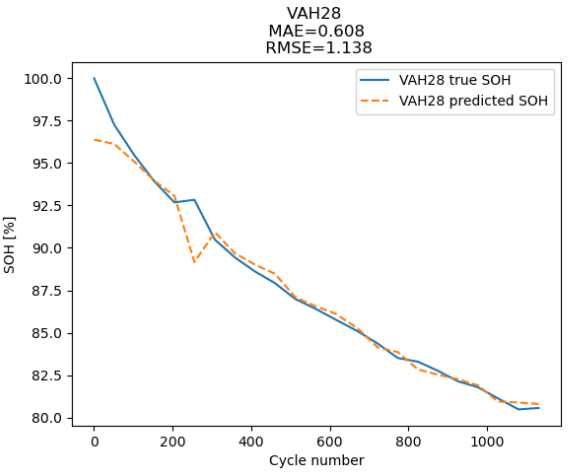

(r) Predicted and true SOH, with GPR, in VAH28

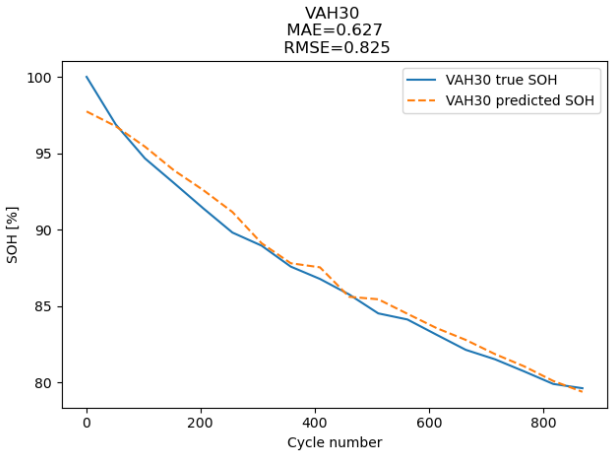

(s) Predicted and true SOH, with GPR, in VAH30

Figure 24: The results of GPR for SOH

F Appendix 6

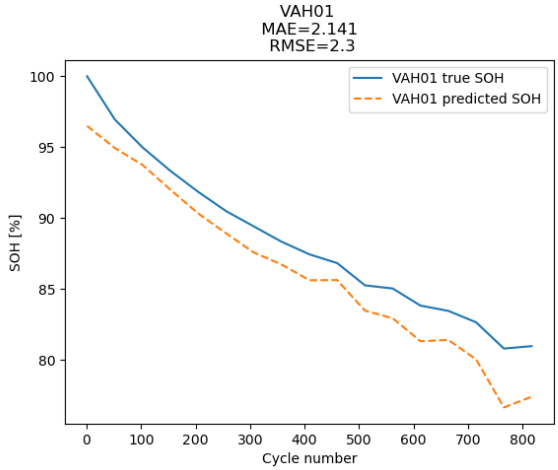

(a) Predicted and true SOH, with MLP, in VAH01

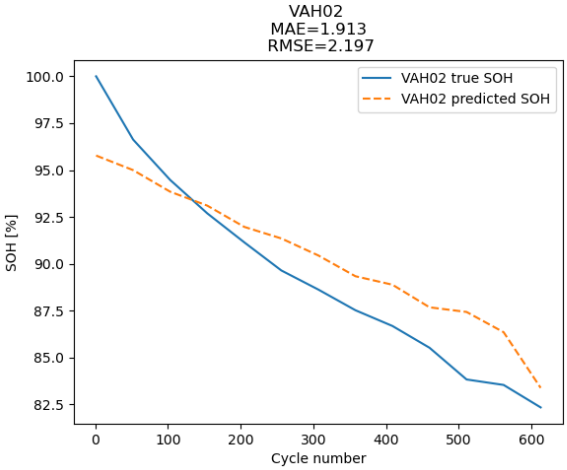

(b) Predicted and true SOH, with MLP, in VAH02

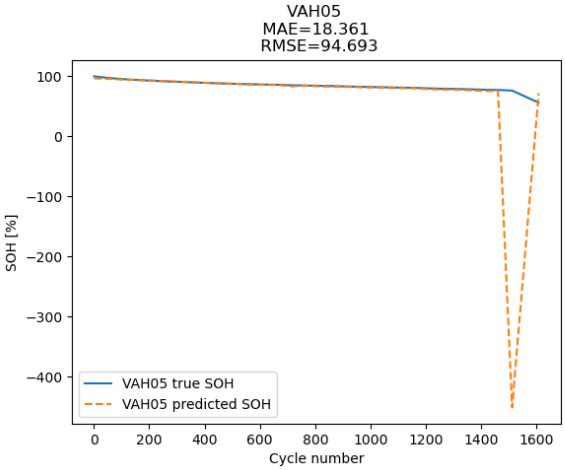

(c) Predicted and true SOH, with MLP, in VAH05

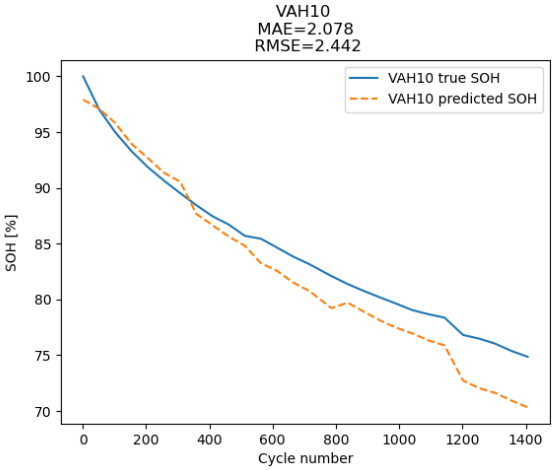

(d) Predicted and true SOH, with MLP, in VAH10

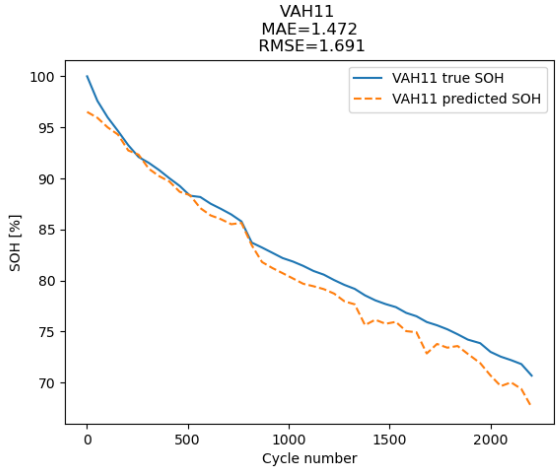

(e) Predicted and true SOH, with MLP, in VAH11

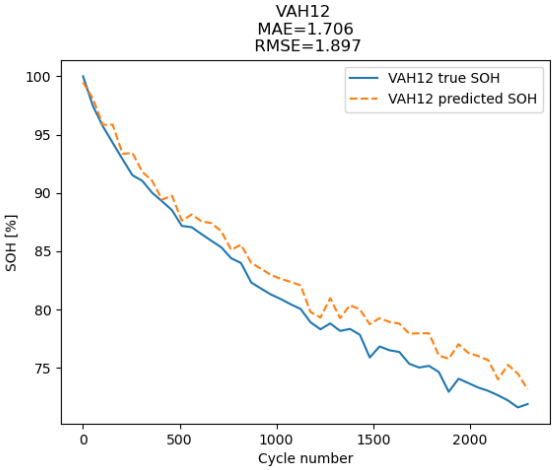

(f) Predicted and true SOH, with MLP, in VAH12

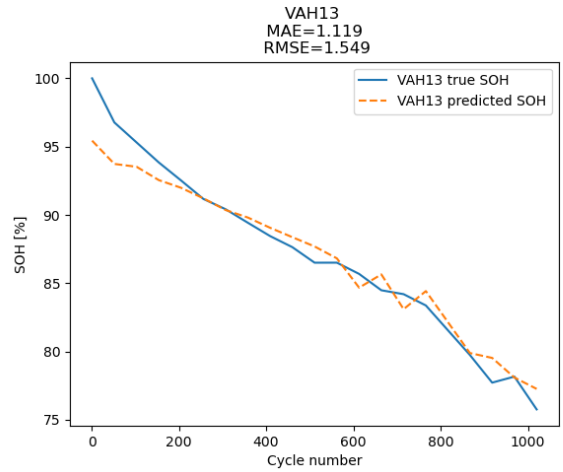

(g) Predicted and true SOH, with MLP, in VAH13

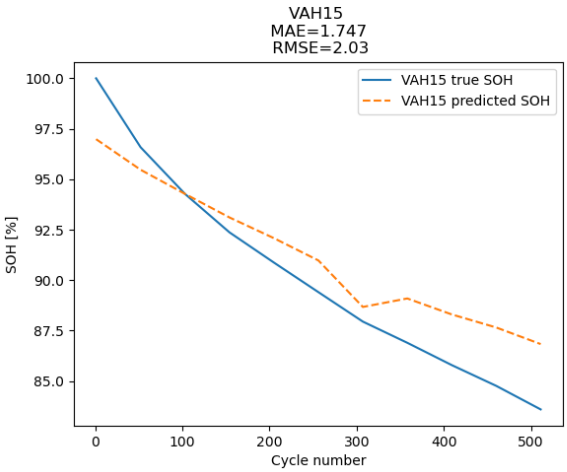

(h) Predicted and true SOH, with MLP, in VAH15

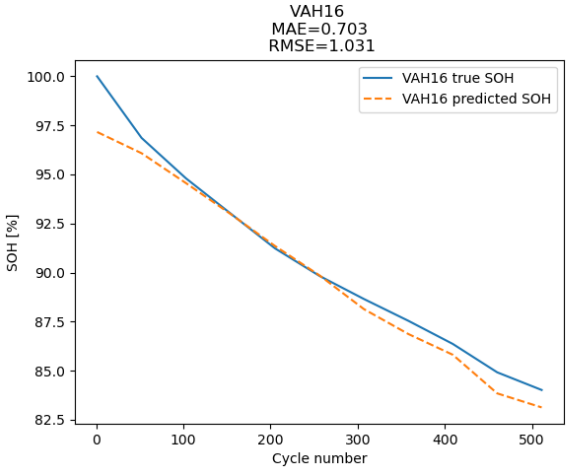

(i) Predicted and true SOH, with MLP, in VAH16

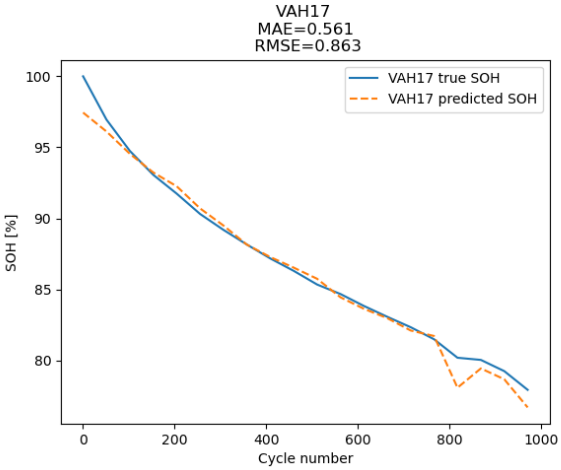

(j) Predicted and true SOH, with MLP, in VAH17

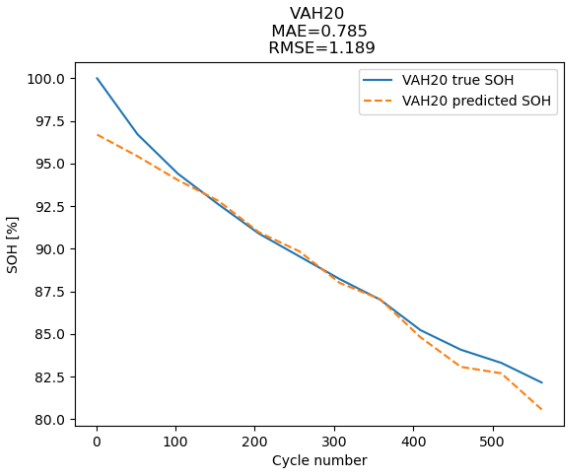

(k) Predicted and true SOH, with MLP, in VAH20

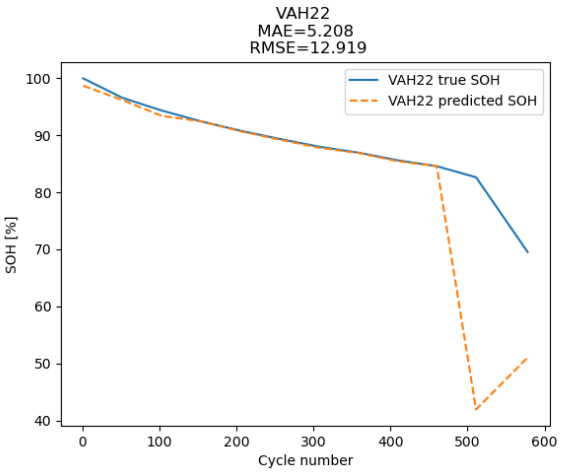

(l) Predicted and true SOH, with MLP, in VAH22

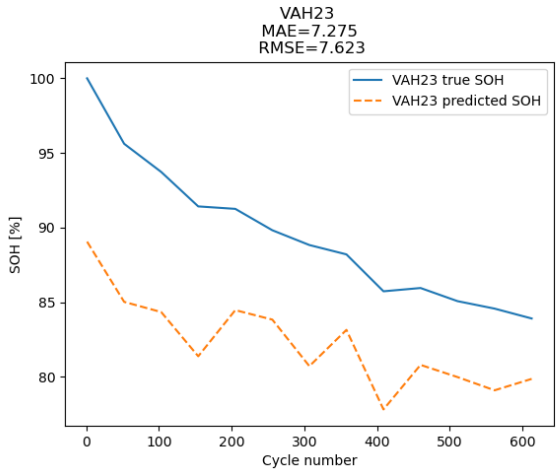

(m) Predicted and true SOH, with MLP, in VAH23

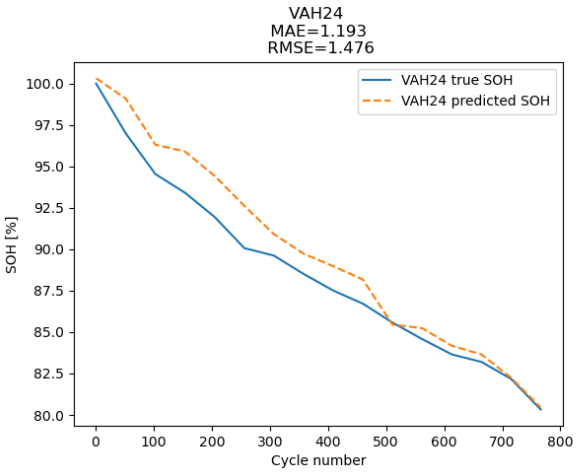

(n) Predicted and true SOH, with MLP, in VAH24

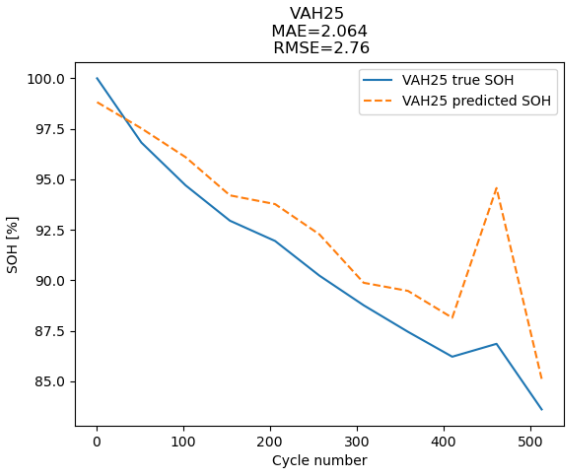

(o) Predicted and true SOH, with MLP, in VAH25

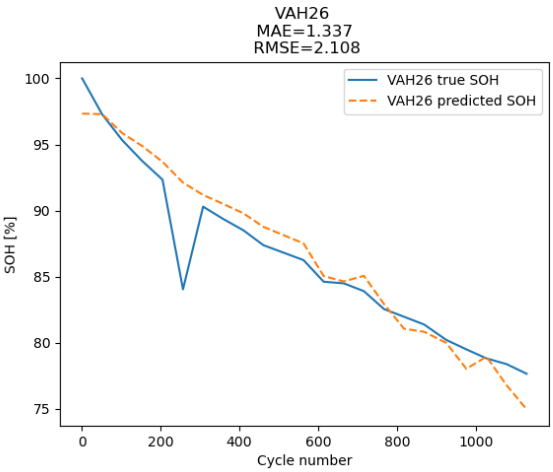

(p) Predicted and true SOH, with MLP, in VAH26

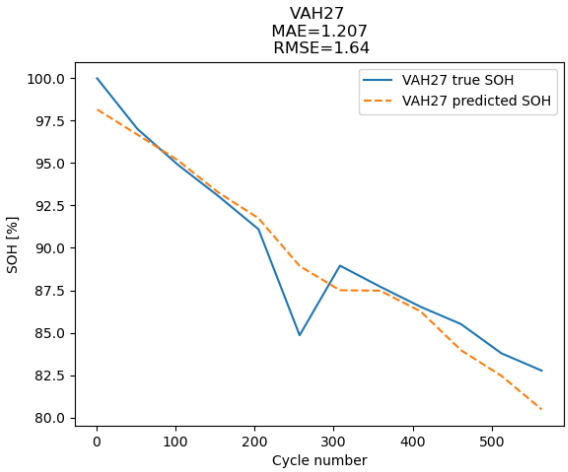

(q) Predicted and true SOH, with MLP, in VAH27

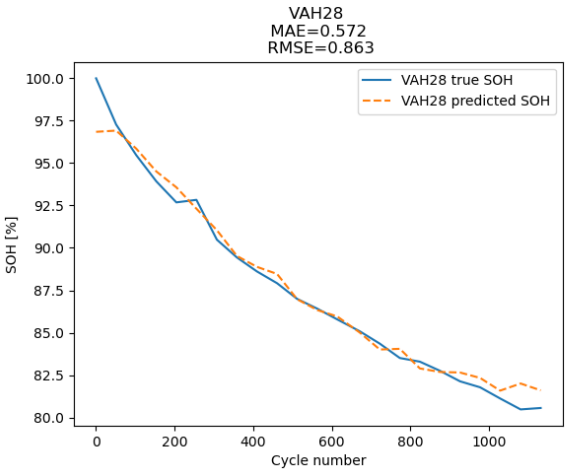

(r) Predicted and true SOH, with MLP, in VAH28

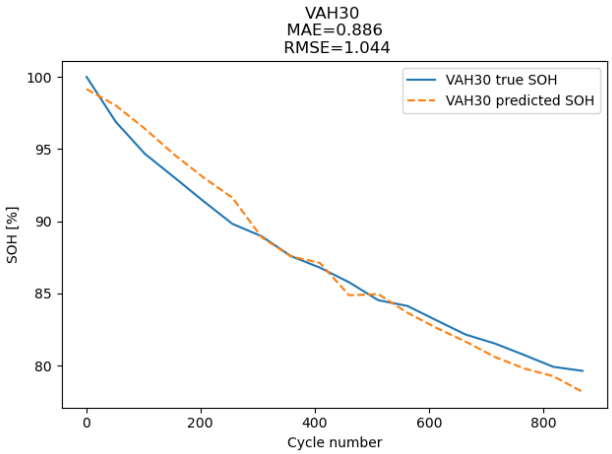

(s) Predicted and true SOH, with MLP, in VAH30

Figure 25: The results of MLP for SOH

G Appendix 7

In Table 10, the predicted and true SOH can be seen within a specific mission profile using SVR. The SOH is determined at every capacity test, and the results are given for every 5^{th} capacity test. It can be seen that the predicted SOH for the first capacity is never 100%. It can be seen in Table 10 that VAH24 has an initial predicted SOH above 100%. Besides, it can be seen in Table 10 that the predicted SOH at the 30^{th} capacity test is above 100% for VAH05. The visualisation of the predicted and true SOH for each mission profile is given in Appendix B. Figure 21(c) shows that the SOH is predicted in the opposite direction, then the true SOH.

		Capacity Test										
		1^{st} [%]	5^{th} [%]	10^{th} [%]	15^{th} [%]	20^{th} [%]	25^{th} [%]	30^{th} [%]	35^{th} [%]	40^{th} [%]	45^{th} [%]	Last [%]
VAH01	Predicted SOH	96.50%	91.40%	86.68%	81.00%	N.A.	N.A.	N.A.	N.A.	N.A.	N.A.	77.97% [$17^{th}test$]
	True SOH	100.00%	91.85%	86.83%	82.66%	N.A.	N.A.	N.A.	N.A.	N.A.	N.A.	80.98% [$17^{th}test$]
VAH02	Predicted SOH	97.40%	91.87%	86.13%	N.A.	N.A.	N.A.	N.A.	N.A.	N.A.	N.A.	81.42% [$13^{th}test$]
	True SOH	100%	91.14%	85.52%	N.A.	N.A.	N.A.	N.A.	N.A.	N.A.	N.A.	82.34% [$13^{th}test$]
VAH05	Predicted SOH	97.17%	93.63%	88.55%	83.80%	81.34%	77.16%	115.31%	N.A.	N.A.	N.A.	71.08% [$31^{th}test$]
	True SOH	100%	92.84%	88.22%	85.14%	82.53%	79.33%	76.29%	N.A.	N.A.	N.A.	56.21% [$31^{th}test$]
VAH10	Predicted SOH	97.36%	92.48%	86.74%	82.91%	80.25%	75.79%	N.A.	N.A.	N.A.	N.A.	74.38% [$28^{th}test$]
	True SOH	100%	91.87%	86.72%	83.16%	79.63%	76.49%	N.A.	N.A.	N.A.	N.A.	74.87% [$28^{th}test$]
VAH11	Predicted SOH	98.51%	95.40%	91.80%	88.86%	84.15%	82.08%	79.22%	77.08%	73.87%	N.A.	70.43% [$44^{th}test$]
	True SOH	100%	93.25%	89.26%	86.48%	82.20%	80.05%	77.70%	75.62%	73.01%	N.A.	70.69% [$44^{th}test$]
VAH12	Predicted SOH	98.67%	93.78%	90.83%	87.71%	84.03%	81.77%	80.96%	79.12%	77.50%	75.20%	74.42% [$46^{th}test$]
	True SOH	100%	92.89%	88.53%	85.34%	81.28%	78.31%	75.89%	75.03%	73.69%	71.61%	71.89% [$46^{th}test$]
VAH13	Predicted SOH	97.64%	93.34%	88.21%	82.61%	N.A.	N.A.	N.A.	N.A.	N.A.	N.A.	74.26% [$20^{th}test$]
	True SOH	100%	92.52%	87.64%	84.20%	N.A.	N.A.	N.A.	N.A.	N.A.	N.A.	75.76% [$20^{th}test$]
VAH15	Predicted SOH	97.21%	91.68%	85.97%	N.A.	N.A.	N.A.	N.A.	N.A.	N.A.	N.A.	84.85% [$11^{th}test$]
	True SOH	100%	90.87%	84.76%	N.A.	N.A.	N.A.	N.A.	N.A.	N.A.	N.A.	83.59% [$11^{th}test$]
VAH16	Predicted SOH	96.60%	91.97%	85.07%	N.A.	N.A.	N.A.	N.A.	N.A.	N.A.	N.A.	83.73% [$11^{th}test$]
	True SOH	100%	91.24%	84.92%	N.A.	N.A.	N.A.	N.A.	N.A.	N.A.	N.A.	84.02% [$11^{th}test$]
VAH17	Predicted SOH	96.74%	92.39%	87.55%	83.68%	N.A.	N.A.	N.A.	N.A.	N.A.	N.A.	79.71% [$20^{th}test$]
	True SOH	100%	91.74%	86.31%	82.34%	N.A.	N.A.	N.A.	N.A.	N.A.	N.A.	77.93% [$20^{th}test$]
VAH20	Predicted SOH	96.51%	91.61%	85.76%	N.A.	N.A.	N.A.	N.A.	N.A.	N.A.	N.A.	82.34% [$12^{th}test$]
	True SOH	100%	90.89%	84.08%	N.A.	N.A.	N.A.	N.A.	N.A.	N.A.	N.A.	82.15% [$12^{th}test$]
VAH22	Predicted SOH	97.23%	91.04%	85.15%	N.A.	N.A.	N.A.	N.A.	N.A.	N.A.	N.A.	73.61% [$12^{th}test$]
	True SOH	100%	90.82%	84.59%	N.A.	N.A.	N.A.	N.A.	N.A.	N.A.	N.A.	69.53% [$12^{th}test$]
VAH23	Predicted SOH	93.12%	91.14%	88.54%	N.A.	N.A.	N.A.	N.A.	N.A.	N.A.	N.A.	86.78% [$13^{th}test$]
	True SOH	100%	91.25%	85.95%	N.A.	N.A.	N.A.	N.A.	N.A.	N.A.	N.A.	83.91% [$13^{th}test$]
VAH24	Predicted SOH	101.79%	96.92%	90.96%	85.02%	N.A.	N.A.	N.A.	N.A.	N.A.	N.A.	84.25% [$16^{th}test$]
	True SOH	100%	91.95%	86.72%	82.18%	N.A.	N.A.	N.A.	N.A.	N.A.	N.A.	80.33% [$16^{th}test$]
VAH25	Predicted SOH	97.07%	92.21%	91.19%	N.A.	N.A.	N.A.	N.A.	N.A.	N.A.	N.A.	83.40% [$11^{th}test$]
	True SOH	100%	91.94%	86.85%	N.A.	N.A.	N.A.	N.A.	N.A.	N.A.	N.A.	83.60% [$11^{th}test$]
VAH26	Predicted SOH	96.40%	93.11%	88.44%	82.62%	77.72%	N.A.	N.A.	N.A.	N.A.	N.A.	73.75% [$22^{th}test$]
	True SOH	100%	92.34%	87.38%	82.55%	78.82%	N.A.	N.A.	N.A.	N.A.	N.A.	77.66% [$22^{th}test$]
VAH27	Predicted SOH	96.70%	91.97%	84.66%	N.A.	N.A.	N.A.	N.A.	N.A.	N.A.	N.A.	80.92% [$12^{th}test$]
	True SOH	100%	91.10%	85.51%	N.A.	N.A.	N.A.	N.A.	N.A.	N.A.	N.A.	82.76% [$12^{th}test$]
VAH28	Predicted SOH	96.16%	93.12%	88.60%	84.26%	82.10%	N.A.	N.A.	N.A.	N.A.	N.A.	81.05% [$23^{th}test$]
	True SOH	100%	92.68%	87.92%	84.36%	81.78%	N.A.	N.A.	N.A.	N.A.	N.A.	80.56% [$23^{th}test$]
VAH30	Predicted SOH	97.42%	92.37%	85.63%	81.82%	N.A.	N.A.	N.A.	N.A.	N.A.	N.A.	79.41% [$18^{th}test$]
	True SOH	100%	91.40%	85.77%	81.52%	N.A.	N.A.	N.A.	N.A.	N.A.	N.A.	79.63% [$18^{th}test$]

Table 10: Results SOH [%] with SVR

In Table 11, the true and predicted SOH for each mission profile can be seen using RF regression. The results are given for every 5^{th} capacity test. Additionally, Table 11 shows a column with the SOH for the last capacity test present in the mission profile. In Table 11 it can be seen that the predicted SOH for the first capacity test is never above 100%, which happened with SVR for VAH24. In Appendix C, the plots of the predicted and true SOH for each mission profile are shown.

		Capacity Test										
		1^{st} [%]	5^{th} [%]	10^{th} [%]	15^{th} [%]	20^{th} [%]	25^{th} [%]	30^{th} [%]	35^{th} [%]	40^{th} [%]	45^{th} [%]	Last [%]
VAH01	Predicted SOH	96.90%	91.31%	85.93%	80.89%	N.A.	N.A.	N.A.	N.A.	N.A.	N.A.	78.32% [$17^{th}test$]
	True SOH	100.00%	91.85%	86.83%	82.66%	N.A.	N.A.	N.A.	N.A.	N.A.	N.A.	80.98% [$17^{th}test$]
VAH02	Predicted SOH	98.36%	91.88%	85.15%	N.A.	N.A.	N.A.	N.A.	N.A.	N.A.	N.A.	80.68% [$13^{th}test$]
	True SOH	100%	91.14%	85.52%	N.A.	N.A.	N.A.	N.A.	N.A.	N.A.	N.A.	82.34% [$13^{th}test$]
VAH05	Predicted SOH	98.42%	94.37%	88.52%	84.31%	82.25%	77.85%	88.98%	N.A.	N.A.	N.A.	72.50% [$31^{th}test$]
	True SOH	100%	92.84%	88.22%	85.14%	82.53%	79.33%	76.29%	N.A.	N.A.	N.A.	56.21% [$31^{th}test$]
VAH10	Predicted SOH	97.82%	92.99%	87.24%	83.71%	80.68%	77.32%	N.A.	N.A.	N.A.	N.A.	76.04% [$28^{th}test$]
	True SOH	100%	91.87%	86.72%	83.16%	79.63%	76.49%	N.A.	N.A.	N.A.	N.A.	74.87% [$28^{th}test$]
VAH11	Predicted SOH	98.69%	93.94%	91.62%	88.09%	84.74%	81.42%	78.86%	76.32%	71.81%	N.A.	70.56% [$44^{th}test$]
	True SOH	100%	93.25%	89.26%	86.48%	82.20%	80.05%	77.70%	75.62%	73.01%	N.A.	70.69% [$44^{th}test$]
VAH12	Predicted SOH	99.19%	92.01%	88.26%	84.96%	80.78%	79.33%	77.96%	75.19%	73.54%	70.68%	71.11% [$46^{th}test$]
	True SOH	100%	92.89%	88.53%	85.34%	81.28%	78.31%	75.89%	75.03%	73.69%	71.61%	71.89% [$46^{th}test$]
VAH13	Predicted SOH	99.12%	92.96%	88.04%	82.87%	N.A.	N.A.	N.A.	N.A.	N.A.	N.A.	74.66% [$20^{th}test$]
	True SOH	100%	92.52%	87.64%	84.20%	N.A.	N.A.	N.A.	N.A.	N.A.	N.A.	75.76% [$20^{th}test$]
VAH15	Predicted SOH	98.72%	90.69%	84.93%	N.A.	N.A.	N.A.	N.A.	N.A.	N.A.	N.A.	83.39% [$11^{th}test$]
	True SOH	100%	90.87%	84.76%	N.A.	N.A.	N.A.	N.A.	N.A.	N.A.	N.A.	83.59% [$11^{th}test$]
VAH16	Predicted SOH	96.81%	91.97%	83.91%	N.A.	N.A.	N.A.	N.A.	N.A.	N.A.	N.A.	82.00% [$11^{th}test$]
	True SOH	100%	91.24%	84.92%	N.A.	N.A.	N.A.	N.A.	N.A.	N.A.	N.A.	84.02% [$11^{th}test$]
VAH17	Predicted SOH	98.84%	91.75%	86.78%	83.10%	N.A.	N.A.	N.A.	N.A.	N.A.	N.A.	78.18% [$20^{th}test$]
	True SOH	100%	91.74%	86.31%	82.34%	N.A.	N.A.	N.A.	N.A.	N.A.	N.A.	77.93% [$20^{th}test$]
VAH20	Predicted SOH	95.91%	89.48%	81.49%	N.A.	N.A.	N.A.	N.A.	N.A.	N.A.	N.A.	77.26% [$12^{th}test$]
	True SOH	100%	90.89%	84.08%	N.A.	N.A.	N.A.	N.A.	N.A.	N.A.	N.A.	82.15% [$12^{th}test$]
VAH22	Predicted SOH	98.96%	90.38%	84.48%	N.A.	N.A.	N.A.	N.A.	N.A.	N.A.	N.A.	80.21% [$12^{th}test$]
	True SOH	100%	90.82%	84.59%	N.A.	N.A.	N.A.	N.A.	N.A.	N.A.	N.A.	69.53% [$12^{th}test$]
VAH23	Predicted SOH	90.84%	89.19%	88.49%	N.A.	N.A.	N.A.	N.A.	N.A.	N.A.	N.A.	87.18% [$13^{th}test$]
	True SOH	100%	91.25%	85.95%	N.A.	N.A.	N.A.	N.A.	N.A.	N.A.	N.A.	83.91% [$13^{th}test$]
VAH24	Predicted SOH	98.82%	95.81%	87.32%	81.45%	N.A.	N.A.	N.A.	N.A.	N.A.	N.A.	81.43% [$16^{th}test$]
	True SOH	100%	91.95%	86.72%	82.18%	N.A.	N.A.	N.A.	N.A.	N.A.	N.A.	80.33% [$16^{th}test$]
VAH25	Predicted SOH	96.18%	90.17%	94.01%	N.A.	N.A.	N.A.	N.A.	N.A.	N.A.	N.A.	83.00% [$11^{th}test$]
	True SOH	100%	91.94%	86.85%	N.A.	N.A.	N.A.	N.A.	N.A.	N.A.	N.A.	83.60% [$11^{th}test$]
VAH26	Predicted SOH	97.41%	92.42%	87.52%	81.47%	77.27%	N.A.	N.A.	N.A.	N.A.	N.A.	75.23% [$22^{th}test$]
	True SOH	100%	92.34%	87.38%	82.55%	78.82%	N.A.	N.A.	N.A.	N.A.	N.A.	77.66% [$22^{th}test$]
VAH27	Predicted SOH	99.12%	91.82%	84.73%	N.A.	N.A.	N.A.	N.A.	N.A.	N.A.	N.A.	81.37% [$12^{th}test$]
	True SOH	100%	91.10%	85.51%	N.A.	N.A.	N.A.	N.A.	N.A.	N.A.	N.A.	82.76% [$12^{th}test$]
VAH28	Predicted SOH	96.80%	91.82%	87.76%	83.71%	81.44%	N.A.	N.A.	N.A.	N.A.	N.A.	80.40% [$23^{th}test$]
	True SOH	100%	92.68%	87.92%	84.36%	81.78%	N.A.	N.A.	N.A.	N.A.	N.A.	80.56% [$23^{th}test$]
VAH30	Predicted SOH	98.20%	93.99%	87.79%	83.87%	N.A.	N.A.	N.A.	N.A.	N.A.	N.A.	81.22% [$18^{th}test$]
	True SOH	100%	91.40%	85.77%	81.52%	N.A.	N.A.	N.A.	N.A.	N.A.	N.A.	79.63% [$18^{th}test$]

Table 11: Results SOH [%] with RF Regression

In Table 12, the true and predicted SOH for each mission profile can be seen using XGBoost. The results are given for every 5^{th} capacity test. Additionally, Table 12 shows a column with the SOH for the last capacity test present in the mission profile. In Table 12 it can be seen that the initial predicted SOH is often closer to 100%, compared to SVR. However, the initial predicted SOH is above 100% for four mission profiles, namely VAH12, VAH13, VAH15, and VAH17.

		Capacity Test										
		1^{st} [%]	5^{th} [%]	10^{th} [%]	15^{th} [%]	20^{th} [%]	25^{th} [%]	30^{th} [%]	35^{th} [%]	40^{th} [%]	45^{th} [%]	Last [%]
VAH01	Predicted SOH	98.49%	91.91%	86.38%	82.00%	N.A.	N.A.	N.A.	N.A.	N.A.	N.A.	77.46% [$17^{th}test$]
	True SOH	100.00%	91.85%	86.83%	82.66%	N.A.	N.A.	N.A.	N.A.	N.A.	N.A.	80.98% [$17^{th}test$]
VAH02	Predicted SOH	99.71%	93.37%	85.03%	N.A.	N.A.	N.A.	N.A.	N.A.	N.A.	N.A.	76.64% [$13^{th}test$]
	True SOH	100%	91.14%	85.52%	N.A.	N.A.	N.A.	N.A.	N.A.	N.A.	N.A.	82.34% [$13^{th}test$]
VAH05	Predicted SOH	99.71%	95.07%	88.16%	84.23%	81.23%	76.89%	88.84%	N.A.	N.A.	N.A.	71.75% [$31^{th}test$]
	True SOH	100%	92.84%	88.22%	85.14%	82.53%	79.33%	76.29%	N.A.	N.A.	N.A.	56.21% [$31^{th}test$]
VAH10	Predicted SOH	97.66%	92.18%	84.64%	83.85%	79.05%	77.59%	N.A.	N.A.	N.A.	N.A.	75.45% [$28^{th}test$]
	True SOH	100%	91.87%	86.72%	83.16%	79.63%	76.49%	N.A.	N.A.	N.A.	N.A.	74.87% [$28^{th}test$]
VAH11	Predicted SOH	99.54%	93.78%	91.55%	89.04%	84.30%	79.53%	79.06%	76.56%	71.70%	N.A.	62.54% [$44^{th}test$]
	True SOH	100%	93.25%	89.26%	86.48%	82.20%	80.05%	77.70%	75.62%	73.01%	N.A.	70.69% [$44^{th}test$]
VAH12	Predicted SOH	100.22%	90.52%	88.95%	85.32%	81.62%	79.70%	76.22%	75.50%	74.72%	74.09%	73.48% [$46^{th}test$]
	True SOH	100%	92.89%	88.53%	85.34%	81.28%	78.31%	75.89%	75.03%	73.69%	71.61%	71.89% [$46^{th}test$]
VAH13	Predicted SOH	100.72%	93.33%	88.17%	83.48%	N.A.	N.A.	N.A.	N.A.	N.A.	N.A.	73.56% [$20^{th}test$]
	True SOH	100%	92.52%	87.64%	84.20%	N.A.	N.A.	N.A.	N.A.	N.A.	N.A.	75.76% [$20^{th}test$]
VAH15	Predicted SOH	100.19%	92.47%	83.78%	N.A.	N.A.	N.A.	N.A.	N.A.	N.A.	N.A.	81.29% [$11^{th}test$]
	True SOH	100%	90.87%	84.76%	N.A.	N.A.	N.A.	N.A.	N.A.	N.A.	N.A.	83.59% [$11^{th}test$]
VAH16	Predicted SOH	98.14%	92.73%	85.02%	N.A.	N.A.	N.A.	N.A.	N.A.	N.A.	N.A.	85.43% [$11^{th}test$]
	True SOH	100%	91.24%	84.92%	N.A.	N.A.	N.A.	N.A.	N.A.	N.A.	N.A.	84.02% [$11^{th}test$]
VAH17	Predicted SOH	100.68%	91.56%	87.27%	84.57%	N.A.	N.A.	N.A.	N.A.	N.A.	N.A.	81.53% [$20^{th}test$]
	True SOH	100%	91.74%	86.31%	82.34%	N.A.	N.A.	N.A.	N.A.	N.A.	N.A.	77.93% [$20^{th}test$]
VAH20	Predicted SOH	99.48%	89.21%	82.51%	N.A.	N.A.	N.A.	N.A.	N.A.	N.A.	N.A.	78.11% [$12^{th}test$]
	True SOH	100%	90.89%	84.08%	N.A.	N.A.	N.A.	N.A.	N.A.	N.A.	N.A.	82.15% [$12^{th}test$]
VAH22	Predicted SOH	99.17%	89.52%	84.08%	N.A.	N.A.	N.A.	N.A.	N.A.	N.A.	N.A.	83.22% [$12^{th}test$]
	True SOH	100%	90.82%	84.59%	N.A.	N.A.	N.A.	N.A.	N.A.	N.A.	N.A.	69.53% [$12^{th}test$]
VAH23	Predicted SOH	91.44%	90.59%	88.36%	N.A.	N.A.	N.A.	N.A.	N.A.	N.A.	N.A.	86.27% [$13^{th}test$]
	True SOH	100%	91.25%	85.95%	N.A.	N.A.	N.A.	N.A.	N.A.	N.A.	N.A.	83.91% [$13^{th}test$]
VAH24	Predicted SOH	99.15%	95.21%	90.33%	83.66%	N.A.	N.A.	N.A.	N.A.	N.A.	N.A.	82.64% [$16^{th}test$]
	True SOH	100%	91.95%	86.72%	82.18%	N.A.	N.A.	N.A.	N.A.	N.A.	N.A.	80.33% [$16^{th}test$]
VAH25	Predicted SOH	96.19%	90.05%	92.86%	N.A.	N.A.	N.A.	N.A.	N.A.	N.A.	N.A.	82.38% [$11^{th}test$]
	True SOH	100%	91.94%	86.85%	N.A.	N.A.	N.A.	N.A.	N.A.	N.A.	N.A.	83.60% [$11^{th}test$]
VAH26	Predicted SOH	98.39%	93.06%	87.81%	81.86%	78.73%	N.A.	N.A.	N.A.	N.A.	N.A.	76.40% [$22^{th}test$]
	True SOH	100%	92.34%	87.38%	82.55%	78.82%	N.A.	N.A.	N.A.	N.A.	N.A.	77.66% [$22^{th}test$]
VAH27	Predicted SOH	99.86%	93.03%	85.70%	N.A.	N.A.	N.A.	N.A.	N.A.	N.A.	N.A.	80.88% [$12^{th}test$]
	True SOH	100%	91.10%	85.51%	N.A.	N.A.	N.A.	N.A.	N.A.	N.A.	N.A.	82.76% [$12^{th}test$]
VAH28	Predicted SOH	98.71%	92.93%	87.47%	85.40%	82.13%	N.A.	N.A.	N.A.	N.A.	N.A.	82.42% [$23^{th}test$]
	True SOH	100%	92.68%	87.92%	84.36%	81.78%	N.A.	N.A.	N.A.	N.A.	N.A.	80.56% [$23^{th}test$]
VAH30	Predicted SOH	98.90%	92.30%	86.63%	81.25%	N.A.	N.A.	N.A.	N.A.	N.A.	N.A.	79.37% [$18^{th}test$]
	True SOH	100%	91.40%	85.77%	81.52%	N.A.	N.A.	N.A.	N.A.	N.A.	N.A.	79.63% [$18^{th}test$]

Table 12: Results SOH [%] with XGBoost

In Table 13, the true and predicted SOH for every 5^{th} capacity test can be seen using GPR. Moreover, there is one column that presents the predicted and true SOH for the last capacity test. From Table 13, it can be seen that the initial predicted SOH are close to 100%. Table 13 presents that the predicted SOH at the 30^{th} capacity test in VAH05 is above 100%, which also happened with the SVR.

		Capacity Test										
		1^{st} [%]	5^{th} [%]	10^{th} [%]	15^{th} [%]	20^{th} [%]	25^{th} [%]	30^{th} [%]	35^{th} [%]	40^{th} [%]	45^{th} [%]	Last [%]
VAH01	Predicted SOH	96.99%	91.37%	86.68%	80.74%	N.A.	N.A.	N.A.	N.A.	N.A.	N.A.	77.45% [$17^{th}test$]
	True SOH	100.00%	91.85%	86.83%	82.66%	N.A.	N.A.	N.A.	N.A.	N.A.	N.A.	80.98% [$17^{th}test$]
VAH02	Predicted SOH	97.71%	91.27%	85.97%	N.A.	N.A.	N.A.	N.A.	N.A.	N.A.	N.A.	81.12% [$13^{th}test$]
	True SOH	100%	91.14%	85.52%	N.A.	N.A.	N.A.	N.A.	N.A.	N.A.	N.A.	82.34% [$13^{th}test$]
VAH05	Predicted SOH	97.54%	93.82%	88.61%	83.72%	81.58%	77.67%	127.96%	N.A.	N.A.	N.A.	71.55% [$31^{th}test$]
	True SOH	100%	92.84%	88.22%	85.14%	82.53%	79.33%	76.29%	N.A.	N.A.	N.A.	56.21% [$31^{th}test$]
VAH10	Predicted SOH	97.54%	92.38%	86.39%	82.41%	79.73%	75.08%	N.A.	N.A.	N.A.	N.A.	73.63% [$28^{th}test$]
	True SOH	100%	91.87%	86.72%	83.16%	79.63%	76.49%	N.A.	N.A.	N.A.	N.A.	74.87% [$28^{th}test$]
VAH11	Predicted SOH	98.26%	94.98%	91.34%	88.38%	83.67%	81.58%	78.67%	76.47%	73.03%	N.A.	69.10% [$44^{th}test$]
	True SOH	100%	93.25%	89.26%	86.48%	82.20%	80.05%	77.70%	75.62%	73.01%	N.A.	70.69% [$44^{th}test$]
VAH12	Predicted SOH	99.46%	94.33%	91.55%	88.57%	85.04%	82.29%	81.58%	80.02%	78.31%	75.87%	74.99% [$46^{th}test$]
	True SOH	100%	92.89%	88.53%	85.34%	81.28%	78.31%	75.89%	75.03%	73.69%	71.61%	71.89% [$46^{th}test$]
VAH13	Predicted SOH	98.18%	93.54%	88.05%	82.47%	N.A.	N.A.	N.A.	N.A.	N.A.	N.A.	73.98% [$20^{th}test$]
	True SOH	100%	92.52%	87.64%	84.20%	N.A.	N.A.	N.A.	N.A.	N.A.	N.A.	75.76% [$20^{th}test$]
VAH15	Predicted SOH	97.63%	91.51%	85.66%	N.A.	N.A.	N.A.	N.A.	N.A.	N.A.	N.A.	84.61% [$11^{th}test$]
	True SOH	100%	90.87%	84.76%	N.A.	N.A.	N.A.	N.A.	N.A.	N.A.	N.A.	83.59% [$11^{th}test$]
VAH16	Predicted SOH	96.90%	91.79%	84.67%	N.A.	N.A.	N.A.	N.A.	N.A.	N.A.	N.A.	83.35% [$11^{th}test$]
	True SOH	100%	91.24%	84.92%	N.A.	N.A.	N.A.	N.A.	N.A.	N.A.	N.A.	84.02% [$11^{th}test$]
VAH17	Predicted SOH	97.08%	92.35%	87.28%	83.20%	N.A.	N.A.	N.A.	N.A.	N.A.	N.A.	78.83% [$20^{th}test$]
	True SOH	100%	91.74%	86.31%	82.34%	N.A.	N.A.	N.A.	N.A.	N.A.	N.A.	77.93% [$20^{th}test$]
VAH20	Predicted SOH	96.64%	91.39%	85.26%	N.A.	N.A.	N.A.	N.A.	N.A.	N.A.	N.A.	81.55% [$12^{th}test$]
	True SOH	100%	90.89%	84.08%	N.A.	N.A.	N.A.	N.A.	N.A.	N.A.	N.A.	82.15% [$12^{th}test$]
VAH22	Predicted SOH	97.85%	91.14%	84.86%	N.A.	N.A.	N.A.	N.A.	N.A.	N.A.	N.A.	67.81% [$12^{th}test$]
	True SOH	100%	90.82%	84.59%	N.A.	N.A.	N.A.	N.A.	N.A.	N.A.	N.A.	69.53% [$12^{th}test$]
VAH23	Predicted SOH	94.48%	92.15%	89.24%	N.A.	N.A.	N.A.	N.A.	N.A.	N.A.	N.A.	87.30% [$13^{th}test$]
	True SOH	100%	91.25%	85.95%	N.A.	N.A.	N.A.	N.A.	N.A.	N.A.	N.A.	83.91% [$13^{th}test$]
VAH24	Predicted SOH	102.83%	97.56%	91.34%	84.94%	N.A.	N.A.	N.A.	N.A.	N.A.	N.A.	83.61% [$16^{th}test$]
	True SOH	100%	91.95%	86.72%	82.18%	N.A.	N.A.	N.A.	N.A.	N.A.	N.A.	80.33% [$16^{th}test$]
VAH25	Predicted SOH	97.50%	92.23%	90.71%	N.A.	N.A.	N.A.	N.A.	N.A.	N.A.	N.A.	82.86% [$11^{th}test$]
	True SOH	100%	91.94%	86.85%	N.A.	N.A.	N.A.	N.A.	N.A.	N.A.	N.A.	83.60% [$11^{th}test$]
VAH26	Predicted SOH	96.64%	93.08%	88.21%	82.25%	77.11%	N.A.	N.A.	N.A.	N.A.	N.A.	72.51% [$22^{th}test$]
	True SOH	100%	92.34%	87.38%	82.55%	78.82%	N.A.	N.A.	N.A.	N.A.	N.A.	77.66% [$22^{th}test$]
VAH27	Predicted SOH	97.10%	91.97%	84.22%	N.A.	N.A.	N.A.	N.A.	N.A.	N.A.	N.A.	80.07% [$12^{th}test$]
	True SOH	100%	91.10%	85.51%	N.A.	N.A.	N.A.	N.A.	N.A.	N.A.	N.A.	82.76% [$12^{th}test$]
VAH28	Predicted SOH	96.38%	93.08%	88.47%	84.13%	81.89%	N.A.	N.A.	N.A.	N.A.	N.A.	80.80% [$23^{th}test$]
	True SOH	100%	92.68%	87.92%	84.36%	81.78%	N.A.	N.A.	N.A.	N.A.	N.A.	80.56% [$23^{th}test$]
VAH30	Predicted SOH	97.74%	92.59%	85.61%	81.86%	N.A.	N.A.	N.A.	N.A.	N.A.	N.A.	79.39% [$18^{th}test$]
	True SOH	100%	91.40%	85.77%	81.52%	N.A.	N.A.	N.A.	N.A.	N.A.	N.A.	79.63% [$18^{th}test$]

Table 13: Results SOH [%] with GPR

In Table 14, the true and predicted SOH for every 5^{th} capacity test can be seen using MLP. Additionally, there is one column that gives the true and predicted SOH for the last capacity test. Table 14 shows that at the 30^{th} capacity test of VAH05 the SOH is predicted at -450.67%.

		Capacity Test										
		1^{st} [%]	5^{th} [%]	10^{th} [%]	15^{th} [%]	20^{th} [%]	25^{th} [%]	30^{th} [%]	35^{th} [%]	40^{th} [%]	45^{th} [%]	Last [%]
VAH01	Predicted SOH	96.50%	90.33%	85.63%	80.04%	N.A.	N.A.	N.A.	N.A.	N.A.	N.A.	77.41% [$17^{th}test$]
	True SOH	100.00%	91.85%	86.83%	82.66%	N.A.	N.A.	N.A.	N.A.	N.A.	N.A.	80.98% [$17^{th}test$]
VAH02	Predicted SOH	95.77%	91.97%	87.68%	N.A.	N.A.	N.A.	N.A.	N.A.	N.A.	N.A.	83.38% [$13^{th}test$]
	True SOH	100%	91.14%	85.52%	N.A.	N.A.	N.A.	N.A.	N.A.	N.A.	N.A.	82.34% [$13^{th}test$]
VAH05	Predicted SOH	96.46%	93.14%	88.10%	83.24%	81.77%	77.88%	-450.67%	N.A.	N.A.	N.A.	71.94% [$31^{th}test$]
	True SOH	100%	92.84%	88.22%	85.14%	82.53%	79.33%	76.29%	N.A.	N.A.	N.A.	56.21% [$31^{th}test$]
VAH10	Predicted SOH	97.91%	92.68%	85.64%	80.76%	77.48%	72.05%	N.A.	N.A.	N.A.	N.A.	70.33% [$28^{th}test$]
	True SOH	100%	91.87%	86.72%	83.16%	79.63%	76.49%	N.A.	N.A.	N.A.	N.A.	74.87% [$28^{th}test$]
VAH11	Predicted SOH	96.51%	92.74%	88.69%	85.52%	80.72%	78.72%	75.76%	73.79%	70.70%	N.A.	67.58% [$44^{th}test$]
	True SOH	100%	93.25%	89.26%	86.48%	82.20%	80.05%	77.70%	75.62%	73.01%	N.A.	70.69% [$44^{th}test$]
VAH12	Predicted SOH	99.49%	93.36%	89.77%	86.71%	82.96%	79.31%	78.74%	77.95%	76.28%	74.50%	73.16% [$46^{th}test$]
	True SOH	100%	92.89%	88.53%	85.34%	81.28%	78.31%	75.89%	75.03%	73.69%	71.61%	71.89% [$46^{th}test$]
VAH13	Predicted SOH	95.44%	91.99%	88.37%	83.10%	N.A.	N.A.	N.A.	N.A.	N.A.	N.A.	77.27% [$20^{th}test$]
	True SOH	100%	92.52%	87.64%	84.20%	N.A.	N.A.	N.A.	N.A.	N.A.	N.A.	75.76% [$20^{th}test$]
VAH15	Predicted SOH	96.98%	92.08%	87.65%	N.A.	N.A.	N.A.	N.A.	N.A.	N.A.	N.A.	86.83% [$11^{th}test$]
	True SOH	100%	90.87%	84.76%	N.A.	N.A.	N.A.	N.A.	N.A.	N.A.	N.A.	83.59% [$11^{th}test$]
VAH16	Predicted SOH	97.16%	91.36%	83.84%	N.A.	N.A.	N.A.	N.A.	N.A.	N.A.	N.A.	83.13% [$11^{th}test$]
	True SOH	100%	91.24%	84.92%	N.A.	N.A.	N.A.	N.A.	N.A.	N.A.	N.A.	84.02% [$11^{th}test$]
VAH17	Predicted SOH	97.45%	92.26%	86.53%	82.11%	N.A.	N.A.	N.A.	N.A.	N.A.	N.A.	76.69% [$20^{th}test$]
	True SOH	100%	91.74%	86.31%	82.34%	N.A.	N.A.	N.A.	N.A.	N.A.	N.A.	77.93% [$20^{th}test$]
VAH20	Predicted SOH	96.70%	90.97%	83.07%	N.A.	N.A.	N.A.	N.A.	N.A.	N.A.	N.A.	80.57% [$12^{th}test$]
	True SOH	100%	90.89%	84.08%	N.A.	N.A.	N.A.	N.A.	N.A.	N.A.	N.A.	82.15% [$12^{th}test$]
VAH22	Predicted SOH	98.70%	90.73%	84.61%	N.A.	N.A.	N.A.	N.A.	N.A.	N.A.	N.A.	51.02% [$12^{th}test$]
	True SOH	100%	90.82%	84.59%	N.A.	N.A.	N.A.	N.A.	N.A.	N.A.	N.A.	69.53% [$12^{th}test$]
VAH23	Predicted SOH	89.06%	84.47%	80.80%	N.A.	N.A.	N.A.	N.A.	N.A.	N.A.	N.A.	79.86% [$13^{th}test$]
	True SOH	100%	91.25%	85.95%	N.A.	N.A.	N.A.	N.A.	N.A.	N.A.	N.A.	83.91% [$13^{th}test$]
VAH24	Predicted SOH	100.32%	94.43%	88.17%	82.25%	N.A.	N.A.	N.A.	N.A.	N.A.	N.A.	80.45% [$16^{th}test$]
	True SOH	100%	91.95%	86.72%	82.18%	N.A.	N.A.	N.A.	N.A.	N.A.	N.A.	80.33% [$16^{th}test$]
VAH25	Predicted SOH	98.82%	93.77%	94.57%	N.A.	N.A.	N.A.	N.A.	N.A.	N.A.	N.A.	85.12% [$11^{th}test$]
	True SOH	100%	91.94%	86.85%	N.A.	N.A.	N.A.	N.A.	N.A.	N.A.	N.A.	83.60% [$11^{th}test$]
VAH26	Predicted SOH	97.33%	93.69%	88.77%	82.94%	78.95%	N.A.	N.A.	N.A.	N.A.	N.A.	74.96% [$22^{th}test$]
	True SOH	100%	92.34%	87.38%	82.55%	78.82%	N.A.	N.A.	N.A.	N.A.	N.A.	77.66% [$22^{th}test$]
VAH27	Predicted SOH	98.16%	91.75%	83.97%	N.A.	N.A.	N.A.	N.A.	N.A.	N.A.	N.A.	80.47% [$12^{th}test$]
	True SOH	100%	91.10%	85.51%	N.A.	N.A.	N.A.	N.A.	N.A.	N.A.	N.A.	82.76% [$12^{th}test$]
VAH28	Predicted SOH	96.85%	93.57%	88.46%	84.01%	82.33%	N.A.	N.A.	N.A.	N.A.	N.A.	81.60% [$23^{th}test$]
	True SOH	100%	92.68%	87.92%	84.36%	81.78%	N.A.	N.A.	N.A.	N.A.	N.A.	80.56% [$23^{th}test$]
VAH30	Predicted SOH	99.15%	93.04%	84.87%	80.59%	N.A.	N.A.	N.A.	N.A.	N.A.	N.A.	78.18% [$18^{th}test$]
	True SOH	100%	91.40%	85.77%	81.52%	N.A.	N.A.	N.A.	N.A.	N.A.	N.A.	79.63% [$18^{th}test$]

Table 14: Results SOH [%] with MLP

H Appendix 8

In Table 15 the predicted and true RUL can be seen within a specific mission profile using SVR. The RUL is determined at every capacity test, but the results in the table are given for every 3^{rd} capacity test to reduce space. In Table 15 it can be seen that the difference between the predicted RUL and true RUL for the last capacity test is significantly high. Moreover, it can be seen that for VAH01, VAH02, and VAH27 the predicted RUL is negative at the end.

		Capacity Test								
		1^{st} [#missions]	3^{rd} [#missions]	5^{th} [#missions]	7^{th} [#missions]	9^{th} [#missions]	11^{th} [#missions]	13^{th} [#missions]	15^{th} [#missions]	Last [#missions]
VAH01	Predicted RUL	465	423	335	270	56	-1	N.A.	N.A.	-65 [$12^{th}test$]
	True RUL	612	510	408	306	204	102	N.A.	N.A.	51 [$12^{th}test$]
VAH02	Predicted RUL	460	407	315	241	52	N.A.	N.A.	N.A.	-35 [$10^{th}test$]
	True RUL	510	408	306	204	102	N.A.	N.A.	N.A.	51 [$10^{th}test$]
VAH05	Predicted RUL	576	532	475	410	343	280	216	N.A.	144 [$15^{th}test$]
	True RUL	765	663	561	459	357	255	153	N.A.	51 [$15^{th}test$]
VAH10	Predicted RUL	556	486	393	318	229	143	N.A.	N.A.	117 [$12^{th}test$]
	True RUL	613	511	409	306	204	102	N.A.	N.A.	51 [$12^{th}test$]
VAH11	Predicted RUL	736	710	643	588	541	482	435	400	390 [$16^{th}test$]
	True RUL	816	714	612	510	408	306	204	102	51 [$16^{th}test$]
VAH12	Predicted RUL	505	467	382	317	265	244	142	N.A.	100 [$15^{th}test$]
	True RUL	765	663	561	459	357	255	153	N.A.	51 [$15^{th}test$]
VAH13	Predicted RUL	531	479	403	316	272	171	N.A.	N.A.	88 [$13^{th}test$]
	True RUL	663	561	459	357	255	153	N.A.	N.A.	51 [$13^{th}test$]
VAH15	Predicted RUL	426	352	264	156	N.A.	N.A.	N.A.	N.A.	76 [$9^{th}test$]
	True RUL	459	357	255	153	N.A.	N.A.	N.A.	N.A.	51 [$9^{th}test$]
VAH16	Predicted RUL	479	431	355	241	N.A.	N.A.	N.A.	N.A.	110 [$9^{th}test$]
	True RUL	459	357	255	153	N.A.	N.A.	N.A.	N.A.	51 [$9^{th}test$]
VAH17	Predicted RUL	458	419	339	255	192	N.A.	N.A.	N.A.	118 [$11^{th}test$]
	True RUL	561	459	357	255	153	N.A.	N.A.	N.A.	51 [$11^{th}test$]
VAH20	Predicted RUL	473	416	315	217	N.A.	N.A.	N.A.	N.A.	128 [$9^{th}test$]
	True RUL	459	357	255	153	N.A.	N.A.	N.A.	N.A.	51 [$9^{th}test$]
VAH22	Predicted RUL	440	349	241	131	N.A.	N.A.	N.A.	N.A.	43 [$9^{th}test$]
	True RUL	459	357	255	153	N.A.	N.A.	N.A.	N.A.	51 [$9^{th}test$]
VAH23	Predicted RUL	210	246	202	164	156	N.A.	N.A.	N.A.	76 [$11^{th}test$]
	True RUL	561	459	357	255	153	N.A.	N.A.	N.A.	51 [$11^{th}test$]
VAH24	Predicted RUL	547	505	399	288	197	N.A.	N.A.	N.A.	82 [$11^{th}test$]
	True RUL	561	459	357	255	153	N.A.	N.A.	N.A.	51 [$11^{th}test$]
VAH25	Predicted RUL	438	393	286	158	21	N.A.	N.A.	N.A.	379 [$10^{th}test$]
	True RUL	512	410	307	205	103	N.A.	N.A.	N.A.	52 [$10^{th}test$]
VAH26	Predicted RUL	494	470	406	302	254	N.A.	N.A.	N.A.	169 [$10^{th}test$]
	True RUL	613	511	409	255	153	N.A.	N.A.	N.A.	51 [$10^{th}test$]
VAH27	Predicted RUL	425	375	290	86	N.A.	N.A.	N.A.	N.A.	-18 [$9^{th}test$]
	True RUL	511	409	307	153	N.A.	N.A.	N.A.	N.A.	51 [$9^{th}test$]
VAH28	Predicted RUL	566	547	480	394	318	241	198	N.A.	161 [$14^{th}test$]
	True RUL	721	619	517	414	312	210	108	N.A.	51 [$14^{th}test$]
VAH30	Predicted RUL	574	501	406	306	234	N.A.	N.A.	N.A.	185 [$10^{th}test$]
	True RUL	510	408	306	204	102	N.A.	N.A.	N.A.	51 [$10^{th}test$]

Table 15: Results RUL [#missions] with SVR

In Table 16 the predicted and true RUL for each mission profile are shown using RF regression. The results are given for every 3^{rd} capacity. Moreover, in Table 16 there is a column for the last capacity test. In Table 16, it can be seen that the final predicted RUL are not negative. It can be seen that the prediction of the RUL is too optimistic for VAH11.

		Capacity Test								
		1^{st} [#missions]	3^{rd} [#missions]	5^{th} [#missions]	7^{th} [#missions]	9^{th} [#missions]	11^{th} [#missions]	13^{th} [#missions]	15^{th} [#missions]	Last [#missions]
VAH01	Predicted RUL	398	367	325	223	86	57	N.A.	N.A.	55 [$12^{th}test$]
	True RUL	612	510	408	306	204	102	N.A.	N.A.	51 [$12^{th}test$]
VAH02	Predicted RUL	517	460	380	345	134	N.A.	N.A.	N.A.	65 [$10^{th}test$]
	True RUL	510	408	306	204	102	N.A.	N.A.	N.A.	51 [$10^{th}test$]
VAH05	Predicted RUL	645	615	570	435	323	259	163	N.A.	96 [$15^{th}test$]
	True RUL	765	663	561	459	357	255	153	N.A.	51 [$15^{th}test$]
VAH10	Predicted RUL	610	537	430	355	238	143	N.A.	N.A.	115 [$12^{th}test$]
	True RUL	613	511	409	306	204	102	N.A.	N.A.	51 [$12^{th}test$]
VAH11	Predicted RUL	716	714	689	664	568	502	465	365	366 [$16^{th}test$]
	True RUL	816	714	612	510	408	306	204	102	51 [$16^{th}test$]
VAH12	Predicted RUL	626	572	449	271	166	150	85	N.A.	78 [$15^{th}test$]
	True RUL	765	663	561	459	357	255	153	N.A.	51 [$15^{th}test$]
VAH13	Predicted RUL	661	574	417	330	263	100	N.A.	N.A.	70 [$13^{th}test$]
	True RUL	663	561	459	357	255	153	N.A.	N.A.	51 [$13^{th}test$]
VAH15	Predicted RUL	457	396	272	159	N.A.	N.A.	N.A.	N.A.	92 [$9^{th}test$]
	True RUL	459	357	255	153	N.A.	N.A.	N.A.	N.A.	51 [$9^{th}test$]
VAH16	Predicted RUL	448	412	342	224	N.A.	N.A.	N.A.	N.A.	102 [$9^{th}test$]
	True RUL	459	357	255	153	N.A.	N.A.	N.A.	N.A.	51 [$9^{th}test$]
VAH17	Predicted RUL	489	424	325	245	181	N.A.	N.A.	N.A.	81 [$11^{th}test$]
	True RUL	561	459	357	255	153	N.A.	N.A.	N.A.	51 [$11^{th}test$]
VAH20	Predicted RUL	427	394	284	216	N.A.	N.A.	N.A.	N.A.	121 [$9^{th}test$]
	True RUL	459	357	255	153	N.A.	N.A.	N.A.	N.A.	51 [$9^{th}test$]
VAH22	Predicted RUL	458	383	289	173	N.A.	N.A.	N.A.	N.A.	78 [$9^{th}test$]
	True RUL	459	357	255	153	N.A.	N.A.	N.A.	N.A.	51 [$9^{th}test$]
VAH23	Predicted RUL	353	346	341	308	320	N.A.	N.A.	N.A.	311 [$11^{th}test$]
	True RUL	561	459	357	255	153	N.A.	N.A.	N.A.	51 [$11^{th}test$]
VAH24	Predicted RUL	467	408	339	274	242	N.A.	N.A.	N.A.	214 [$11^{th}test$]
	True RUL	561	459	357	255	153	N.A.	N.A.	N.A.	51 [$11^{th}test$]
VAH25	Predicted RUL	477	436	310	163	63	N.A.	N.A.	N.A.	554 [$10^{th}test$]
	True RUL	512	410	307	205	103	N.A.	N.A.	N.A.	52 [$10^{th}test$]
VAH26	Predicted RUL	593	542	430	277	196	N.A.	N.A.	N.A.	104 [$10^{th}test$]
	True RUL	613	511	409	255	153	N.A.	N.A.	N.A.	51 [$10^{th}test$]
VAH27	Predicted RUL	505	415	323	155	N.A.	N.A.	N.A.	N.A.	62 [$9^{th}test$]
	True RUL	511	409	307	153	N.A.	N.A.	N.A.	N.A.	51 [$9^{th}test$]
VAH28	Predicted RUL	633	572	476	366	250	120	88	N.A.	81 [$14^{th}test$]
	True RUL	721	619	517	414	312	210	108	N.A.	51 [$14^{th}test$]
VAH30	Predicted RUL	644	554	461	349	271	N.A.	N.A.	N.A.	213 [$10^{th}test$]
	True RUL	510	408	306	204	102	N.A.	N.A.	N.A.	51 [$10^{th}test$]

Table 16: Results RUL [#missions] with RF regression tree

In Table 17 the predicted and true RUL for each mission profile are shown using XGBoost. The results are given for every 3^{rd} capacity. It can be seen in Table 17, that the prediction of the RUL is too optimistic for VAH11, which is the same as RF Regression.

		Capacity Test								
		1^{st} [#missions]	3^{rd} [#missions]	5^{th} [#missions]	7^{th} [#missions]	9^{th} [#missions]	11^{th} [#missions]	13^{th} [#missions]	15^{th} [#missions]	Last [#missions]
VAH01	Predicted RUL	484	458	401	279	67	46	N.A.	N.A.	32 [$12^{th}test$]
	True RUL	612	510	408	306	204	102	N.A.	N.A.	51 [$12^{th}test$]
VAH02	Predicted RUL	568	451	375	273	78	N.A.	N.A.	N.A.	65 [$10^{th}test$]
	True RUL	510	408	306	204	102	N.A.	N.A.	N.A.	51 [$10^{th}test$]
VAH05	Predicted RUL	656	617	573	460	417	314	198	N.A.	55 [$15^{th}test$]
	True RUL	765	663	561	459	357	255	153	N.A.	51 [$15^{th}test$]
VAH10	Predicted RUL	597	449	392	279	246	110	N.A.	N.A.	81 [$12^{th}test$]
	True RUL	613	511	409	306	204	102	N.A.	N.A.	51 [$12^{th}test$]
VAH11	Predicted RUL	757	764	737	695	621	575	520	369	371 [$16^{th}test$]
	True RUL	816	714	612	510	408	306	204	102	51 [$16^{th}test$]
VAH12	Predicted RUL	643	532	382	305	200	228	87	N.A.	77 [$15^{th}test$]
	True RUL	765	663	561	459	357	255	153	N.A.	51 [$15^{th}test$]
VAH13	Predicted RUL	681	596	405	324	262	122	N.A.	N.A.	29 [$13^{th}test$]
	True RUL	663	561	459	357	255	153	N.A.	N.A.	51 [$13^{th}test$]
VAH15	Predicted RUL	460	365	238	141	N.A.	N.A.	N.A.	N.A.	78 [$9^{th}test$]
	True RUL	459	357	255	153	N.A.	N.A.	N.A.	N.A.	51 [$9^{th}test$]
VAH16	Predicted RUL	479	415	277	208	N.A.	N.A.	N.A.	N.A.	93 [$9^{th}test$]
	True RUL	459	357	255	153	N.A.	N.A.	N.A.	N.A.	51 [$9^{th}test$]
VAH17	Predicted RUL	516	443	345	255	177	N.A.	N.A.	N.A.	100 [$11^{th}test$]
	True RUL	561	459	357	255	153	N.A.	N.A.	N.A.	51 [$11^{th}test$]
VAH20	Predicted RUL	450	349	250	199	N.A.	N.A.	N.A.	N.A.	103 [$9^{th}test$]
	True RUL	459	357	255	153	N.A.	N.A.	N.A.	N.A.	51 [$9^{th}test$]
VAH22	Predicted RUL	460	356	249	147	N.A.	N.A.	N.A.	N.A.	56 [$9^{th}test$]
	True RUL	459	357	255	153	N.A.	N.A.	N.A.	N.A.	51 [$9^{th}test$]
VAH23	Predicted RUL	303	343	290	210	252	N.A.	N.A.	N.A.	212 [$11^{th}test$]
	True RUL	561	459	357	255	153	N.A.	N.A.	N.A.	51 [$11^{th}test$]
VAH24	Predicted RUL	499	417	324	266	219	N.A.	N.A.	N.A.	150 [$11^{th}test$]
	True RUL	561	459	357	255	153	N.A.	N.A.	N.A.	51 [$11^{th}test$]
VAH25	Predicted RUL	454	413	299	161	36	N.A.	N.A.	N.A.	434 [$10^{th}test$]
	True RUL	512	410	307	205	103	N.A.	N.A.	N.A.	52 [$10^{th}test$]
VAH26	Predicted RUL	665	554	446	265	178	N.A.	N.A.	N.A.	102 [$10^{th}test$]
	True RUL	613	511	409	255	153	N.A.	N.A.	N.A.	51 [$10^{th}test$]
VAH27	Predicted RUL	548	408	330	135	N.A.	N.A.	N.A.	N.A.	55 [$9^{th}test$]
	True RUL	511	409	307	153	N.A.	N.A.	N.A.	N.A.	51 [$9^{th}test$]
VAH28	Predicted RUL	691	603	512	347	297	166	100	N.A.	73 [$14^{th}test$]
	True RUL	721	619	517	414	312	210	108	N.A.	51 [$14^{th}test$]
VAH30	Predicted RUL	654	423	384	317	262	N.A.	N.A.	N.A.	231 [$10^{th}test$]
	True RUL	510	408	306	204	102	N.A.	N.A.	N.A.	51 [$10^{th}test$]

Table 17: Results RUL [#missions] with XGBoost

In Table 18 the predicted and true RUL for each mission profile are shown using GPR. The results are given for every 3^{rd} capacity. The prediction of the RUL is very optimistic for VAH11, and VAH12.

		Capacity Test								
		1^{st} [#missions]	3^{rd} [#missions]	5^{th} [#missions]	7^{th} [#missions]	9^{th} [#missions]	11^{th} [#missions]	13^{th} [#missions]	15^{th} [#missions]	Last [#missions]
VAH01	Predicted RUL	491	453	364	294	73	35	N.A.	N.A.	19 [$12^{th}test$]
	True RUL	612	510	408	306	204	102	N.A.	N.A.	51 [$12^{th}test$]
VAH02	Predicted RUL	445	391	307	240	105	N.A.	N.A.	N.A.	62 [$10^{th}test$]
	True RUL	510	408	306	204	102	N.A.	N.A.	N.A.	51 [$10^{th}test$]
VAH05	Predicted RUL	678	640	579	474	354	256	176	N.A.	100 [$15^{th}test$]
	True RUL	765	663	561	459	357	255	153	N.A.	51 [$15^{th}test$]
VAH10	Predicted RUL	436	386	307	237	162	108	N.A.	N.A.	92 [$12^{th}test$]
	True RUL	613	511	409	306	204	102	N.A.	N.A.	51 [$12^{th}test$]
VAH11	Predicted RUL	477	487	483	468	446	381	337	304	296 [$16^{th}test$]
	True RUL	816	714	612	510	408	306	204	102	51 [$16^{th}test$]
VAH12	Predicted RUL	480	455	369	293	236	211	110	N.A.	78 [$15^{th}test$]
	True RUL	765	663	561	459	357	255	153	N.A.	51 [$15^{th}test$]
VAH13	Predicted RUL	631	580	482	330	269	136	N.A.	N.A.	63 [$13^{th}test$]
	True RUL	663	561	459	357	255	153	N.A.	N.A.	51 [$13^{th}test$]
VAH15	Predicted RUL	425	347	257	147	N.A.	N.A.	N.A.	N.A.	88 [$9^{th}test$]
	True RUL	459	357	255	153	N.A.	N.A.	N.A.	N.A.	51 [$9^{th}test$]
VAH16	Predicted RUL	510	447	350	228	N.A.	N.A.	N.A.	N.A.	119 [$9^{th}test$]
	True RUL	459	357	255	153	N.A.	N.A.	N.A.	N.A.	51 [$9^{th}test$]
VAH17	Predicted RUL	522	453	360	256	186	N.A.	N.A.	N.A.	122 [$11^{th}test$]
	True RUL	561	459	357	255	153	N.A.	N.A.	N.A.	51 [$11^{th}test$]
VAH20	Predicted RUL	506	431	312	204	N.A.	N.A.	N.A.	N.A.	121 [$9^{th}test$]
	True RUL	459	357	255	153	N.A.	N.A.	N.A.	N.A.	51 [$9^{th}test$]
VAH22	Predicted RUL	432	350	249	146	N.A.	N.A.	N.A.	N.A.	80 [$9^{th}test$]
	True RUL	459	357	255	153	N.A.	N.A.	N.A.	N.A.	51 [$9^{th}test$]
VAH23	Predicted RUL	241	267	216	177	146	N.A.	N.A.	N.A.	106 [$11^{th}test$]
	True RUL	561	459	357	255	153	N.A.	N.A.	N.A.	51 [$11^{th}test$]
VAH24	Predicted RUL	351	340	305	229	167	N.A.	N.A.	N.A.	102 [$11^{th}test$]
	True RUL	561	459	357	255	153	N.A.	N.A.	N.A.	51 [$11^{th}test$]
VAH25	Predicted RUL	484	420	313	173	64	N.A.	N.A.	N.A.	175 [$10^{th}test$]
	True RUL	512	410	307	205	103	N.A.	N.A.	N.A.	52 [$10^{th}test$]
VAH26	Predicted RUL	604	556	452	278	207	N.A.	N.A.	N.A.	114 [$10^{th}test$]
	True RUL	613	511	409	255	153	N.A.	N.A.	N.A.	51 [$10^{th}test$]
VAH27	Predicted RUL	545	475	354	136	N.A.	N.A.	N.A.	N.A.	65 [$9^{th}test$]
	True RUL	511	409	307	153	N.A.	N.A.	N.A.	N.A.	51 [$9^{th}test$]
VAH28	Predicted RUL	615	577	490	361	256	168	133	N.A.	105 [$14^{th}test$]
	True RUL	721	619	517	414	312	210	108	N.A.	51 [$14^{th}test$]
VAH30	Predicted RUL	343	308	251	185	141	N.A.	N.A.	N.A.	116 [$10^{th}test$]
	True RUL	510	408	306	204	102	N.A.	N.A.	N.A.	51 [$10^{th}test$]

Table 18: Results RUL [#missions] with GPR

In Table 19 the predicted and true RUL for each mission profile are shown using MLP. The results are given for every 3^{rd} capacity. It can be seen in Table 19, that the RUL prediction for VAH11 is again optimistic. Moreover, the RUL is predicted negative at VAH01 and VAH05.

		Capacity Test								
		1^{st} [#missions]	3^{rd} [#missions]	5^{th} [#missions]	7^{th} [#missions]	9^{th} [#missions]	11^{th} [#missions]	13^{th} [#missions]	15^{th} [#missions]	Last [#missions]
VAH01	Predicted RUL	681	525	391	262	57	-2	N.A.	N.A.	-18 [$12^{th}test$]
	True RUL	612	510	408	306	204	102	N.A.	N.A.	51 [$12^{th}test$]
VAH02	Predicted RUL	619	513	388	318	72	N.A.	N.A.	N.A.	22 [$10^{th}test$]
	True RUL	510	408	306	204	102	N.A.	N.A.	N.A.	51 [$10^{th}test$]
VAH05	Predicted RUL	706	598	451	357	244	92	-51	N.A.	-92 [$15^{th}test$]
	True RUL	765	663	561	459	357	255	153	N.A.	51 [$15^{th}test$]
VAH10	Predicted RUL	590	483	339	250	140	70	N.A.	N.A.	68 [$12^{th}test$]
	True RUL	613	511	409	306	204	102	N.A.	N.A.	51 [$12^{th}test$]
VAH11	Predicted RUL	1013	966	882	821	775	725	671	632	630 [$16^{th}test$]
	True RUL	816	714	612	510	408	306	204	102	51 [$16^{th}test$]
VAH12	Predicted RUL	687	623	493	406	334	265	136	N.A.	92 [$15^{th}test$]
	True RUL	765	663	561	459	357	255	153	N.A.	51 [$15^{th}test$]
VAH13	Predicted RUL	642	519	421	361	259	99	N.A.	N.A.	18 [$13^{th}test$]
	True RUL	663	561	459	357	255	153	N.A.	N.A.	51 [$13^{th}test$]
VAH15	Predicted RUL	466	354	258	167	N.A.	N.A.	N.A.	N.A.	88 [$9^{th}test$]
	True RUL	459	357	255	153	N.A.	N.A.	N.A.	N.A.	51 [$9^{th}test$]
VAH16	Predicted RUL	594	496	317	140	N.A.	N.A.	N.A.	N.A.	2 [$9^{th}test$]
	True RUL	459	357	255	153	N.A.	N.A.	N.A.	N.A.	51 [$9^{th}test$]
VAH17	Predicted RUL	515	408	326	251	203	N.A.	N.A.	N.A.	141 [$11^{th}test$]
	True RUL	561	459	357	255	153	N.A.	N.A.	N.A.	51 [$11^{th}test$]
VAH20	Predicted RUL	578	472	293	111	N.A.	N.A.	N.A.	N.A.	50 [$9^{th}test$]
	True RUL	459	357	255	153	N.A.	N.A.	N.A.	N.A.	51 [$9^{th}test$]
VAH22	Predicted RUL	467	349	257	147	N.A.	N.A.	N.A.	N.A.	69 [$9^{th}test$]
	True RUL	459	357	255	153	N.A.	N.A.	N.A.	N.A.	51 [$9^{th}test$]
VAH23	Predicted RUL	416	286	301	314	266	N.A.	N.A.	N.A.	281 [$11^{th}test$]
	True RUL	561	459	357	255	153	N.A.	N.A.	N.A.	51 [$11^{th}test$]
VAH24	Predicted RUL	632	521	382	302	296	N.A.	N.A.	N.A.	269 [$11^{th}test$]
	True RUL	561	459	357	255	153	N.A.	N.A.	N.A.	51 [$11^{th}test$]
VAH25	Predicted RUL	606	510	329	207	77	N.A.	N.A.	N.A.	368 [$10^{th}test$]
	True RUL	512	410	307	205	103	N.A.	N.A.	N.A.	52 [$10^{th}test$]
VAH26	Predicted RUL	672	599	494	300	198	N.A.	N.A.	N.A.	114 [$10^{th}test$]
	True RUL	613	511	409	255	153	N.A.	N.A.	N.A.	51 [$10^{th}test$]
VAH27	Predicted RUL	551	456	329	148	N.A.	N.A.	N.A.	N.A.	43 [$9^{th}test$]
	True RUL	511	409	307	153	N.A.	N.A.	N.A.	N.A.	51 [$9^{th}test$]
VAH28	Predicted RUL	691	634	537	413	331	283	243	N.A.	211 [$14^{th}test$]
	True RUL	721	619	517	414	312	210	108	N.A.	51 [$14^{th}test$]
VAH30	Predicted RUL	551	443	317	202	144	N.A.	N.A.	N.A.	105 [$10^{th}test$]
	True RUL	510	408	306	204	102	N.A.	N.A.	N.A.	51 [$10^{th}test$]

Table 19: Results RUL [#missions] with MLP

I Appendix 9

If the EOL-threshold is set to 80%, only 9 mission profiles reach the EOL. In Table 20 it can be seen that the following mission profiles reach the EOL, when the threshold is set to 80% of its initial measured capacity: VAH05, VAH10, VAH11, VAH12, VAH13, VAH17, VAH22, VAH26 and VAH30. The mission number is given when the battery reaches its EOL (#Missions until EOL). Besides, there is a column that highlights how many capacity tests are present until the battery reaches its EOL.

	VAHXX	#Missions until EOL	# Capacity tests until EOL
MP1	VAH01	N.A.	N.A.
MP2	VAH02	N.A.	N.A.
MP3	VAH05	1256	25
MP7	VAH10	990	20
MP8	VAH11	1276	25
MP9	VAH12	1176	24
MP10	VAH13	867	17
MP11	VAH15	N.A.	N.A.
MP12	VAH16	N.A.	N.A.
MP13	VAH17	919	19
MP14	VAH20	N.A.	N.A.
MP15	VAH22	578	12
MP16	VAH23	N.A.	N.A.
MP17	VAH24	N.A.	N.A.
MP18	VAH25	N.A.	N.A.
MP19	VAH26	976	19
MP20	VAH27	N.A.	N.A.
MP21	VAH28	N.A.	N.A.
MP22	VAH30	817	17

Table 20: All mission profiles (MP1-MP22, excluding MP4, MP5, and MP6) with EOL-threshold set to 80% of the initial measured capacity

If the EOL-threshold is set to 80%, 9 mission profiles can be used. The number of train observations is 170. Therefore, it is chosen to generate 3 folds. The division of folds have the following characteristics:

- Fold 1: number of train observations is 116. The number of test observations is 54, based on the files VAH11, VAH17, VAH22
- Fold 2: number of train observations is 112. The number of test observations is 58, based on the files VAH05, VAH26, VAH30
- Fold 3: number of train observations is 112. The number of test observations is 58, based on the files VAH10, VAH12, VAH13

In Figure 26 the relative importance of the features can be seen. It is chosen to follow the same procedure as for the EOL-threshold of 85%. Hence, 65% of the features are selected.

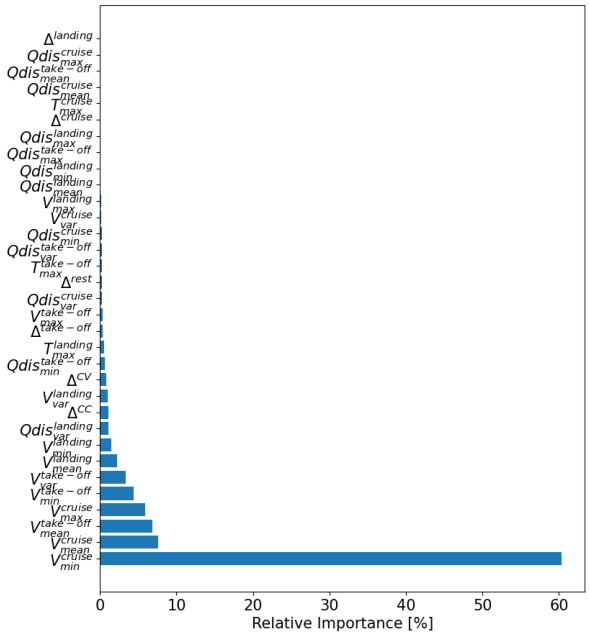

Figure 26: Feature importance RUL with EOL-threshold 80%

The selected features are:

- Charge-related features: CC time ($\Delta^{CC,m,c}$), CV time ($\Delta^{CV,m,c}$), rest time ($\Delta^{rest,m,c}$)
- Discharge-related features: minimum voltage during take-off, cruise, and landing ($V^{phase,m,c}_{min}$); maximum voltage during take-off and cruise ($V^{phase,m,c}_{max}$); mean voltage during take-off, cruise, and landing ($V^{phase,m,c}_{mean}$); variance voltage during take-off, and landing ($V^{phase,m,c}_{var}$); variance discharge capacity during take-off, cruise, and landing ($Qdis^{phase,m,c}_{var}$); minimum discharge capacity during take-off, and cruise ($Qdis^{phase,m,c}_{min}$); duration of take-off ($\Delta^{phase,m,c}$)
- Temperature-related features: maximum temperature during take-off, and landing ($T^{phase,m,c}_{max}$)

	MAE	RMSE	MAPE
SVR	109.32	129.51	0.47
RF Regression	161.53	182.22	0.54
XGBoost	153.43	166.88	0.54
GPR	**110.06**	**120.69**	**0.36**
MLP	238.19	418.76	1.73

Table 21: Results - RUL prediction [#missions], EOL-threshold 80%.

I.1 Results SVR RUL 80%

Model	Hyperparameters
Support Vector Regression	$Kernel = linear$ $Tolerance = 98.12$ $C = 0.87$ $\epsilon = 109.12$

Table 22: Optimized hyperparameters for RUL with EOL 80% using SVR

		Capacity Test								
		1^{st} [#missions]	4^{th} [#missions]	7^{th} [#missions]	10^{th} [#missions]	13^{th} [#missions]	16^{th} [#missions]	19^{th} [#missions]	22^{nd} [#missions]	Last [#missions]
VAH05	Predicted RUL	919	810	706	580	472	371	280	172	75 [$24^{th}test$]
	True RUL	1255	1102	949	796	643	490	337	153	51 [$24^{th}test$]
VAH10	Predicted RUL	952	796	651	525	409	278	N.A.	N.A.	191 [$19^{th}test$]
	True RUL	989	836	682	529	376	204	N.A.	N.A.	51 [$19^{th}test$]
VAH11	Predicted RUL	1155	1095	984	915	825	783	625	552	496 [$25^{th}test$]
	True RUL	1275	1122	969	816	663	510	357	204	51 [$25^{th}test$]
VAH12	Predicted RUL	954	881	742	673	570	507	381	323	306 [$23^{th}test$]
	True RUL	1175	1022	869	716	563	410	255	102	51 [$23^{th}test$]
VAH13	Predicted RUL	921	822	676	595	469	N.A.	N.A.	N.A.	368 [$16^{th}test$]
	True RUL	866	713	560	407	254	N.A.	N.A.	N.A.	101 [$16^{th}test$]
VAH17	Predicted RUL	816	687	527	411	287	227	N.A.	N.A.	42 [$18^{th}test$]
	True RUL	918	765	612	459	306	153	N.A.	N.A.	51 [$18^{th}test$]
VAH22	Predicted RUL	658	459	272	100	N.A.	N.A.	N.A.	N.A.	430 [$11^{th}test$]
	True RUL	577	424	271	118	N.A.	N.A.	N.A.	N.A.	67 [$11^{th}test$]
VAH26	Predicted RUL	892	787	611	521	315	183	N.A.	N.A.	106 [$18^{th}test$]
	True RUL	975	822	668	515	311	158	N.A.	N.A.	51 [$18^{th}test$]
VAH30	Predicted RUL	967	802	639	501	374	N.A.	N.A.	N.A.	247 [$16^{th}test$]
	True RUL	816	663	510	357	204	N.A.	N.A.	N.A.	51 [$16^{th}test$]

Table 23: Results RUL [#missions], EOL-threshold 80%, with SVR

	MAE	RMSE	MAPE
VAH05	169.84	196.36	0.27
VAH10	47.67	59.73	0.31
VAH11	185.53	228.07	0.94
VAH12	121.16	138.85	0.54
VAH13	156.65	167.92	0.59
VAH17	54.44	62.37	0.13
VAH22	63.38	116.26	0.0.58
VAH26	34.11	43.4	0.14
VAH30	151.1	152.66	0.7
Average	109.32	129.51	0.47

Table 24: Results RUL,using SVR, with EOL-threshold 80%

I.2 Results RF Regression RUL 80%

Model	Hyperparameters
Random Forest Regression Tree	$\#Trees = 3$ $MaxDepth = 20$ $MinSampleLeaf = 2$ $MinSampleSplit = 7$ $Criterion = SquaredError$

Table 25: Optimized hyperparameters for RUL with EOL 80% using RF regression tree

		Capacity Test								
		1^{st} [#missions]	4^{th} [#missions]	7^{th} [#missions]	10^{th} [#missions]	13^{th} [#missions]	16^{th} [#missions]	19^{th} [#missions]	22^{nd} [#missions]	Last [#missions]
VAH05	Predicted RUL	921	831	771	509	382	310	198	136	109 [$24^{th}test$]
	True RUL	1255	1102	949	796	643	490	337	153	51 [$24^{th}test$]
VAH10	Predicted RUL	1201	906	695	550	479	373	N.A.	N.A.	178 [$19^{th}test$]
	True RUL	989	836	682	529	376	204	N.A.	N.A.	51 [$19^{th}test$]
VAH11	Predicted RUL	1159	1159	1119	1022	1022	1022	606	422	318 [$25^{th}test$]
	True RUL	1275	1122	969	816	663	510	357	204	51 [$25^{th}test$]
VAH12	Predicted RUL	986	928	851	629	398	336	99	99	99 [$23^{th}test$]
	True RUL	1175	1022	869	716	563	410	255	102	51 [$23^{th}test$]
VAH13	Predicted RUL	1032	860	679	478	391	N.A.	N.A.	N.A.	164 [$16^{th}test$]
	True RUL	866	713	560	407	254	N.A.	N.A.	N.A.	101 [$16^{th}test$]
VAH17	Predicted RUL	878	558	538	228	166	206	N.A.	N.A.	87 [$18^{th}test$]
	True RUL	918	765	612	459	306	153	N.A.	N.A.	51 [$18^{th}test$]
VAH22	Predicted RUL	891	737	537	327	N.A.	N.A.	N.A.	N.A.	610 [$11^{th}test$]
	True RUL	577	424	271	118	N.A.	N.A.	N.A.	N.A.	67 [$11^{th}test$]
VAH26	Predicted RUL	829	744	571	510	189	179	N.A.	N.A.	115 [$18^{th}test$]
	True RUL	975	822	668	515	311	158	N.A.	N.A.	51 [$18^{th}test$]
VAH30	Predicted RUL	1201	1013	695	550	438	N.A.	N.A.	N.A.	166 [$16^{th}test$]
	True RUL	816	663	510	357	204	N.A.	N.A.	N.A.	51 [$16^{th}test$]

Table 26: Results RUL [#missions], EOL-threshold 80%, with XGBoost

	MAE	RMSE	MAPE
VAH05	194.58	214.11	0.35
VAH10	92.21	125.51	0.33
VAH11	247.53	285.26	0.82
VAH12	96.3	115.34	0.22
VAH13	119.37	127.48	0.29
VAH17	94.27	115.28	0.25
VAH22	284.12	301.19	1.54
VAH26	66.92	78.65	0.22
VAH30	258.5	277.19	0.86
Average	161.53	182.22	0.54

Table 27: Results RUL,using RF Regression, with EOL-threshold 80%

I.3 Results XGBoost RUL 80%

Model	Hyperparameters
XGBoost	$\#Estimators = 29$
	$MaxDepth = 16$
	$Gamma = 0.85$
	$MinChildWeight = 13$
	$Colsamplebytree = 0.75$
	$Learningrate = 0.275$
	$subsample = 0.88$

Table 28: Optimized hyperparameters for RUL with EOL 80% using XGBoost

		Capacity Test								
		1^{st} [#missions]	4^{th} [#missions]	7^{th} [#missions]	10^{th} [#missions]	13^{th} [#missions]	16^{th} [#missions]	19^{th} [#missions]	22^{nd} [#missions]	Last [#missions]
VAH05	Predicted RUL	1028	799	654	637	427	346	185	126	115 [$24^{th}test$]
	True RUL	1255	1102	949	796	643	490	337	153	51 [$24^{th}test$]
VAH10	Predicted RUL	1011	929	725	596	489	262	N.A.	N.A.	137 [$19^{th}test$]
	True RUL	989	836	682	529	376	204	N.A.	N.A.	51 [$19^{th}test$]
VAH11	Predicted RUL	1162	1148	1139	1075	1033	997	641	506	383 [$25^{th}test$]
	True RUL	1275	1122	969	816	663	510	357	204	51 [$25^{th}test$]
VAH12	Predicted RUL	1024	932	805	635	475	389	193	92	93 [$23^{th}test$]
	True RUL	1175	1022	869	716	563	410	255	102	51 [$23^{th}test$]
VAH13	Predicted RUL	1031	876	665	562	397	N.A.	N.A.	N.A.	216 [$16^{th}test$]
	True RUL	866	713	560	407	254	N.A.	N.A.	N.A.	101 [$16^{th}test$]
VAH17	Predicted RUL	847	743	528	416	189	129	N.A.	N.A.	66 [$18^{th}test$]
	True RUL	918	765	612	459	306	153	N.A.	N.A.	51 [$18^{th}test$]
VAH22	Predicted RUL	792	669	449	248	N.A.	N.A.	N.A.	N.A.	643 [$11^{th}test$]
	True RUL	577	424	271	118	N.A.	N.A.	N.A.	N.A.	67 [$11^{th}test$]
VAH26	Predicted RUL	856	694	538	409	118	113	N.A.	N.A.	109 [$18^{th}test$]
	True RUL	975	822	668	515	311	158	N.A.	N.A.	51 [$18^{th}test$]
VAH30	Predicted RUL	1006	996	809	600	410	N.A.	N.A.	N.A.	228 [$16^{th}test$]
	True RUL	816	663	510	357	204	N.A.	N.A.	N.A.	51 [$16^{th}test$]

Table 29: Results RUL [#missions], EOL-threshold 80%, with XGBoost

	MAE	RMSE	MAPE
VAH05	178.43	195.64	0.32
VAH10	70.38	77.52	0.29
VAH11	263.9	294.05	0.94
VAH12	82.83	89.59	0.19
VAH13	139.88	145.91	0.37
VAH17	63.61	74.69	0.18
VAH22	247.92	273.63	1.44
VAH26	96.92	109.16	0.27
VAH30	236.99	241.75	0.86
Average	153.43	166.88	0.54

Table 30: Results RUL,using XGBoost, with EOL-threshold 80%

I.4 Results GPR RUL 80%

Model	Hyperparameters
GPR	$Alpha = 1.0$ $Kernel = RBF(length\_scale = 467.05)$

Table 31: Optimized hyperparameters for RUL with EOL 80% using GPR

		Capacity Test								
		1^{st} [#missions]	4^{th} [#missions]	7^{th} [#missions]	10^{th} [#missions]	13^{th} [#missions]	16^{th} [#missions]	19^{th} [#missions]	22^{nd} [#missions]	Last [#missions]
VAH05	Predicted RUL	1038	957	832	637	465	316	208	102	33 [$24^{th}test$]
	True RUL	1255	1102	949	796	643	490	337	153	51 [$24^{th}test$]
VAH10	Predicted RUL	858	780	650	521	387	240	N.A.	N.A.	158 [$19^{th}test$]
	True RUL	989	836	682	529	376	204	N.A.	N.A.	51 [$19^{th}test$]
VAH11	Predicted RUL	866	899	904	876	800	753	546	436	355 [$25^{th}test$]
	True RUL	1275	1122	969	816	663	510	357	204	51 [$25^{th}test$]
VAH12	Predicted RUL	857	841	691	591	436	345	177	115	100 [$23^{th}test$]
	True RUL	1175	1022	869	716	563	410	255	102	51 [$23^{th}test$]
VAH13	Predicted RUL	948	901	713	594	403	N.A.	N.A.	N.A.	261 [$16^{th}test$]
	True RUL	866	713	560	407	254	N.A.	N.A.	N.A.	101 [$16^{th}test$]
VAH17	Predicted RUL	793	651	468	332	197	132	N.A.	N.A.	28 [$18^{th}test$]
	True RUL	918	765	612	459	306	153	N.A.	N.A.	51 [$18^{th}test$]
VAH22	Predicted RUL	667	498	319	173	N.A.	N.A.	N.A.	N.A.	0 [$11^{th}test$]
	True RUL	577	424	271	118	N.A.	N.A.	N.A.	N.A.	67 [$11^{th}test$]
VAH26	Predicted RUL	941	835	598	476	223	85	N.A.	N.A.	28 [$18^{th}test$]
	True RUL	975	822	668	515	311	158	N.A.	N.A.	51 [$18^{th}test$]
VAH30	Predicted RUL	790	738	618	484	347	N.A.	N.A.	N.A.	221 [$16^{th}test$]
	True RUL	816	663	510	357	204	N.A.	N.A.	N.A.	51 [$16^{th}test$]

Table 32: Results RUL [#missions], EOL-threshold 80%, with GPR

	MAE	RMSE	MAPE
VAH05	136.92	146.34	0.25
VAH10	46.58	58.44	0.23
VAH11	191.73	215.59	0.71
VAH12	124.38	145.3	0.23
VAH13	155.83	158.28	0.46
VAH17	104.05	110.56	0.27
VAH22	70.15	71.28	0.31
VAH26	53.53	64.71	0.19
VAH30	107.37	115.68	0.57
Average	110.06	120.69	0.36

Table 33: Results RUL,using GPR, with EOL-threshold 80%

I.5 Results MLP RUL 80%

Model	Hyperparameters
MLP	$Activation = identity$
	$Batchsize = 64$
	$Firstlayerneurons = 10$
	$Secondlayerneurons = 100$
	$Thirdlayerneurons = 90$

Table 34: Optimized hyperparameters for RUL with EOL 80% using MLP

		Capacity Test								
		1^{st} [#missions]	4^{th} [#missions]	7^{th} [#missions]	10^{th} [#missions]	13^{th} [#missions]	16^{th} [#missions]	19^{th} [#missions]	22^{nd} [#missions]	Last [#missions]
VAH05	Predicted RUL	971	881	741	568	420	297	160	8	-131 [$24^{th}test$]
	True RUL	1255	1102	949	796	643	490	337	153	51 [$24^{th}test$]
VAH10	Predicted RUL	1057	883	732	575	447	302	N.A.	N.A.	221 [$19^{th}test$]
	True RUL	989	836	682	529	376	204	N.A.	N.A.	51 [$19^{th}test$]
VAH11	Predicted RUL	1453	1408	1262	1148	1023	980	724	609	532 [$25^{th}test$]
	True RUL	1275	1122	969	816	663	510	357	204	51 [$25^{th}test$]
VAH12	Predicted RUL	1017	946	683	554	368	253	12	-90	-119 [$23^{th}test$]
	True RUL	1175	1022	869	716	563	410	255	102	51 [$23^{th}test$]
VAH13	Predicted RUL	1087	956	703	568	333	N.A.	N.A.	N.A.	182 [$16^{th}test$]
	True RUL	866	713	560	407	254	N.A.	N.A.	N.A.	101 [$16^{th}test$]
VAH17	Predicted RUL	832	712	552	436	313	254	N.A.	N.A.	73 [$18^{th}test$]
	True RUL	918	765	612	459	306	153	N.A.	N.A.	51 [$18^{th}test$]
VAH22	Predicted RUL	661	535	367	211	N.A.	N.A.	N.A.	N.A.	-7799 [$11^{th}test$]
	True RUL	577	424	271	118	N.A.	N.A.	N.A.	N.A.	67 [$11^{th}test$]
VAH26	Predicted RUL	1029	914	687	566	283	110	N.A.	N.A.	50 [$18^{th}test$]
	True RUL	975	822	668	515	311	158	N.A.	N.A.	51 [$18^{th}test$]
VAH30	Predicted RUL	1133	954	783	621	500	N.A.	N.A.	N.A.	365 [$16^{th}test$]
	True RUL	816	663	510	357	204	N.A.	N.A.	N.A.	51 [$16^{th}test$]

Table 35: Results RUL [#missions], EOL-threshold 80%, with MLP

	MAE	RMSE	MAPE
VAH05	200.48	204.74	0.51
VAH10	76.13	85.24	0.42
VAH11	354.4	362.24	1.24
VAH12	160.38	169.04	0.57
VAH13	159.2	174.49	0.36
VAH17	41.02	48.2	0.13
VAH22	814.2	2374.13	11.03
VAH26	46.67	59.03	0.1
VAH30	291.19	291.76	1.24
Average	238.19	418.76	1.73

Table 36: Results RUL,using MLP, with EOL-threshold 80%

J Appendix 10

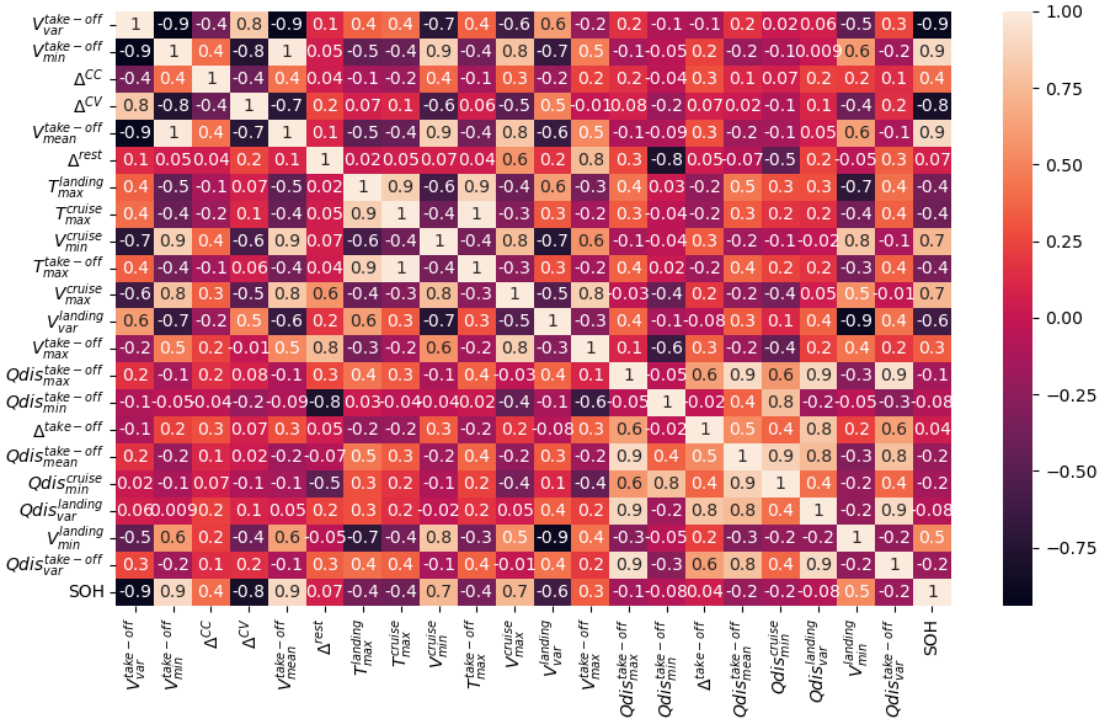

Figure 27: Correlation matrix of the selected features for the SOH prediction

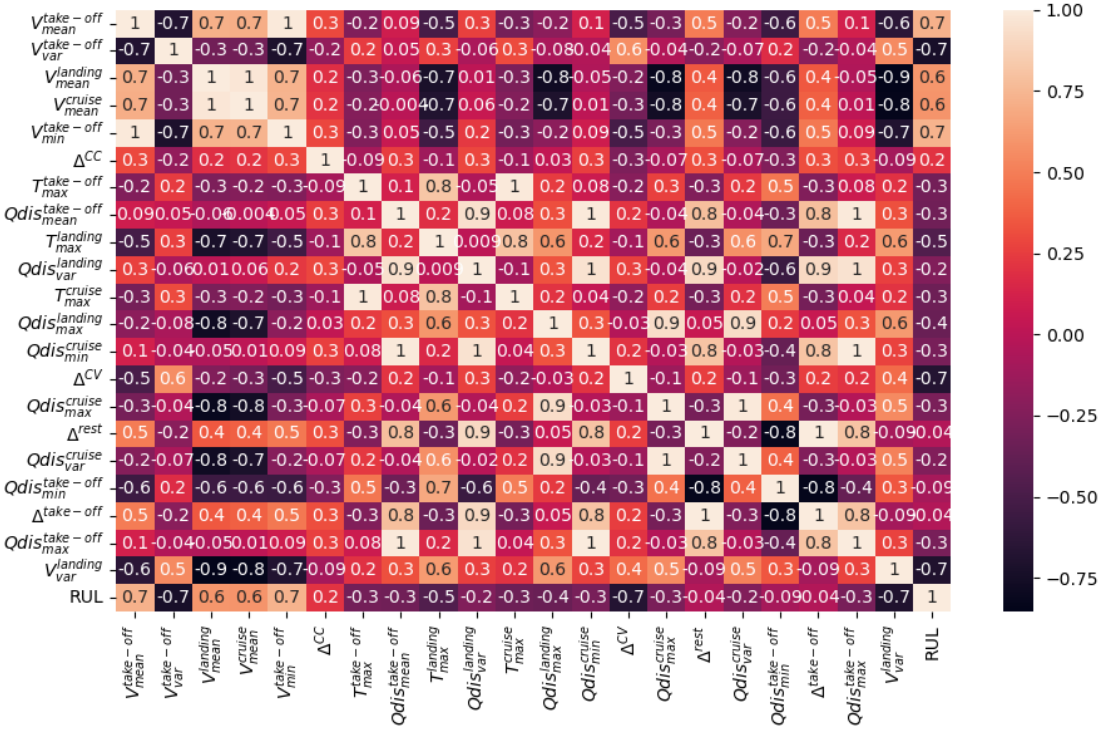

Figure 28: Correlation matrix of the selected features for the RUL prediction

K Appendix 11

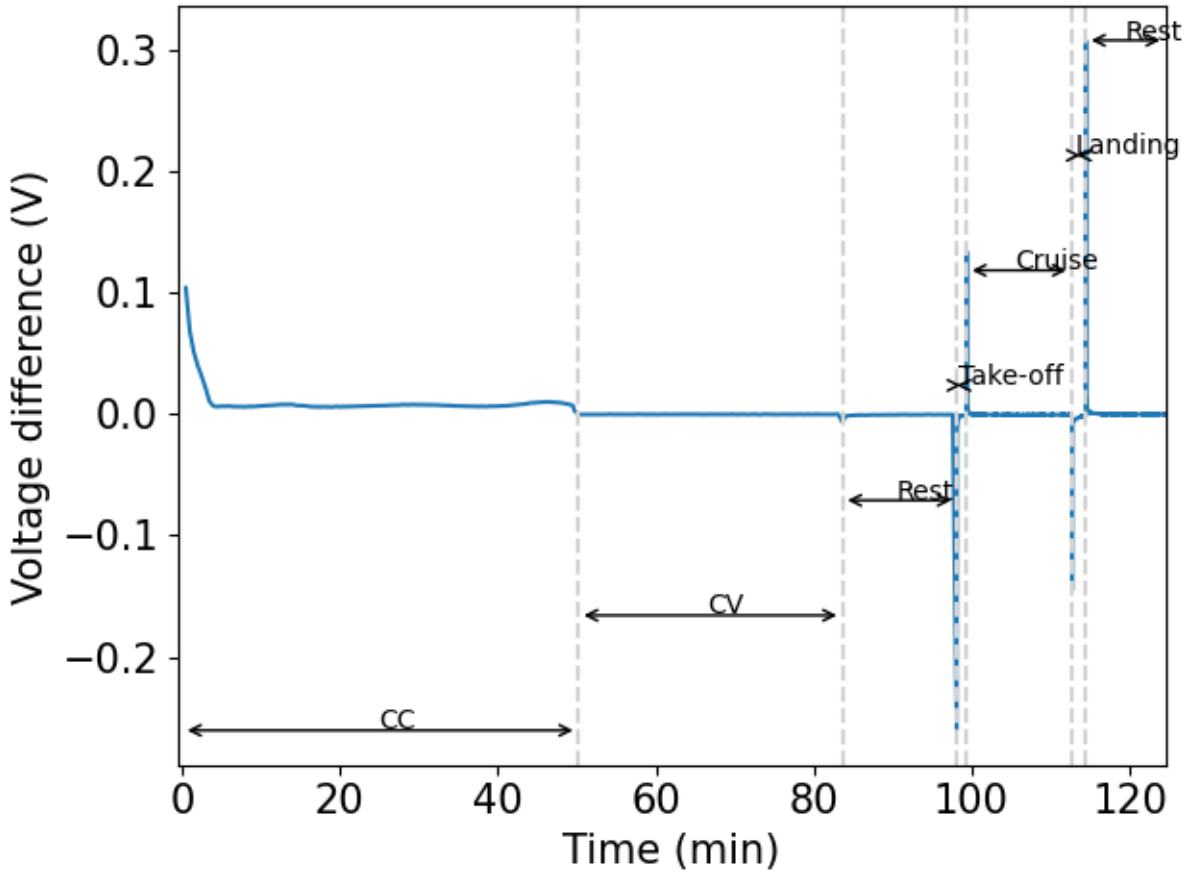

Figure 29: Difference of the voltage within the first capacity test for VAH01